THE ANALYSIS OF MODEL MEASUREMENTS CONCERNING THE BEHAVIOUR OF MOORED SHIPS IN LONG WAVES

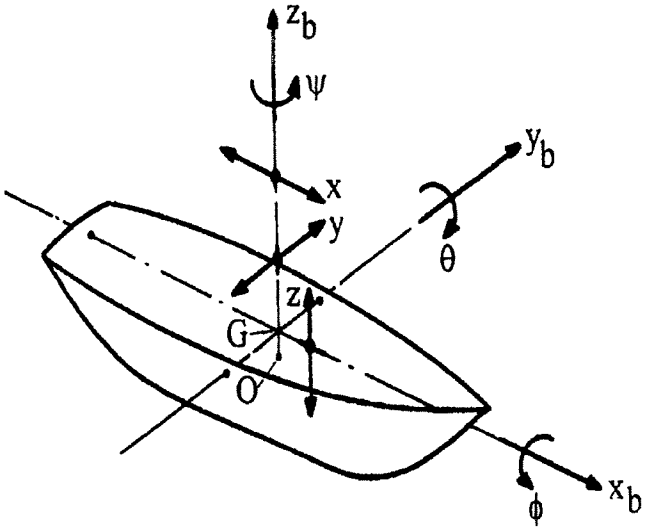

Jadwiga Sarneel
728182

DECEMBER 2000

MSc PROJECT

DELFT UNIVERSITY OF TECHNOLOGY, FACULTY OF CIVIL ENGINEERING AND GEOSCIENCES, SECTION OF HYDRAULIC ENGINEERING

COMMITTEE:

- PROF. IR. H. LIGTERINGEN
- PROF. DR. IR. J.A. BATTJES
- IR. R. GROENVELD
- IR. H. MOES
- PROF. DR. IR. J.A. PINKSTER

Preface

This report is the result of my MSc-project at the Faculty of Civil Engineering and Geosciences at Delft University of Technology. It is conducted within the Section of Hydraulic and Offshore Engineering, Chair Ports and Inland Waterways. Prof. Ir. H. Ligteringen and Ir. R. Groenveld have been very helpful during the process of this project.

The project involves the disciplines Hydromechanics and Ship Hydromechanics as well. I would like to thank Prof. Dr. Ir. J. A. Battjes and Prof. Dr. Ir. J. A. Pinkster for their knowledge and support in these fields.

Especially I would like to thank Ir. H. Moes and Ir. J. van Aswegen for their help during my stay at the CSIR, Stellenbosch.

Hopefully the results of this project contribute to the development of a simple model to describe the behaviour of moored ships subjected to incident waves.

Jadwiga Sarneel.

Abstract

When designing a new port it is important to predict the operation efficiency of the port. In this respect, it is desirable to predict the possible downtime of a new port in an early phase of the design process. Downtime depends strongly on the moored ship motions.

In the past decades several numerical models were developed to predict the behaviour of moored ships in waves. They are referred to as Six Degree of Freedom (SDF) models. These models, such as TERMSIM and BAS, are complex and require quite detailed input data. This detailed information is not available in the planning phase of a new port. Consequently, it is desirable to estimate possible downtime by means of a simple model that estimates the ship's behaviour without detailed input data.

With this in mind Delft University of Technology started a research programme that consists of a number of MSc- projects possibly leading to a PhD-project. The research objective of the programme is to investigate the possibilities of simplification of the models used nowadays. In this respect the aim is to find straightforward relationships to describe the behaviour of moored ships subjected to incident waves. It is emphasized that this simplified model is not meant to replace the Six Degree of Freedom models. The simple model is a valuable design tool, to be used in an early stage of the port development process.

This report covers one of the MSc-projects defined as *"The analysis of model measurements concerning the behaviour of moored ships in long wave"*. It concerns the model tests of the planned "Coega Harbour" in South Africa. Part of this project is carried out in South Africa, at CSIR (Council for Scientific and Industrial Research), where data of the model tests are available. The aim of the project is to gain insight in the importance of the various parameters and their mutual relations. An important issue is the validation of relationships mentioned in the literature. The main objective is to derive straightforward relations between motions of a moored ship and the wave field near the ship

Hypotheses with regard to the surge, sway and roll motion are derived from the theory of a moored ship. These hypotheses are verified using the data measured in the physical model. This data is limited to one type of ship moored with one type of mooring system inside one specific harbour. Consequently, the conclusions do not contain general validity. Nonetheless, the results present tools that contribute to the understanding of the response of a moored ship to incident waves. The following conclusions result from validation of the hypotheses:

- The surge motion relates linearly to the low frequency significant wave height with a value that is not varying significantly with the peak period of the incident short wave spectrum.

- The roll motion is proportional to the high frequency significant wave height. The ratio between the ship motions and the wave height is not constant for different wave fields. The ratio is a function of the peak period that appears to be influenced by the natural period of roll.

- For the sway motion a proportionality between this ship motion and the significant wave height is observed. The ratio between the ship motion and the wave field is a function of the peak period. This function increases with increasing peak period and appears to be influenced by the natural period of roll.

Because of the linear relation between the surge motion and the low frequency wave field it is assumed that the system of the moored ship can be represented by a linear mass-spring system. To verify the assumed representation, the energy spectrum of the surge motion is calculated and compared to the measured energy spectrum. This comparison shows that the calculated surge motion is of the same magnitude as the measured surge motion. The ratio of the calculated and the measured significant surge motion is between 0.4 and 1.8 for all considered wave fields and directions.

Mol et al. (1985) also schematised the moored ship as a linear damped mass spring system with one degree of freedom. They formulated an empirical relation on the basis that the dynamic motion is the static value multiplied by a coefficient (C_X) that represents the dynamic influence. Mol et al. (1985) found C_X values ranging between 1 and 3, with an average of 1.7. The value of C_X found for the measured data of the Coega model tests is 1.8, which is within the range found by Mol et al. (1985).

Roll motions calculated for a free-floating ship overestimate the motions of a moored ship. It is advised to include the mooring system in order to derive more accurate results. Sway motions calculated for a free-floating ship provide a fairly accurate representation of the moored ship motions. By taking into account the coupling with the roll motion the calculations can be improved.

The physical model study of the Coega harbour was not conducted in order to investigate the behaviour of moored ships in general. It is recommendable to conduct a physical model study of which the research objective is primarily to derive relations describing the ship's behaviour. This study should investigate more than the ships response to incident waves. The mooring system and ship characteristics should be varied in order to investigate their influence on the ship's behaviour.

The results of this physical model study should be compared to prototype measurements in order to validate the conclusions of the study. It is this writer's opinion that a simple computer (spreadsheet) programme can be developed after the conduction of a comprehensive physical model study.

Table of contents

List of figures

List of tables

List of symbols

If any of the symbols in this list is used for any other purpose as defined here then this will be mentioned in the text.

Roman Symbols

a	hydrodynamic mass coefficient
b	hydrodynamic damping coefficient
B	breadth
c	restoring spring coefficient
C_B	block coefficient
d	water depth
E	absorbed energy
f	frequency
f_p	peak frequency
F	force
g	gravitational force
H_{hi}	significant wave height high frequency
H_{lo}	significant wave height low frequency
H_{mo}	significant wave height
H_s	significant wave height
$H_{s,\,long}$	significant wave height long waves
k	wave number
k_t	stiffness of mooring system parallel to quay-line
K_{eff}	effective elasticity coefficient
$K_{fenders}$	elastic coefficients of the fenders
K_{lines}	elastic coefficients of the mooring lines
L_{bp}	length between perpendiculars
L_B	basin length
L_{oa}	length over all
m	mass
m_o	zeroth moment
s	compression of fender
S	energy spectral density
t	time
T_n	natural period
T_P	peak period, period of most energetic frequency
u	velocity
x	displacement
X	surge motion; translation along the x-axis
$X_{horizontal}$	horizontal ship motions
X_{mo}	significant surge displacement
y	sway motion; translation along the y-axis
Y_{mo}	significant sway displacement
z	heave motion; translation along the z-axis

Greek Symbols

γ	spectral peak enhancement factor
ε	phase angle
ζ	wave amplitude
ς^*	reduced wave elevation
θ	pitch motin; rotation around the y-axis
λ	wave length
σ^2	variance
∇	displacement
φ	direction of incident waves
ϕ	roll motion; rotation around the x-axis
Φ_{mc}	significant roll angle
ψ	yaw motion; rotation around the z-axis
ω	angular frequency

1. Introduction

Initiation of the project

When designing a new port it is important to predict the operation efficiency of the port. In this respect, it is desirable to predict the possible downtime of a new port in an early phase of the design process. Downtime depends strongly on the moored ship motions.

In the past decades several numerical models were developed to predict the behaviour of moored ships in waves. They are referred to as Six Degree of Freedom (SDF) models. These models, such as TERMSIM and BAS, are complex and require quite detailed input data. This detailed information is not available in the planning phase of a new port. Consequently, it is desirable to estimate possible downtime by means of a simple model that estimates the ship's behaviour without detailed input data.

With this in mind Delft University of Technology started a research programme that consists of a number of MSc- projects possibly leading to a PhD-project. The research objective of the programme is to investigate the possibilities of simplification of the models used nowadays. It is emphasized that this simplified model is not meant to replace the Six Degree of Freedom models. The simple model is a valuable design tool, to be used in an early stage of the port development process.

This report covers one of the MSc-projects defined as "The analysis of model measurements concerning the behaviour of moored ships in long waves." It concerns the model tests of the planned "Coega Harbour" in South Africa. This harbour will be located in Algoa Bay, near Port Elizabeth (see Figure 1.1). Appendix 1.a shows a bathymetric chart of Algoa Bay. Part of this project is carried out in South Africa, at CSIR (Council for Scientific and Industrial Research), where data of the model tests are available.

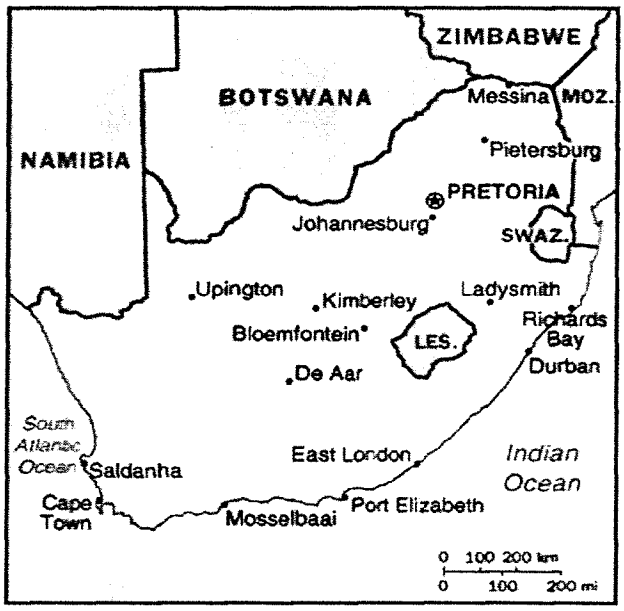

Figure 1.1. Map of South Africa

Figure 1.2 gives an overview of how this report is built up. The basis of this MSc-project is described in Chapter 2. The problem definition and research objective formulated in this chapter influence all of the following chapters. The Chapters 3 and 4 are fairly independent. Chapter 3 presents the theory of a moored ship in waves. It commences with background information of moored ships in waves. Points of view of several sources are discussed and empirical relations are mentioned. In Chapter 4 the Coega model tests are described. It is described which tests were performed and how the model tests were conducted. The relevant reports of the CSIR are mentioned as well.

Chapter 5 combines the two preceding chapters. It investigates to what extent the theory is applicable to the model tests. Hypotheses are derived from this combination of the theory and the model tests. These hypotheses concern the relation between the waves and the ship motions. Verification of the hypotheses and application to the model ship takes place in Chapter 6.

Lastly, Chapter 7 summarizes the conclusions following from the preceding chapters. Furthermore, recommendations for the future are made.

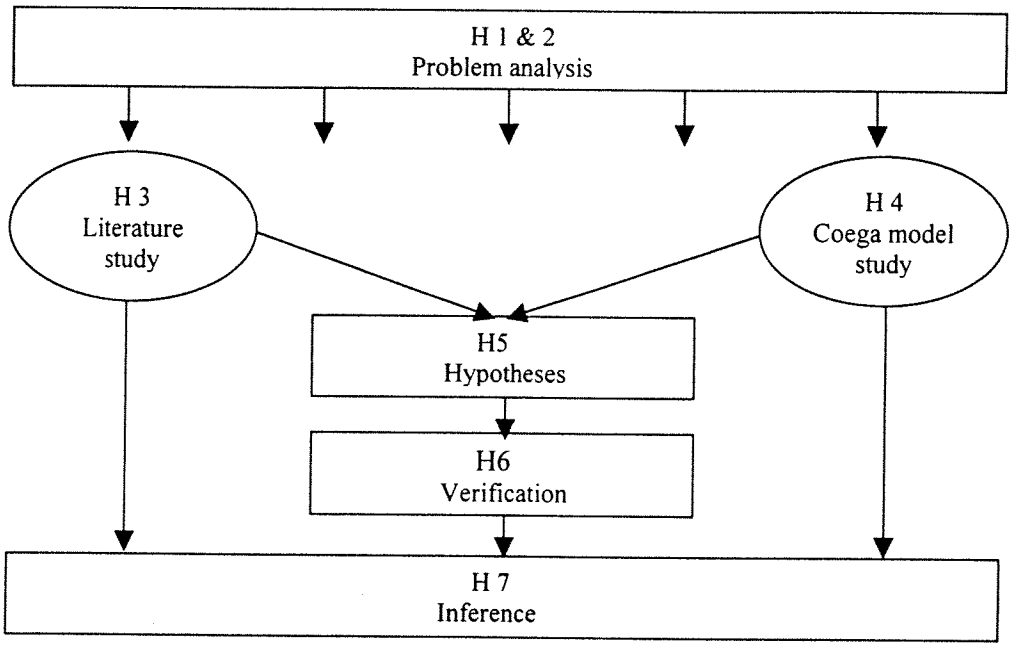

Figure 1.2. Set-up of the report

2. Problem analysis

Scope of the project

This chapter describes the problem definition and the research objectives. Because the MSc-project is part of a large research programme distinction is made between the problem definition and research objective of the programme and those of the MSc-project. A good understanding of the research programme is of importance in order to define the MSc-project. The scope of the research programme is given in Section 2.1. Subsequently, Sections 2.2 and 2.3 contain respectively the problem definition and research objective of the MSc-project.

2.1. Introduction

The research objective of the programme is to investigate the possibilities of a simplification of the Six Degree of Freedom models. In this respect the aim is to find straightforward relationships between ship motions and waves at the position of the ship.

The wave fields outside a port and inside a port are not identical. It is assumed that the designers of a new port have some knowledge of the wave field outside the harbour. With the layout of the future harbour the wave field inside the port can be determined. Next, the ship motions need to be predicted from the wave field near the ship. For this prediction relations of general validity are necessary.

This MSc-project attempts to derive relations between the ship motions and the wave field at the position of the ship. This is done by means of the test results of the model of "Coega Harbour". Both the wave fields inside and outside the port are measured as well as the ship motions. The wave field inside the port (near the ship) and the measured ship motions are used to derive relations of general validity. The wave field outside the port is used to investigate existing relations of the significant wave height with the low frequency significant wave height.

Figure 2.1 gives a schematisation of the abovementioned. For the sake of simplicity, the wave field in this figure is identified by the wave height. Other parameters, such as the wave direction and the wave period, also influence the motions of moored ships and are treated in this report as well.

The following symbols are to identify the wave field and the ship motions:

- H_{mo} = significant wave height (m)
- H_{lo} = low frequency significant wave height (m)
- H_{hi} = high frequency significant wave height (m)
- X_{mo} = significant surge displacement (m)
- Y_{mo} = significant sway displacement (m)
- Φ_{mo} = significant roll angle (°)
- T_P = peak period of the wave spectrum (s)
- φ = direction of incident waves (°)

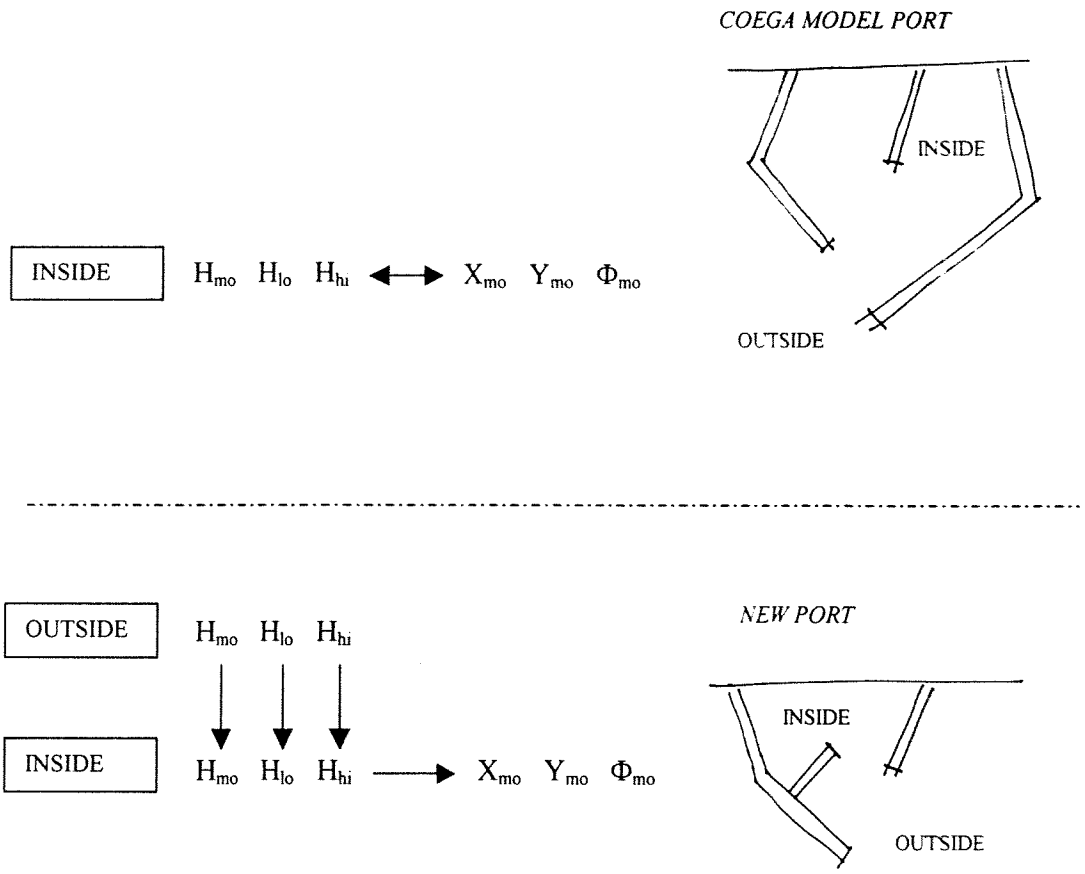

Figure 2.1. Schematisation of this MSc-project in relation to the development of a new port

The term 'general validity' as mentioned before requires elucidation. Three pitfalls need to be considered:

- The relations derived in this report ensue from results of a model test. The coefficients found for these relations cannot simply be used in prototype situations. For this reason, effort is made to derive dimensionless coefficients.
- In a physical model phenomena can occur that are not present in reality. These model effects need to be eliminated in order to come to useful relations.
- The Coega model tests represent merely one type of ship and one type of mooring system. Coefficients found using the test results apply only for this type of ship with this type of mooring system.

2.2. Problem definition

There is no simple model available to predict the motions of moored ships in response to incident waves. To estimate the ship's behaviour during the planning phase of a port such a model is required. This is the problem definition of the research programme. The problem definition of the MSc-project is a derivative of that of the research programme:

"There are no straightforward relationships available to describe the behaviour of moored ships subjected to incident waves."

2.3. Research objective

The aim of the project is to gain insight in the importance of the various parameters and their mutual relations. An important issue is the validation of relationships mentioned in the literature. The main objective is to come to simple relationships to describe the behaviour of moored ships. With this, the research objective is:

"To derive straightforward relations between motions of a moored ship and the wave field near the ship."

It is emphasised that this project is limited to one type of ship that is moored inside a harbour.

3. Literature study

Theory behind the moored ship

3.1. Introduction

This chapter treats the theory of moored ships in waves. This theory is the basis for the formulation of hypotheses in Chapter 5.

The system of a moored ship can be divided into three components: the wave field, the mooring system and the ship itself. These three components are very closely related to each other and are therefore hard to discuss separately. Nonetheless, it is tried in Section 3.2 to give some general information without looking into the relations between these components. After reviewing the incoming waves (Section 3.2.1), the mooring system (Section 3.2.2) and the ship (Section 3.2.3) these three aspects are put together in Section 3.2.4.

Subsequently, Section 3.3 presents the most important outcomes of a literature study concerning all the aspects of a moored ship. Emphasis is given to the relation between the waves and the response motions of the ship. This section contains citations from publications. The author's opinion is expressed both in the choice of citations and in several remarks.

3.2. Theory of moored ships

The total system of a moored ship is divided into three sub-systems, which are handled separately. These three systems are the wave field, the ship and the mooring system. Most of the information in this section comes from sources like "Offshore hydromechanics" (Journée and Massie, 2000) and "Basic ship theory" (Rawson and Tupper, 1983), which are considered to be of general validity. This in contrast to the sources in Section 3.3 that are regarded as hypotheses that can or cannot be valid.

3.2.1. Waves

There are two different types of wind generated wave fields: sea and swell. Contrary to sea, swell consists of waves that are no longer under the influence of wind. Swell can travel long distances without any wind. The main period of sea varies between 5 to 12 seconds. Swell can be divided into waves with periods between 10 to 25 seconds and waves with periods greater than 30 seconds.

Waves with a period of 30 sec or more are considered low frequency waves or long waves. There is a distinction between free long waves, like seiches and tidal waves, and bound long waves. Bound long waves are waves accompanying sea and/or swell. The bound long wave travels with the short period wave group celerity. The trough of these bound waves coincides with high short waves. Their crests coincide with low short waves. This is illustrated in Figure 3.1

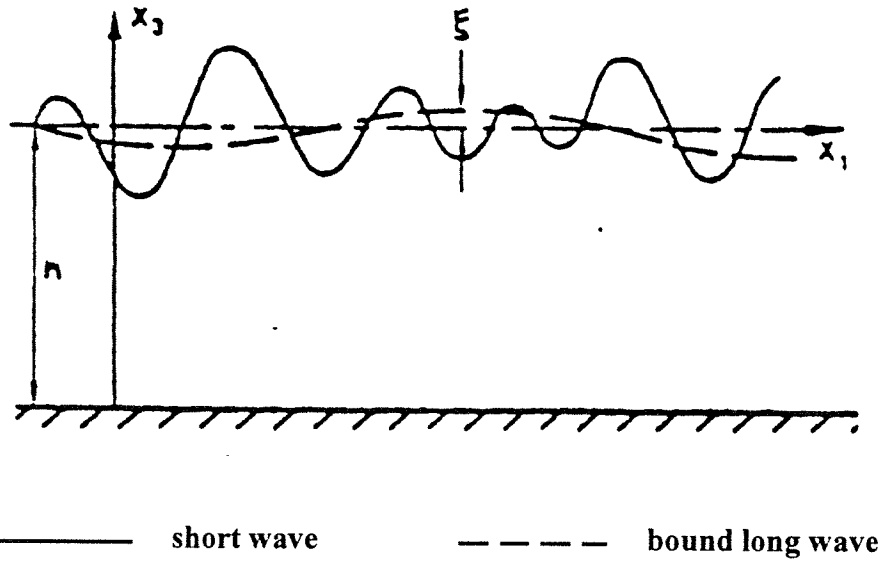

Figure 3.1. Bound long waves accompanying short waves

In an irregular wave field there are four possible forces acting on the ship:

- First order wave forces
- Low-frequency wave forces
- Mean wave drift forces
- Second order slowly varying wave drift forces

By the time that a wave field has reached the harbour entrance it has been influenced by a lot of factors. Important phenomena are refraction and shoaling. When entering more shallow water bound long waves refract earlier than the short long waves to which they are bound. The wave direction of the long waves changes while the wave direction of the short waves will not change until even more shallow water is reached. From that point the long waves are no longer fully bound to the short waves.

Inside the harbour diffraction and reflection are important phenomena. The layout of the harbour determines how and to what extent waves near the entrance penetrate the harbour and reach the quay.

Measures that can be taken to reduce (short period) wave heights are amongst others, breakwaters, quay structures, bank structures and the harbour layout. It is impossible to fully avoid penetration of long waves into the harbour except when the harbour is completely closed. Therefore it is harder to reduce long waves in a harbour than it is for short period waves.

Usually the amplitude of long waves in open sea is small. Because of non-linear effects these waves are being enlarged when they reach the coast. Inside the harbour this effect can be even stronger if the wave period is the same as the natural period of the harbour. This resonance is a linear effect. It can only be avoided by changing the layout of the harbour.

3.2.2. Mooring system

In general, the mooring system has two main requirements: it has to be safe and it must prohibit major movements of the vessel that would have an adverse effect on operational efficiency and availability of the berth for operation.

The complete mooring system consists of mooring lines and fenders. The effective elasticity coefficient of this system (K_{eff}) is equal to the sum of the elastic coefficients of the mooring lines (K_{lines}) and the fenders ($K_{fenders}$).

- $$\overline{K}_{eff} = \overline{K}_{lines} + \overline{K}_{fenders} \tag{3-1}$$

The way these mooring lines and fenders are placed relative to the moored ship is of great importance for the reaction of the ship to the waves. Mooring lines are best placed symmetrically with regard to the centre of gravity of the ship. This way the forces acting on the ship are distributed evenly. Preferably, the mooring lines are placed more or less horizontal to counteract the horizontal motions of the ship. It is recommended that the angle with the horizontal is less than 25 to 30 degrees.

In addition, the position of the fenders is of importance. The location of the fenders relative to the centre of gravity affects the coupling of motions (see Section3.2.3). The configuration of the fenders influences the motions of the moored ship as well. For example, to reduce the roll motion of a ship it can be useful to place the fenders vertically scattered instead of concentrated at one elevation.

Mooring lines can be steel wires, polypropylene ropes or a combination of those two. The spring constant of the load-deflection characteristics of the latter is much smaller than that of the first (Shiraishi, 1998). After repeated use the mooring lines lose their elastic properties.

Figure 3.2 demonstrates a conventional mooring-layout. Bow and stern lines are attached to the respective ends of the vessel and usually make an angle of around 45° with the quay. Larger angles are not recommended. Lines with an angle of 45° provide some degree of both lateral and longitudinal restraint. Breasting lines are nearly normal to the quay and provide only lateral restraint. Spring lines run fore and aft, usually at an angle of 5° to 10° to the quay and provide only longitudinal restraint.

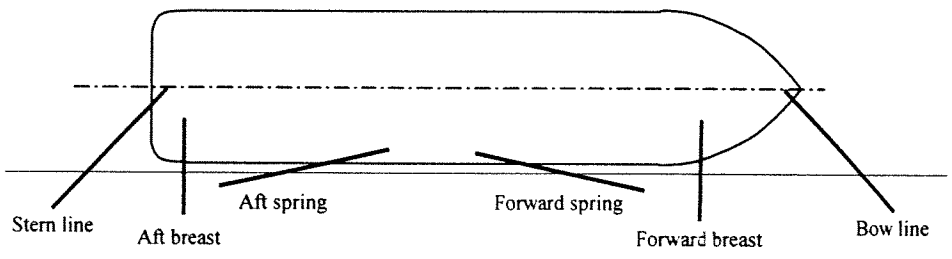

Figure 3.2. Conventional mooring layout

Bruun (1989) divides fenders into two categories:

- protective fenders (energy absorbing protective pad)
- impact fenders (during berthing manoeuvres)

In this report the focus is on protective fenders because the berthing process is beyond the scope of the investigation.

The absorption of energy by one particular fender can be computed from its deformation diagram:

$$E = \int_0^s F(s)ds \qquad (3\text{-}2)$$

in which
E = absorbed energy
F = force
s = compression of fender

Figure 3.3 shows examples of deformation diagrams for three different systems: hydraulic fenders, rubber fenders and buckling fenders.

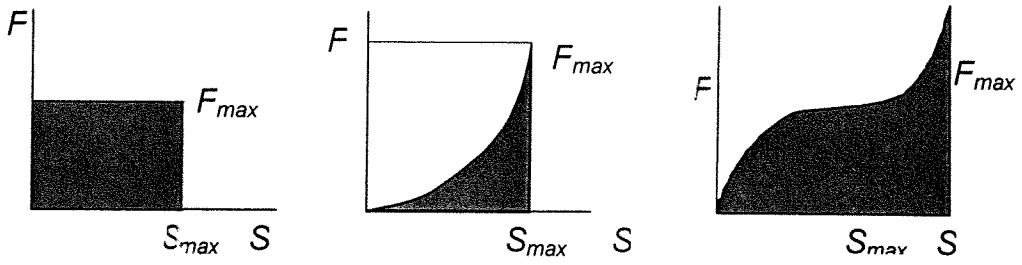

"Hydraulic fenders" "Rubber fenders" "Buckling fenders"

Figure 3.3 Deformation diagram for fenders

3.2.3. Ships

A ship can be categorised by several characteristics. Prime parameters are volume, mass and linear dimensions. The main characteristics are summarised:

- Length over all, L_{oa}
- Length between perpendiculars, L_{bp}
- Breadth, B
- Draught, d
- Freeboard, F
- Displacement, ∇
- Block coefficient, C_B $\qquad C_B = \nabla / [L \times B \times d]$

The length over all is the horizontal distance between two vertical lines; one tangent to the ship's bow and one to the ship's stern. The length between perpendiculars is the horizontal distance between the point of intersection of the ship's bow and the waterline and the vertical line through the axis of the rudder of the ship. The breadth is the maximum distance between the two sides of the ship. The draught is the maximum distance between the water level and the keel of the ship. The displacement of a ship is the volume of the submerged part of that ship. The only form coefficient that is mentioned here is the block coefficient. Appendix 2 gives an overview of all the form coefficients and their mutual relations.

The level of initial stability of a ship depends mainly on the meta centre height (GM). This is the distance between the meta centre (M) of a ship and its centre of gravity (G). The meta centre itself depends on the centre of buoyancy (B). See Figure 3.4. In formula (Schneekluth, 1987):

- $\overline{GM} = \overline{KB} + \overline{BM} - \overline{KG}$ (3-3)

in which
GM = distance between the centre of gravity and the meta centre
KB = distance between the keel and the centre of buoyancy
BM = distance between the centre of buoyancy and the meta centre
KG = distance between the keel and the centre of gravity

The higher the meta centre, relative to the centre of gravity, the better the initial stability of a ship. A change in stability means a change in natural roll frequency of the ship.

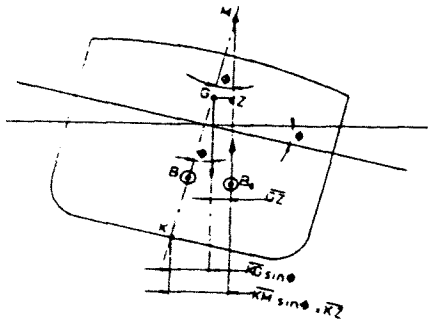

Figure 3.4. Meta-centre height

Any floating body has six degrees of freedom. To completely define the ship motion it is necessary to consider movements in all these modes (see Figure 3.5). The motions are defined as movements of the centre of gravity of the ship and rotations about a set of orthogonal axes through the centre of gravity. The axes move with the mean forward speed (in case of a sailing ship) but are otherwise fixed in space. This is referred to as a body bound coordinate system.

- Surge, x (translation along the x-axis)
- Sway, y (translation along the y-axis)
- Heave, z(translation along the z-axis)
- Roll, ϕ (rotation around the x-axis)
- Pitch, θ (rotation around the y-axis)
- Yaw, ψ (rotation around the z-axis)

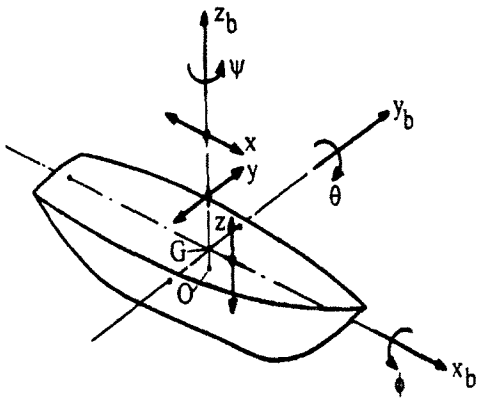

Figure 3.5. Ship motions

Surge, sway and yaw are referred to as the horizontal motions of the ship. Heave is the only true vertical motion. Often roll and pitch are also referred to as vertical motions. However, they include some motion in horizontal direction. Heave, roll and pitch motions of a free floating ship are oscillatory motions. This means that, if a ship is displaced in one of these modes from its equilibrium by some force, it will oscillate until the motion is damped out whenever that force is removed (Muckle, 1987). Vertical motions mainly correspond to the short wave frequency while horizontal motions correspond to both the short wave frequency and to the long wave frequency.

In considering the response of the ship to the sea it is important to determine the natural periods of oscillation in the various modes (Muckle, 1987). The natural period (per motion) is a function of vessel size and mooring outfit. The natural period of roll is in the range of the periods of wind waves. The natural period of surging, yawing and swaying is relatively long. For pitch and heave the mooring system is of negligible importance. Then the natural periods of a free floating ship in still water can be considered.

In general, whenever a ship is moored all the motions are coupled. There is however a difference in the magnitude of this coupling between the six motions. The coupling between heave and pitch is very profound. If a ship is symmetrical about its longitudinal centre plane, the longitudinal motions (pitch and heave) are uncoupled from the lateral motions (sway, yaw and roll) (Rawson and Tupper, 1983).

In case the centre of gravity is not at equal height as the fender, coupling occurs between the roll motion and the sway motion (see Figure 3.6). In that case the sway motion, in addition to the waves, excites the roll motions. Ueda and Shiraishi (1984) confirm this interaction between the swaying and the rolling motions.

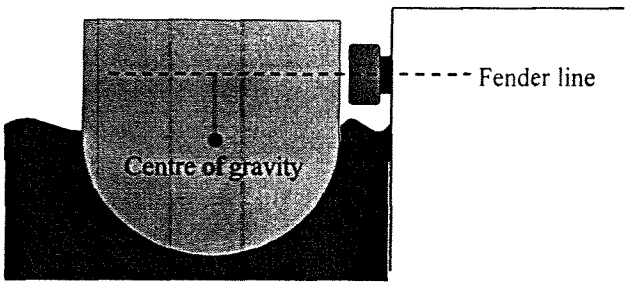

Figure 3.6. Coupling between roll and sway motion

Vis and Keuning, 1979

"A considerable part of the surge and sway motion is subharmonic, because of excitation in these natural periods by wave groups. The subharmonic response of the roll motion is caused by the coupling with sway motion."

3.2.4. Moored ship in waves

The dynamic behaviour of a ship depends on both the characteristics of the ship and the mooring system. This behaviour can be described by Newton's second law:

$$\sum_{j=1}^{6} M_{kj} \cdot \ddot{x}_j = F_k^e \qquad k = 1,2,\ldots..6 \tag{3-4}$$

in which

M_{kj} = representative of the inertia matrix of the ship

$\ddot{x}$ = representative of the acceleration vector of all six degrees of freedom

F_k^e = representative of all external forces and moments acting on the ship

These external forces acting on the ship are divided into:

- F_w = wave forces
- F_h = hydrodynamic forces due to ship motions
- F_r = hydrostatical restoring forces
- F_m = mooring line forces
- F_f = fender forces

Hydrodynamic forces and moments (F_h) are induced by harmonic oscillations of the rigid body moving in the undisturbed surface of the fluid. Wave exciting forces and moments (F_w) are produced by waves coming in on the restrained body. The equation of motions results from the definition of the hydrodynamic and the wave exciting forces. For more detailed information about these forces reference is made to Journée and Massie (2000). Here the equation of motion for heave of a free-floating ship is presented:

$$(m+a)\cdot\ddot{x} + b\cdot\dot{x} + c\cdot x = a\cdot\ddot{\varsigma}^* + b\dot{\varsigma}^* + c\varsigma^* \tag{3-5}$$

in which

m = mass of the body
a = hydrodynamic mass coefficient
b = hydrodynamic damping coefficient
c = restoring spring coefficient
x = displacement
ς^* = reduced water surface elevation

Due to the mooring system the ship's response includes non-linear components. Consequently, the hydrodynamic forces cannot be described by means of a formulation in the frequency domain. A formulation in the time domain is required. For more detailed information reference is made to Van Oortmerssen (1976).

In the time domain, the wave elevation of irregular waves is represented by the sum of a large number of regular waves (in the frequency domain):

$$\varsigma(t) = \sum_{n=1}^{N} \varsigma_{an} \cos(k_n x - \omega_n t + \varepsilon_n) \tag{3-6}$$

in which

ζ_{an} = wave amplitude n^{th} component
ω_n = circular frequency n^{th} component
k_n = wave number n^{th} component
ε_n = random phase angle n^{th} component

The water level amplitude, ζ_{an}, can be expressed in terms of the energy spectral density, $S_\zeta(\omega_n)$:

$$S_\varsigma(\omega_n)\cdot d\omega = \tfrac{1}{2}\varsigma_{an}^2 \tag{3-7}$$

in which dω is an infinitely small frequency interval

The variance of the water surface elevation. $\sigma^2\varsigma$, is equal to the area under the spectrum:

$$\sigma_\varsigma^2 = \int_0^\infty S_\varsigma(\omega)\cdot d\omega \tag{3-8}$$

The significant wave height is defined as:

$$H_{mo} = 4\sqrt{m_0} = 4\sqrt{\sigma_\varsigma^2} \tag{3-9}$$

in which m_0 is the zeroth moment of the spectrum.

Figure 3.7 contains a graphical interpretation of the relation between the wave spectrum and the (irregular) waves. The response spectrum of a ship is included as well. For more detailed information reference is made to Journée and Massie (2000).

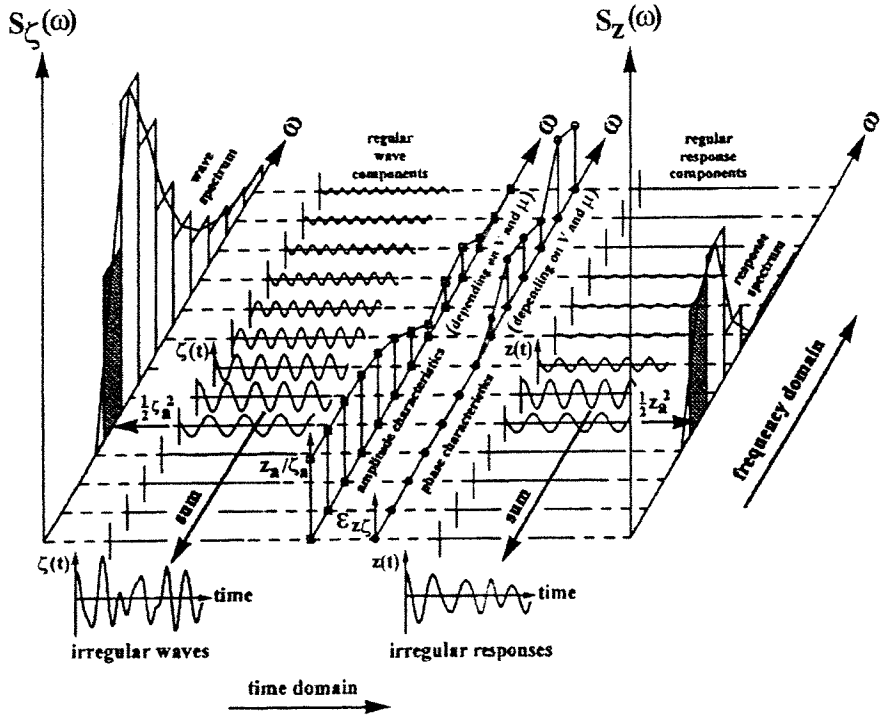

Figure 3.7. Wave spectrum and response spectrum in time and frequency domain

3.3. Findings concerning moored ships

The system of a moored ship is very complex and difficult to describe analytically. In the past scientists have tried to find patterns in the behaviour of moored ships. This section presents a review of their findings. As mentioned earlier these findings are not considered to be generally valid. They are mainly used as basis in the drawing up of hypotheses in Chapter 5.

Knowledge and perspective have changed over the years. Therefore, the four sections are subdivided in two periods of time, before and after 1990. The year 1990 is arbitrary. Furthermore, several citations are presented as an illustration of and support to the text.

3.3.1. Introduction

Information about waves is usually available as energy spectrum (frequency domain) while the non-linear behaviour of ships requires a formulation in the time domain. Three sources of information are available when investigating moored ship motions:

- Physical modelling
- Prototype measurement
- Numerical simulation

Often a combination of these sources is used to enlarge the validity of the investigation. Shiraishi et al. (1999[2]) compared several numerical simulation models used to evaluate ship motions and mooring forces.

Simplifications are often used in the representation of the complex system of a moored ship. Those simplifications should be considered during the analysis of the results.

> Massie, 1973
> *"One must be very careful that significant information about the motion of a non-linear system is not lost or hidden when a problem is linearised."*

3.3.2. Waves

Long period waves play an important role with respect to large moored ships since the natural periods of horizontal motions are typically within the range of 30 seconds to 2 minutes. As the damping at these frequencies is small a significant response of the moored ship can occur even in case of relatively small wave heights. Excessive horizontal motions are caused by resonance between the long period waves and the natural periods of the moored ship. This leads to the conclusion that when a ship is exposed to long period waves significant horizontal motions can be expected.

Before 1990

Van den Bunt (1973) investigated the influence of the wave height, wave period and wave direction on the mooring line and fender forces. The ship (displacement is 320 000 m³) and the mooring layout are not varied in the model study. Both regular and irregular waves were applied. Unexpected high forces occurred in irregular waves. Van den Bunt (1973) concluded that the time varying drift forces were the cause of these high forces. The mooring system was the same during the test with regular and with irregular waves. Therefore the non-linearity of the mooring system could not be the cause of the high forces.

Serious mooring problems occurred at a harbour in San Nicolas Bay leading to breaking of mooring lines and damage to the pier. It was assumed that the horizontal water motion at the pier was the most important factor leading to these mooring difficulties. *Keith* (1973) conducted a study to define the wave action in the harbour. He concluded that the low frequency ship motion was not correlated to the low frequency water motion. He found that the swell excited the ship and that the low frequency ship motion resulted from the mooring system.

Bowers (1977) showed theoretically that natural oscillations of a harbour could be excited by long period waves travelling at the group velocity. When a group period is close to a natural period of the harbour, resonance will occur.

Wave grouping has a significant influence on the impact from waves. Since the phase spectrum influences wave grouping, *Burcharth* (1980) questioned whether or not random phase type of wave generators could be used in model studies without introducing unacceptable errors. For that reason, he compared the probability distribution of the wave groups for both field waves and laboratory waves. He concluded that the random phase generator could be used when dealing with pure storm waves.

For the design of harbours it is of importance that the long waves in nature are correctly represented in a physical model. In this respect research was carried out (*Bowers*, 1980) in order to programme wave generators to produce the appropriate long waves in the model. He concluded that undesirable waves could be minimised by adding an appropriate long period movement of the wave generator.

Sand (1982) also investigated the long wave errors in traditional model test with only first order wave generation. He concluded that a first order control signal could not be considered sufficient when the natural bounded long wave amplitudes are small. The magnitude of the error depends on the ratio of the water depth to the wave height.

Barthel et al. (1983) continued this investigation with the aim of suppressing the spurious long waves in physical models. In first order wave generation the boundary condition at the wave board are not fulfilled for the bounded long waves. This leads to various spurious free long waves. The general equations and the solution for a rotating and translating waves board are presented and verified by means of laboratory experiments.

Barthel et al. (1983) distinguish three types of free long waves in a physical model:

- Local disturbance waves, associated with first order local disturbances
- Displacement waves, due to wave board displacement
- Parasitic long waves, originating from group bounded long waves that are generated naturally

All are spurious long waves that have to be suppressed in physical modelling. When the parasitic long waves are not of the same magnitude as the displacement long waves this suppression was successful, according to Barthel et al. (1983). He found that if these two types of waves were of comparable magnitude, reflection and resonance effects led to inconclusive test results.

1990-present

Barthel and Mansard (1994) carried out a physical model of a 35 000 dwt bulk carrier moored in a lagoon harbour to investigate the penetration of long period waves inside that lagoon. The propagation of irregular waves through an access channel, past a breakwater and into the lagoon was studied. Both the modification of the irregular waves and the effects of various breakwater layouts were evaluated. In order to increase the validity of the results non-linear characteristics and hysteresis of the mooring lines and fenders were taken into account.

Barthel and Mansard (1994) state that shoaling of groups and their associated group-bounded long waves induces breaking of the first order (short) waves. The long waves then detach themselves from the group and continue to travel at free wave velocity. As mentioned in Section 3.2.1 this detaching of long waves also occurs in case the short waves do not break because of a change in wave direction.

During the model tests first order waves were hardly visible inside the lagoon. Long waves of low amplitude were present and induced significant motions of the vessel. It was concluded that the surge motion was most sensitive to these long waves. Additionally, it was found that enlarging the breakwater at the entrance led to smaller surge motions inside the harbour. Accordingly, longer breakwaters lead to less penetration of low frequency waves inside the lagoon. Groynes interrupt the orbital current associated with the long waves. Therefore, a combination of a short breakwater near the entrance and a pair of groynes near the vessel also led to reduction of the surge motion.

Vis and Mol, 1985

"Natural period of dynamic response of the moored vessel is close to the period of the long waves. Damping at these frequencies is small"

Mol et al., 1985

"The effect of bound long waves is basically the same as the effect of free long waves and the combined action of both types of long waves are the main cause of the horizontal motions and line forces of a moored ship."

Ueda and Shiraishi, 1988

"When a ship is exposed to long period waves ship motions become larger than in short period waves."

Shiraishi, 1998

"It was found that the energy of short period wave components was diminished by the wave diffraction at the breakwater. On the other hand, long period wave components exceeding 100 seconds remained just as strong as before. Long period waves inside the harbour generate the large low-frequency ship motions."

"The low-frequency surge motions of ships are generated by long-period waves in the port. The amplitude becomes extremely large when the natural period of surge motion is almost equal to the dominant period of long-period waves."

Kubo and Sakakibara, 1999

"It is well known that large ship motions are caused by the resonance of both the natural period of surge mode and that of the long-period waves that exist inside the harbour."

3.3.3. Ship motions

This section describes several investigations that were performed in order to enlarge understanding of moored ship motions. In Section 3.2.1 a distinction is made between short period (high frequency) waves and long period (low-frequency) waves. The motions of a ship are often referred to as harmonic (wave frequency), subharmonic (frequency lower than wave frequency) and super harmonic (frequency higher than wave frequency) motions.

Subharmonic ship motions can have the following origins:

- non-linear and asymmetric elastic character of mooring lines and fenders
- second order slowly varying wave drift force
- long periodic waves, like seiches and surf beats, may cause subharmonic motions, particularly if the harbour configuration tends to amplify these phenomena

Before 1990

Wilson (1973) examined, on a theoretical basis, the circumstances in which a moored ship resonates longitudinally with a periodic "surge". Note that here "surge" is used to describe long wave action. Wilson only includes standing long waves inside the harbour basin (seiches). The response of the ship is shown to be dependent primary on the degree of initial tightness of the mooring system. The magnitude of the seiches and the location of the ship within it are also important. Only seiches with periods of 2 minutes and less are capable of causing serious resonant motion. The mass of the ship is said to be of minor importance in longitudinal motion. Both large and small ships react in much the same way, provided that they are similarly moored.

In view of the abovementioned Wilson (1973) concluded that tight mooring of ships is an effective antidote to longitudinal wave action, provided that the harbour is impervious to high frequency waves. It should be noted that tight mooring of ships leads to large forces in the mooring lines. Therefore this solution to unwanted ship motions could lead to problems in a different field.

To further elucidate the motions of ships moored in the presence of waves *Russell* (1959) carried out some highly idealized experiments. A body, having the same cross sectional shape as a 32 000 dwt tanker was allowed to oscillate under the influence of waves. A stiff spring and in the opposite direction a soft spring represented the fenders and mooring lines respectively.

The experiments showed that the moored ship moved more than a free-floating ship in almost all experiments. It was found that the movements of the ship could be kept to a minimum either by use of very stiff mooring lines or by a combination of soft fenders and soft mooring ropes. Very tight mooring systems can lead to large mooring forces. This should be taken into account. The tension in the mooring lines and the forces on the fenders were least when the load-deflection characteristics of the fenders were very low.

Russell (1959) concludes that the wave height might be of less importance than the type of mooring system considering moored ship motions. It is noted that the influence of the wave period is not contemplated in this investigation. Lastly, the value of these highly idealized experiments is questionable.

The motion of a ship moored against stiff fenders and subjected to wave action consists of a series of bounces. In mono-frequency waves this (subharmonic) motion can be remarkably regular. Consequently, resonance can occur which leads to movements considerably larger than if the ship were free floating. For that reason *Lean* (1971) analysed the simple case of sideways movement in mono-frequency waves Coupling between roll and the horizontal motions is not taken into account.

To illustrate the presence of subharmonic motions a model of a bulk carrier with a displacement of 40 000 m^3 was moored with soft mooring lines against a plate with sixteen stiff fenders. The model was moored beam on to the incident waves and the movements of the ship were examined over a range of high and low frequencies. Note that the analysis is valid only for mono-frequency waves and is not simply applicable for real sea situations.

Lean (1971) concluded that reduction in movement is possible by application of a steady force toward the quay by means of inextensible lines. That way, however, high mooring line forces occur and subharmonic oscillations can still be present Furthermore, the ship motions are still greater than in case of a free floating ship or a ship moored with soft mooring lines and soft fenders.

1990-present

A significant problem in harbours is the excessive motion of moored ships caused by long wave action. *Raichlen et al.* (undated) noted that the low frequency oscillations leading to problems are between 40 seconds and 200 seconds. The origin of such long period waves is investigated is the scope of two mooring basins in the Port of Long Beach near Los Angeles. Physical model studies are conducted in order to define ways of reducing the long waves at these two sites. The outcomes of this investigation by Raichlen are specifically for the two investigated basins.

Subsequently, *Headland and Poon* (1998) present a numerical model for ship motion analyses. This model is applied for the long wave problem in the Port of Long Beach. The approach is a combination of physical and numerical models. Physical model results are used to define boundary conditions for and calibration of the numerical model. The numerical model calculates harbor basin response, the ships hydrodynamic coefficients (added mass and damping coefficients) and the first and second order wave forces in the time domain. Furthermore, the ship motions are computed in the time domain.

In view of expansion plans of the Ports of Los Angeles and Long Beach (California) a monitoring system was operated in these ports (*Mc Gehee*, 1991). The main goal was to monitor the response of ships to long period waves. Also the mooring lines and fender reactions were investigated. Five ships (9 500 dwt to 70 000 dwt) were monitored. Furthermore, the harbour resonance was measured for comparison to a three-dimensional physical model. All the measured data was used to calibrate and verify the numerical model of moored ship response of Headland and Poon (1998).

Mc Gehee (1991) concluded that slacking mooring lines increases and tightening mooring lines reduces ship motions and that mooring systems consisting of tighter lines react more strongly to higher frequency motions. The tight mooring lines prevent, as it were, the low frequency ship motions. The maximum measured ship motions are typically due to surge, sway and roll. Heave shows the lowest amplitudes.

Shiraishi (1998) investigated the low-frequency ship motions due to long period waves in harbours. His investigation was threefold:

- analyses of field observations of low frequency ship motions and waves obtained inside and outside the ports
- simulation of ship motions by means of a numerical model
- evaluation of the mooring system's ability to reduce low frequency ship motions by means of numerical simulation and field observation

The field observations were conducted in three ports in Japan: Tomakomai Port, Noshiro Port and Sendai Port. The investigation of the Noshiro Port is described in Section 3.3.3, see *Shiraishi et al* (undated). The numerical model was based on a second order differential equation of motion with six degrees of freedom. The model included the non-linearity of the mooring system.

The numerical model was used to reproduce ship motions and fender deformations in the port on the Honshu Island of Japan (*Shiraishi et al*, 1999). Here fender damages were observed and the conditions (mooring system, waves, winds) during these damages are known. The influence of the wave direction is investigated for a 40 000 dwt ore carrier moored in the ocean facing port.

The direction of the incoming waves influences the ship motions considerably. When a ship is exposed to waves of which the direction comes close to perpendicular to the quay line (the wave angle exceeds 60°), swaying and rolling become distinct. For surging, the amplitude becomes large when the wave angle is less than 30° (head waves). See Figure 3.8.

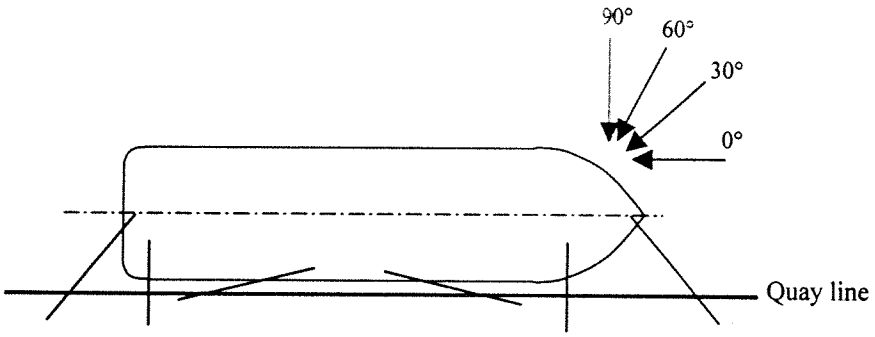

Figure 3.8. Direction of incident waves

At ocean facing ports it can be expected that the influence of long period waves is large leading to considerable low frequency ship motions. Accordingly, Shiraishi (1999) found that surging increased significantly when taking into account the long period components. Fender deflections became large when the wave period was long because surging and swaying are large at those conditions. The difference in fender deflection due to waves of various wave periods is however smaller than due to changes in wave direction.

3.3.4. Mooring system

Stiffness of the mooring outfit influences ship motions and mooring line forces significantly. Ship motions generally decrease with a stiffer mooring system (steel wires) and mooring forces diminish with a softer mooring line system (polypropylene ropes).

Before 1990

Wilson (1973) discussed the general equations of motion in six degrees of freedom of a moored ship. He included the coupling between motions and the non-linear restraints of the mooring lines and fenders. Subsequently, he solved the equation numerically for the surge motion of a 200 000 dwt tanker moored in head sea including the non-linear restraint and damping. Damping in surge motion is small. He found that long period waves with low wave heights together with moderate wind waves or swells could lead to significant surge amplitudes. He investigated different mooring layouts to restrain the surge motions and concluded the following:

> *"Control of the motion by brute force would thus be an unrewarding and uneconomic solution to the problem except insofar as it may help the ship to ride out the contingency of a dangerous combination of short and long-period waves."*

It is noted that low frequency waves can penetrate a harbour during long periods of time and that "riding out" is, thus, not the solution to low frequency wave related problems. Furthermore, it is noted that the solution as presented by Wilson (1973) includes some simplifications. For instance, the ship is represented by a rectangular block. Physical modelling and prototype measurements can verify the theory for various types of ships.

Ueda et al. (1984) developed a numerical simulation program which analyses ship motions and mooring forces in time domain. The program includes irregularities of wave forces and non-linear characteristics of the mooring system. The results of the numerical simulations were compared to results of a hydraulic model test with a 10 000 dwt cargo ship. Both the effects of wave and wind action and the effects of mooring system on ship motions were investigated.

As a result of onshore wind the neutral position of the sway motion moves closer to the fender so that the deformation of the fender increases. With increasing wind speed Ueda et al. (1984) found that the period of the swaying motion gradually decreased to the value of the wave period and the amplitude became small. It is noted that the effect of the wind force is the same as pretensioned mooring lines. When the onshore wind speed is relatively low the wind force to compress the fenders is small. In that case the fender characteristics have a great influence on ship motions. In that case Ueda et al. (1984) found a large subharmonic sway motion caused by the asymmetry of the load-deflection characteristic of the mooring system

O'Brien (1985) investigated the slow drift oscillations of a 55 000 dwt bulk carrier moored in head sea at a six-buoy spread mooring system at Cape Cuvier in Australia. This was conducted by means of a numerical model. Field measurements served to calibrate the model. The influence of the mooring system to the response of the vessel was investigated for both regular and irregular long waves.

Since there was no quay present and the ship was moored in head waves no large lateral motions were expected. Nonetheless, significant lateral motions were observed during the field measurements. This demonstrates the importance of coupling between longitudinal and lateral motions. It was concluded that minimisation of these lateral motions depended mainly on the tensioning of the mooring lines. The type, sizing and number of mooring lines appeared to be of less importance.

1990-present
Breaking accidents of mooring lines occurred at a 60 000 dwt bulk carrier berth. *Shiraishi et al.* (undated) estimated that this was due to long wave action in the harbour. Resonance of the natural period of surge and the long period waves led to significant long period ship motions. The natural period of a ship depends, partly, on the mooring system. By means of a numerical simulation, Shiraishi et al. (undated) investigated the countermeasure by mooring system under long period waves.

The countermeasure consisted of modifications of mooring lines and fenders and of creation of additional mooring dolphins. The 100 mm diameter nylon mooring lines were replaced by polypropylene ropes with a nylon tail mooring lines. The latter are more elastic. Pneumatic fenders replaced the existing buckling fenders. The number of mooring lines and the pretension were not altered.

Due to these changes the natural period of surge changed from 140 s to 80 s. Furthermore, the modifications restrained the subharmonic sway motions induced by the asymmetric mooring system. It is noted that Shiraishi et al. (undated) tried to prevent the undesirable results of the long period waves instead of reducing the long wave action inside the harbour.

3.3.5. Operation efficiency

In the previous sections mention has been made of the fact that long waves, and thus the period of waves, play an important role in the response of the ship. This section describes several investigations that point out the importance of this to the operation efficiency of a harbour. Harbour tranquillity has always been evaluated in terms of the wave height inside the harbour. It is suggested that berth efficiency can be evaluated more realistically by the moored ship motions rather than the wave height. Therefore, the proper berth design of ports, especially ports that are built in open sea areas, must be examined from viewpoint of moored ship motions instead of wave height.

> DiCastro et al., undated
>
> *'Since the periods of resonance of the harbour and the horizontal modes of motion (surge, sway, yaw) of the moored ship are in the range of long waves (more than about 20 seconds), and since the long waves are better transmitted into the harbour, it is very important to consider the contribution of long waves to the motion of ships in the harbour. Most of the energy in the long wave range is a result of non-linear wave-wave interaction that takes place in the shoaling zone.'*

> Shiraishi et al., undated
>
> *"Moored ship oscillations become larger when the influence of long- period waves is strong, even if the wave height inside the harbour is small. Therefore, the proper berth design of ports that are build in open sea areas must be examined from the viewpoint of moored ship oscillations."*

Cargo handling is occasionally interrupted or suspended if movements of the ship exceed the allowable ship motions. According to *Ueda and Shiraishi* (1988), the operation efficiency of a port, then, should be defined based on the allowable ship motions for cargo handling. They suggested that, when a ship is exposed to long period waves, the operation efficiency calculated based on the allowable ship motions might be smaller than that based solely on the wave height in front of the berth.

The investigation was carried out at the Sendai Port, the Onahama Port and the Kashima Port in Japan. Here it had been considered that cargo handling was influenced by ship motions due to the action of long period waves. The allowable ship motions were estimated in terms of type and size of ship and of cargo handling equipment by means of numerical simulations. Subsequently inquiries were sent to almost all cargo-handling operators in Japan. So, the provisional figures resulting from the numerical simulation were evaluated and revised.

Ueda and Shiraishi (1988) concluded that the most important motions causing suspension of cargo handling are surge and heave. It is noted that significant surge motion could be expected since long period waves were present in the investigated ports. Long wave action causes significant heave motion in case the length of the ship is small compared to the wavelength. A large variety of ships has been investigated. Table 3.1 shows the allowable ship motions as proposed by Ueda and Shiraishi (1988).

Table 3.1. Allowable ship motions according to Ueda and Shiraishi (1988)

	Component of ship motions:					
Type of ship	Surge (m)	Sway (m)	Heave (m)	Roll (°)	Pitch (°)	Yaw (°)
Gen. Cargo	0	0.75 *	0.5	2.5	1.0	1.5
Grain Carriers	0	0.5 *	0.5	1.0	1.0	1.0
Ore Carriers	1.0	0 *	0.5	3.0	1.0	1.0
Oil Carriers	1.0	0.75 *	0.5	3.0	1.5	1.5

*) Amplitude of swaying in one direction, away from the berth, other significant peak to peak values.

In 1992 the motions of the ships at berth in Sendai New Harbour led to failure of the loading operations. Since the wave heights were less than the allowable wave heights for these loading operations *Nagai et al.* (1994) analysed the wave data in order to find a cause for the large ship motions. He found that the motions were caused by bound long waves. Accordingly the harbour tranquillity should be evaluated in terms of more than just the wave height at a berth. The wave period and other factors such as wind conditions and the scale of the vessel should also be taken into account.

3.4. Empirical relations regarding ship motions

Several investigations concerning the motions of moored ships in waves led to relations, for instance relations between the ship motions and the waves. This section presents some relevant findings of four different sources.

Van Oorschot (1976)

Van Oorschot (1976) investigated the subharmonic components in hawser and fender forces. He found that the slowly varying wave drift force was the dominant parameter with respect to the behaviour of a large moored ship. The harmonic wave forces and the harmonic ship motions of a free-floating ship generally related fairly well linearly to the wave amplitude. However, in case of a (tightly) moored ship in a non-linear mooring system, the linear approach could no longer be justified.

He concluded that the subharmonic components formed a substantial part of the total horizontal ship motions or mooring forces. This appeared particularly true in more exposed locations. In irregular waves the subharmonic components increased in proportion to H_S^2. They also continuously increased with increasing peak period of the energy spectrum (T_P), for both sway and surge. In formula:

$$X_{horizontal} \propto H_S^2 \tag{3-10}$$

Van Oorschot (1976) concluded that altering the mooring system could, to some extent, reduce subharmonic motions. However, the effect of a variation of the mooring characteristics seemed to be fairly unpredictable.

Mol et al. (1985)

While studying the motions of moored vessels Mol et al. (1985) developed semi-empirical relations to calculate surge motions and line forces. The relations are based upon Newton's second law of motions. Linearity and frequency dependency form significant problems in this respect.

"Some force components can be coupled directly to specific motions, other force components can be neglected. Schematising the moored vessel as a linear damped mass spring system with one degree of freedom, heuristic formulas are found on the basis that the dynamic force or motion is the static value multiplied by a coefficient that represents the dynamic influence."

The result for the surge motion in formula:

$$X_s = C_x \cdot H_{sl} \sqrt{\frac{g \cdot M}{d \cdot k_l}} \tag{3-11}$$

in which:
X_S = significant surge displacement
C_x = coefficient
M = mass of vessel
d = water depth
H_{sl} = long period significant wave height
k_l = stiffness of mooring system parallel to quay-line

In other words the relation between low frequency horizontal motions and waves is as follows:

- $X_{horizontal} \propto H_{S,long}$ (3-12)

It was assumed that the following relationship holds for bound long waves in shallow water:

- $H_{S,long} = \frac{0.08}{d^2} \cdot T_P^2 \cdot H_S^2$ (3-13)

The dimension of the coefficient of 0.08 in this relation is equal to that of the gravitational coefficient in SI-units (m/s²). So the relation changes into:

- $H_{S,long} = 8 \cdot 10^{-3} \cdot \frac{g \cdot T_P^2 \cdot H_S^2}{d^2}$ (3-14)

Herewith, the relation between low frequency motions and waves becomes:

- $X_{horizontal} \propto H_S^2 \cdot T_P^2$ (3-15)

Deelen (1984)

The previously mentioned study of Mol et al. (1985) is partly based on the ship motion study for the port of Sines carried out by Deelen (1984). By means of a hydraulic model study he investigated the response of three different vessels moored with various mooring layouts under various wave conditions. The following ships were used:

- 15 000 dwt general cargo ship
- 35 000 dwt container vessel
- 70 000 dwt coal ship

The study resulted in the following conclusions:

For the steel wire configuration the relation between the wave height and ship motions or maximum mooring forces is predominantly linear:

- $X_{ship} \propto H_S$ (3-16)

- $F_{max} \propto H_S$ (3-17)

The behaviour of the configuration with all propylene ropes is more subharmonic with rather large ship motions and reduced mooring line forces.

The horizontal motions of a ship moored with steel wires have a mixed harmonic and subharmonic character. For a constant wave height the surge, sway and roll motions strongly depend on the peak period of the spectrum. The effect of the peak period on the heave, pitch and yaw motion is small.

The relation between the low frequency significant wave height and subharmonic horizontal motions is nearly linear. This is also true for the relation between the low frequency significant wave height and maximum mooring line forces. In formula:

- $X_{horizontal} \propto H_{S,long}$ (3-18)
- $F_{max} \propto H_{S,long}$ (3-19)

According to the model results the maximum mooring line forces increase with the square root of the mooring line stiffness.

- $F_{max} \propto \sqrt{k}$ (3-20)

Deelen (1984) found that pretensioned mooring lines suppressed especially the subharmonic surge motion, reducing in this way also the maximum mooring line force Furthermore he recommended that all mooring lines be approximately equally loaded.

Vis and Keuning (1979)

Vis and Keuning (1979) executed a technical design study on ship motions, as part of the hydraulic studies concerning the Yanbu industrial complex port. To determine the ship motions and the mooring line and fender forces a model study of a 20 000 dwt tanker and a 150 000 dwt tanker was conducted. The study included both beam and oblique waves. The mooring layout was not altered during the different tests but the stiffness of the mooring lines varied. The following is concluded concerning wave heights, mooring line forces, peak periods and ship motions:

It was found that the stiffness of the mooring system determined the mooring line and fender forces. A mooring system with all steel wires led to unacceptable high mooring line forces. Reduction of the stiffness (load-elongation characteristics) reduced the mooring line forces considerably. Compared to the situation of beam waves the mooring line forces are reduced for quartering waves.

The mooring line forces vary quite linear with the significant wave height for beam waves in case of a 20 000 dwt tanker. However, this does not hold for a 150 000 dwt tanker. The linear relation can be explained by the high stiffness of the steel wires. For the 150 000 dwt tanker this stiffness is relatively lower, hence, the relation is not linear.

For oblique waves there is a tendency of less than linear increase of the forces with the significant wave height. This non-linear relation is also found in the ship motions. For linear springs, the mooring line forces increase with the square root of the spring stiffness.

The mooring line and fender forces and the displacements of the ship increase with an increase in the peak period of the wave spectrum. However, there is certainly no linear relation between force and period due to the resonance in the ship motions. The true shape of this function is difficult to predict. This is found for both beam and oblique waves.

The influence of pretension of the steel wires was also investigated. Two situations were tested: a pretension of 1 kN and of 75 kN in each line. No significant influence on the mooring line forces or the ship motions was noted.

In tests with oblique waves Vis and Keuning (1979) found that a phase relation between the roll and the sway motions led to higher forces in the stern and aft breast line. When both rotations were in phase, this resulted in a cumulative effect on the translations in the aft ship and counteracting effect in the fore ship for positive yaw and roll angles.

4. Coega model study

Description of the model tests regarding the Coega harbour

This chapter presents the physical model study of the Coega harbour. The long wave investigation (see Section 4.1) gave rise to the execution of this model study. The study itself is described in Section 4.2. This mainly contains the set up of the tests, the calibrations and the resulting output.

Finally, Section 4.3 treats a report that discusses and interprets the results obtained from the measurements of vessel motions in the physical model.

It is emphasised that this chapter provides an overview of the investigations that were conducted by the CSIR in Stellenbosch (South Africa). The execution of the tests is not part of this MSc-project. This chapter is solely a report of how the tests were conducted. The purpose of this chapter is to gain knowledge of the value of the results.

4.1. Long wave investigation

It was identified in a feasibility study that long waves could occur in the Coega. If such long waves would indeed occur this might adversely affect the safe mooring of ships in the port, especially when long wave height amplification due to harbour resonance occurs. Therefore, it appeared justified to investigate the occurrence and magnitude of long waves in Algoa Bay. In this section the approach of the investigation and important conclusions and recommendations are summarized. For a more detailed description of the study reference is made to the report: "Coega Harbour: Long wave conditions in the harbour" (Moes, 1997).

First, the possibility of occurrence and the height of long waves at the entrance of the Coega harbour are estimated by means of theory. Several theories are compared with long waves measured along the Cape west coast. The theoretical values developed by Barthel (1983) are accepted as conservative estimates of long wave heights.

Subsequently, the possible amplification of long waves inside the harbour is determined. With the help of numerical modelling it is established which specific wave periods lead to resonance. Resonance results in amplified vertical water motion at anti-node areas and amplified horizontal water motion at node areas. This can form a problem for the moored ships. By adjusting the layout of the harbour basin the amplification factors can be reduced or the nodes of the long wave resonant pattern can be shifted to areas that do not affect the moored ships.

Resonance in the Coega port layout was investigated by means of a numerical model. Three different harbour layouts were tested. The third layout, with two basins created to the south of the jetty, resembles the layout in the physical model of the Coega harbour the most (see Figure 4.1).

The mooring conditions for small craft in the corner just north of the jetty appear to be a problem. This is the location of the ore-(off)loading berth. It was suggested that this potential problem should be carefully investigated, both numerically and in the 3-D physical model.

Another recommendation made by this investigation concerns the layout of the basins. The layouts of the basins appear to bring about adverse long wave conditions for the mooring of vessels and should probably not be rectangular. After investigating alternative layouts of these basins, the resonance conditions should again be carefully checked.

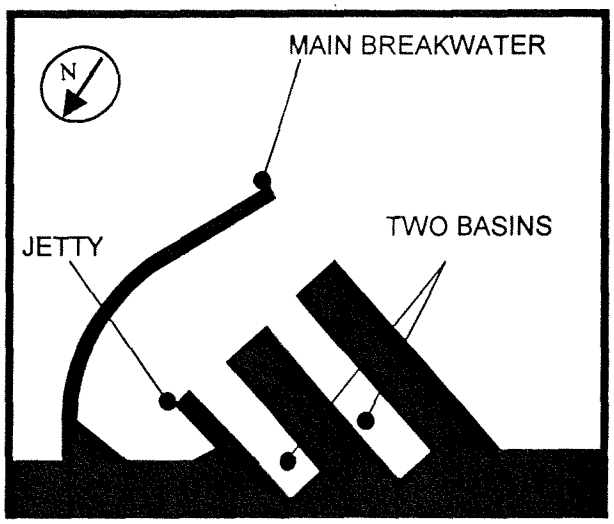

Figure 4.1. Coega harbour layout as tested for long wave amplification in numerical model

The final conclusion of the investigation is as follows: "All the above is based on theory. It will be essential to determine the actual presence of long waves in the Coega area by appropriate wave measurement and subsequent long wave analysis. Once this has been completed the actual effect of long waves on the ships moored in the harbour can be determined through physical and/or numerical modelling."

4.2. Model and analysis conditions

This section provides a description of the measurement system and methodology used in the physical model study. Also the accuracies that can be obtained for the tests are reviewed. Reference is made to the progress reports: "Coega Harbour: Model tests of moored ship motions at the ore quay, progress report no. 1 and no. 2" (Moes and Van Aswegen, 1999[1, 2]).

The study concerns the measurements of ship motions in six degrees of freedom. The ship motions as well as the associated mooring line forces are determined from measurements in a 1:100 scale physical undistorted fixed-bed model of the Coega harbour. Except for wave-generated currents no other currents were specifically simulated during the tests.

4.2.1. Model layout

The layout of the future Coega harbour as indicated in Figure 4.2 has been reproduced in the model. Appendix 1.b shows the bathymetry chart of the area surrounding the future Coega harbour. Figure 4.3 shows a schematic overview of the model test basin with an intermediate phase of the port (only one basin). The wave generators are positioned for the simulation of easterly wave conditions. Waves are generated within a sector of about +15° to −15° relative to the perpendicular direction at the wave generators. The original position of the wave generators is 112.5° relative to True North (waves travelling into 292.5°). The mooring conditions are tested initially for wave directions of 110° and 128°. Later, when testing wave directions of 140° and 160°, relocation of the wave generators is necessary.

The ore-(off)loading quay is located in the NW'ly sector of the harbour basin. The solid vertical quay wall has an orientation of 325°. A rubble mound groyne protects the head of the quay. The ship is moored on starboard, with the bow directed out. The harbour basin depth at the quay is −16.0 m Chart Datum (CD). The moored ship conditions are tested at a constant mean tide level of +1.00 m CD. The average ship's draught is 12.5 m. Consequently the average underkeel clearance of the ship is 4.5 m. The relative underkeel clearance is expressed as the ratio of the mean water depth over the average ship's draught, which is in this case 1.36.

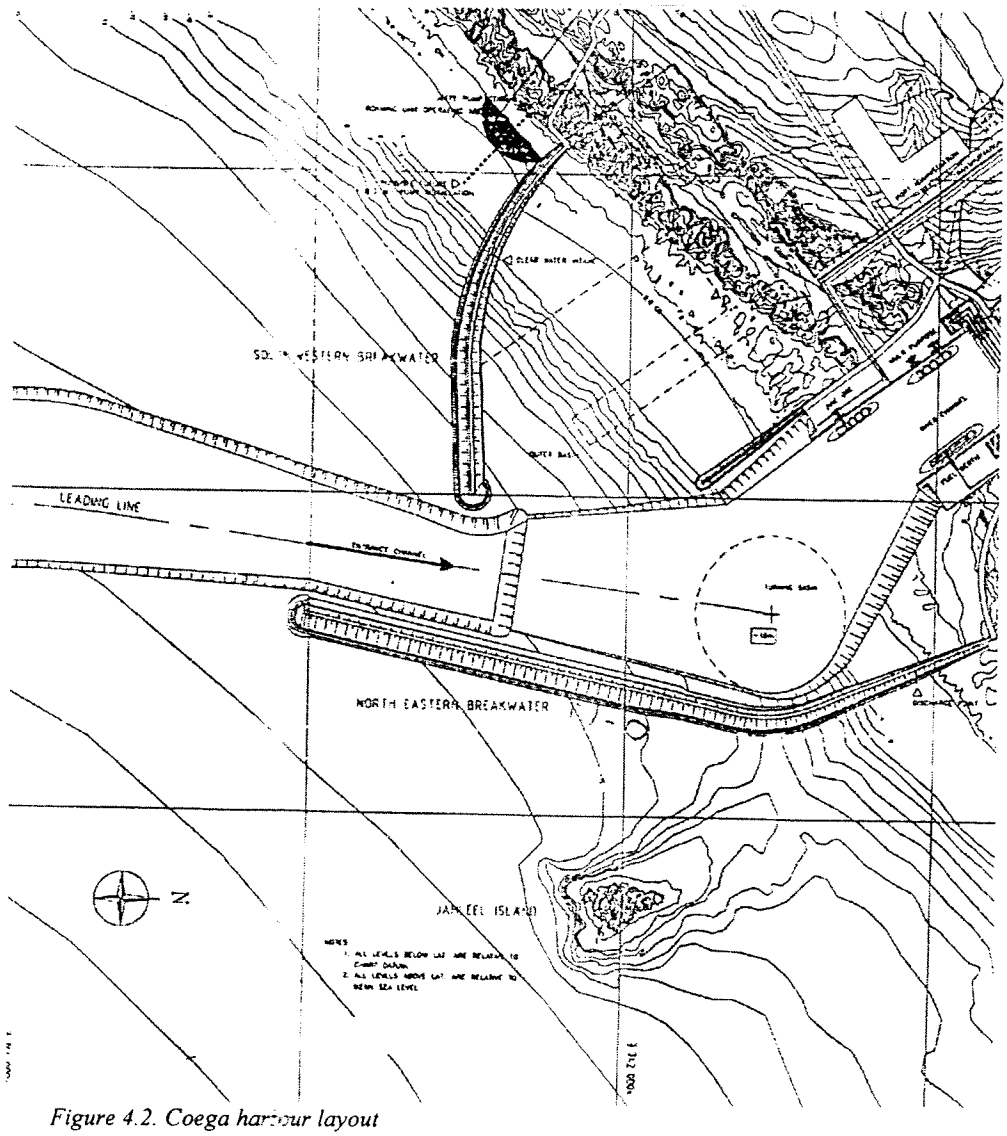

Figure 4.2. Coega harbour layout

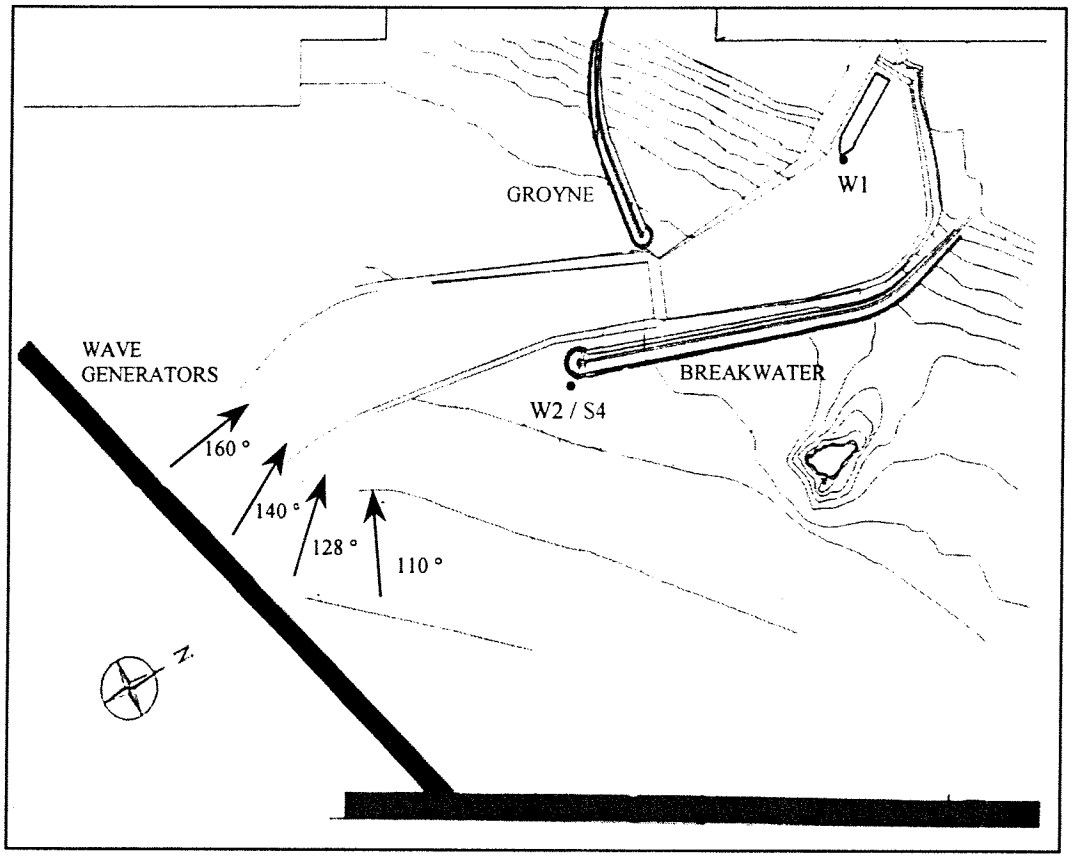

Figure 4.3. Model layout of the Coega harbour

4.2.2. The model ship

Set up of the model

The ship used for the mooring studies is a 1:100 scale model of a 65 000 dwt Panamax bulk carrier. The prototype ship has a length between perpendiculars of 243.4 m, a beam width of 32.2 m and a fully laden design draught of 12.5 m. The model ship represents a coal bulk carrier in its fully laden condition. It is loaded with lead weight blocks to obtain an average draught of 12.5 m, with a 1.0 m trim at the stern. This leads to a draught of 13.0 m at the stern and 12.0 m at the bow.

The model ship contains a conventional single propeller stern section and a bulbous bow. The stern section is designed without the propeller. The model ship does not have bilge keels. Ships of this size are often equipped with bilge keels for roll stabilization. Roll motions of the model ship could, therefore, be larger than of a ship with bilge keels.

The principal dimensions and loading conditions of the prototype ship are listed in Appendix 3. For a 1:100 undistorted geometric model scale, the time scale is 1:10 and the volume, mass and force scale is 1:1 000 000. For more information about scale factors reference is made to Appendix 4.

Calibration and results

The draught, the position of the centre of gravity and the longitudinal and transverse moments of inertia of the laden ship together determine the loading condition. The following guidelines are used:

- The vertical position of the centre of gravity above the keel (KG) of the laden ship is taken as 0.75 times the draught (D) at full loading.
- The longitudinal position of the centre of gravity (LCG) for even-keel loading will be equal to the longitudinal position of the centre of buoyancy of the ship and will be 0.55 times the length between perpendiculars.
- The transverse radius of gyration (k_{xx}) can be taken 0.35 times the beam (B), although this value may actually vary between about 0.28·B and 0.4·B. The model value will be determined experimentally from the natural roll period.
- The longitudinal radius of gyration (k_{yy}) of the laden ship is accepted as 0.28 times the length between perpendiculars.

The appropriate loading and inertia conditions for the model are obtained by following a standard calibration procedure. This procedure includes the positioning and distribution of lead blocks inside the ship's hull to ensure that the model draught, trim, centre of gravity and longitudinal and transverse moments of inertia are as close as possible to the required values.

The finally obtained model ship loading and inertia characteristics are shown in Table 4.1 and Appendix 4 where they are compared with the target values. The model values are expressed in prototype quantities.

Table 4.1. Comparison of model and prototype characteristics

Description	Target value (prototype value)	Value obtained (prototype value)	Difference
KG	9.4 m	9.76 m	+ 3.8 %
LCG	134 m	118.9 m (trim)	--
GM_T	3.8 m	2.87 m	- 24 %
T_θ (roll)	11.6 s	11.92 s	+ 2.8 %
T_ϕ (pitch)	9.7 s	--	--
k_{xx}	11.3 m	9.954 m	(- 14 %)
k_{yy}	68.2 m	65.383 m	- 4.1 %

The target values for a coal carrier are used here, under the assumption that the mass densities of coal and zinc ore are of the same order. Within the uncertainty about and the variability of these values, the model ship can be accepted as representing a typical 65 000 dwt bulk carrier.

4.2.3. Wave field

Set up of the model

Irregular waves are generated in the model in three consecutive cycles of 4 min by a bank of wave generators. The wave spectra have a JONSWAP spectral shape, with a spectral peak enhancement factor $\gamma = 3.3$. The phases of the wave frequency components are chosen randomly for the composition of the time series of the waves.

For each of the four wave directions (110°, 128°, 140°, 160°) the following wave conditions (in prototype quantities) are simulated:

- Wave height (H_{mo}) = 2 m, with peak period (T_P) = 10, 12, 14, 16 and 18 s
- Wave height (H_{mo}) = 4 m, with peak period (T_P) = 10, 12, 14, 16 and 18 s
- Wave height (H_{mo}) = 6 m, with peak period (T_P) = 10, 12, 14, 16 and 18 s

Wave heights next to the ship are measured with a conventional array of eight wave probes cantilevered from a measuring bridge. The centre of the probe array in the harbour basin (W1) is positioned just at the port side off the bow of the moored ship. Wave heights are also measured from a measuring bridge at a position near the tip of the main breakwater (W2). The twelve-probe array in this case is positioned near the position where in prototype the S4 wave measuring instrument is deployed. See Figure 4.3 for an overview of the model basin. The wave conditions are measured both at W2 and W1.

Calibration and results

The measured significant wave heights at the W2 position and inside the harbour (at W1) are listed in Tables a, b, c and d of Appendix 5. It can be seen from these tables that the actual wave height at W2 agree within 6% of the target wave heights. The wave heights in the basin (W1) are about 10% of the wave heights at W2.

Moes and Van Aswegen (1999) note that long period waves, with a period of around 200 s (prototype), are manifest in the mooring basin. Long wave analysis of prototype measurements at the S4 position also indicates the presence of long period wave energy around 200 s. The long wave heights are of the order of 15% of the significant swell wave height. This ratio agrees with the results of long wave measurements at the Cape West Coast, as well as with theoretical computations of bound long waves. Therefore, Moes and Van Aswegen (1999) conclude that the long waves in the Coega model can be accepted as realistic.

It is noted that the long waves, with a period of around 200 s, measured at S4 consist without the influence of the (planned) harbour. The long waves measured in the mooring basin can result from the layout of the harbour. Consequently, it can not be concluded that the long waves in the Coega model are realistic on the basis of the abovementioned argument.

4.2.4. Mooring system

Set up of the model

The ship is moored on starboard at the outer berth as can be seen in Figure 4.4. This figure shows the general mooring layout used in the model tests. The centre of gravity is chosen as origin for the motions of the ship. The position of the moored ship is with its bow 40 m from the SE'ly edge of the quay section. This allows bowlines at an angle of about 30° relative to the ship's longitudinal axis. The mooring line layout, with the line positions and dimensions, is shown in Appendix 6.

The fender characteristics are chosen to represent "Vredestein Gigant" fenders of dimensions d_o = 1.925 m (external diameter), d_i = 1.100 m (internal diameter) and l = 3.300 m (length). The elastic properties of this fender type are reproduced in the model by two sections of linear stiffness:

- 2.3 MN/m (prototype value) for deflection of up to 1.1 m (prototype value)
- 30 MN/m (prototype value) for deflections larger than 1.1 m (prototype value)

Polypropylene lines are chosen for the mooring lines. These lines are accepted to have a breaking strength per single line of 1 000 kN (prototype). Similarly to the fenders, the elastic characteristics of the lines are represented by two sections of linear stiffness:

- 7.5% elongation at 40% of breaking strength (stiffness 1)
- 14.6% elongation at 100% of breaking strength (stiffness 2)

It is accepted that the lines are tight but have no pretension when the ship rests against fenders. The mooring layout of the prototype ship consists of 14 lines; three bow lines, three stern lines, two breast lines fore, two spring lines fore, two breast lines aft and two spring lines aft. These lines are reproduced in the model by six mooring lines; one bow line, one stern line, one breast line fore, one spring line fore, one breast line aft and one spring line aft (see Figure 4.4).

The elastic characteristics of the fenders (load-deflection) and mooring lines (load-elongation) are shown in Appendix 7.

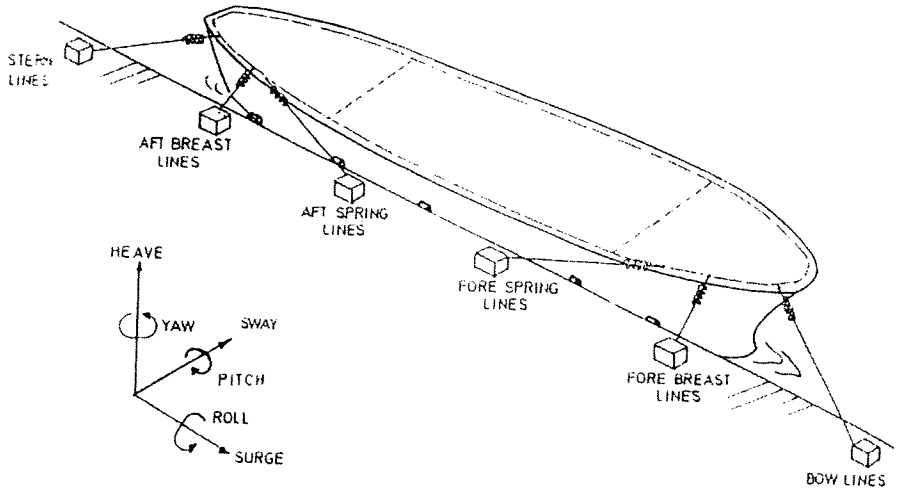

Figure 4.4. Layout of the mooring lines for the model ship

Calibration and results

The six model mooring lines are calibrated against the linearised stiffness of the prototype lines. The actual mooring line lengths, as represented in the model, are listed in Table 4.2. These lengths agree with the target requirement of 14.6% line elongation at breaking strength. Hence, it can be concluded that the mooring lines represent the chosen elastic characteristics

Table 4.2. Mooring line length and stiffness as used in the model

Line No.	Line length (m)	No. of lines	Stiffness 1 (kN/m)	Stiffness 2 (kN/m)
1	59	3	237	396
2	34	2	329	521
3	55	2	196	287
4	57	2	188	290
5	30	2	408	515
6	56	3	291	395

4.2.5. Measurements of ship motion

Set up of the model

The ship motions are determined relative to the centre of gravity (G) of the ship. The six points on the ship at which the ship motions are measured, are located on the ship's deck. The deck of the ship is located 17.5 m above the keel. The position of the six points relative to the projection of G to the deck is illustrated in Figure 4.5.

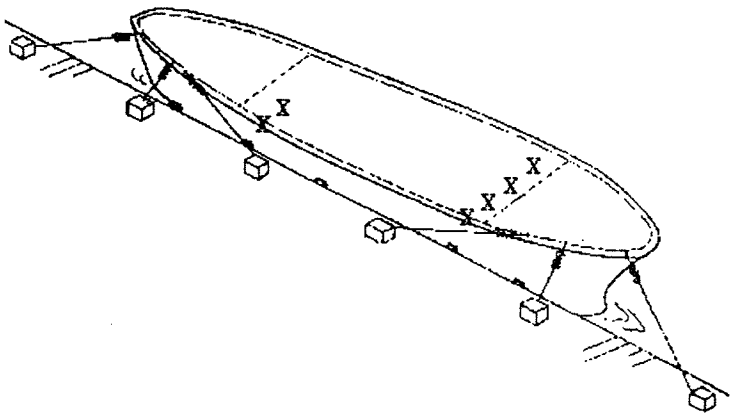

Figure 4.5. Location of the six measured points

The ship motions in six degrees of freedom are monitored by a digital video camera, linked to a PC. This camera is placed at a distance of 16.25 m off the quay edge where the ship is moored. The portside of the ship is recorded. The lens is zoomed in to obtain a maximum size picture containing sets of strip markings. The pixel co-ordinates of black and white images (strip markings) of known dimensions on the parallel body section of the ship are located. The recordings are processed by dedicated software, developed specifically for the Coega model tests.

Recording of the ship moored in its rest position is done before waves are generated. This provides reference positions for the subsequent ship motions. After the waves are generated, recording only starts after a steady state of the waves, water levels and ship motions is reached. Once this state is reached, video frames are recorded at a standard frequency of 25 Hz (prototype). These recordings are called keograms. As an example, Appendix 8 shows such a keogram. Before analysis takes place, the keograms are interpolated at 20 Hz resulting in a series of up to 8 192 records at 0.5 s (prototype) interval. This allows standard Fast Fourier Transformation (FFT) spectral analysis, as also used for wave recordings.

Calibration and results

The basic calibration of the keogram analysis is based on determining the pixel scale factor for the various positions on the ship. Once the camera is set up in a fixed position, these values will stay constant. Using the known dimensions of the paper and strips on the ship, the pixel scale factors are checked through a dynamic calibration. It is concluded, by Moes and Van Aswegen (1999), that the keogram analysis can be used with confidence and with an accuracy of at least 0.1 m (prototype).

The result of the analysis is the determination of the six principal motions of the ship. These motions allow the determination of the displacement of the attachment points of the mooring lines on the ship. From this the elongation of the mooring lines and their associated mooring line forces are calculated. The time series of the forces are truncated since the mooring forces remain zero for any negative elongation of the mooring line.

From the principal ship motions the transverse displacements of the contact points of the fenders against the ship's hull are computed. Positive values indicate a movement of the ship's hull into the direction of the quay and into the fenders. Negative values indicate a movement away from the quay and the fenders. Using the load deflection characteristics of the fenders the forces in the fenders are determined. The time series of these forces are also truncated since the fender force remains zero for any negative displacement of the ship's hull.

Lastly, from the principal ship motions relative to the ship's rest position the vertical displacements of the keel points of the ship and the maximum downward displacement are computed. The projection of the six selected keel points on the deck of the ship is shown in Figure 4.6.

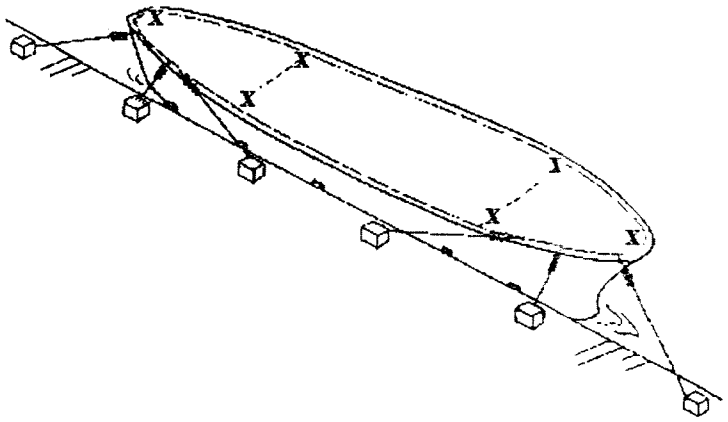

Figure 4.6. Projection of the six keel points on the plane of the deck

4.2.6. Results of the test series

The motions and forces are spectrally analysed at two frequency ranges. The horizontal motions (surge, sway, yaw) are basically of low frequency. Therefore, their motion displacements are sampled at every fourth value (0.5 Hz prototype). This yields a good spectral resolution at the low frequency range. The same process is followed for the mooring line displacements and forces. The vertical motions (heave, roll, pitch) are analysed for each recorded value (2 Hz prototype). The dividing line between the low frequencies and the high frequencies is at 0.003 Hz.

The result of a spectral analysis is a plotted output containing the most relevant spectral values. Appendix 9 shows the output of the test conditions with a significant wave height of 6 m and a wave direction of 160°. Both the wave conditions (at W1 and W2) and the ship motions (surge, sway and yaw) are displayed. The choice for these specific test results is explained in Chapter 5. Note that the rotational values of roll are indicated in units of meters but these should be read as units of degrees.

In Appendix 10 nine characteristics are listed for each of the principal motions. These characteristics are derived from the spectral analysis of each test condition. The listed values are the average spectral values obtained from three measured time series for each condition. The following nine characteristics are listed:

- Mean = mean value of the time series of the principal motion
- H1 = difference between maximum and minimum value of the time series
- H_{max} = maximum successive peak-to-trough value
- H_{mo} = four times the square root of the zero moment of the spectrum $4\sqrt{mo}$
- T_p = period at the peak value of the spectrum
- H_{lo} = H_{mo} value of only the low frequency part of the spectrum
- T_{plo} = period of the peak value of the low frequency part of the spectrum
- H_{hi} = H_{mo} value of only the high frequency part of the spectrum
- T_{phi} = period of the peak value of the high frequency part of the spectrum

From these figures Moes and Van Aswegen (1999) conclude:

- The relatively large mean sway values for the 6 m wave height (prototype) and the higher peak periods indicate that the average position of the ship for these conditions is at some distance from the fenders (up to about 0.3 m). Except for the sway motion, the principal motions are almost symmetric. The asymmetry of the sway motions is caused by difference in elasticity of the mooring lines and the fenders. The surge motions are much larger than the other principal motions. This can be attributed to the high elasticity of the mooring lines in the ship's longitudinal direction. With more than the present number of mooring lines attached, or with pre-tensioned lines, or with stiffer lines, the ship motions could be reduced.

- The values of H_{mo} for surge, sway, yaw and heave are very close to the corresponding H_{lo} values. This indicates that almost all energy associated with the horizontal ship motions and the heave motion is in the low-frequency domain. In case of heave, this is mainly due to the vessel following the low frequency water level motions quasi-statically. Roll and pitch respond more directly to the swell waves.

- In general, it appears that the peak values of the oscillations for al principal motions are reasonably well Rayleigh distributed. For statistical (design) purposes a Rayleigh distribution could, therefore, be used to determine the maximum expected oscillation from the significant oscillation (H_{mo} values).

4.3. Assessment of operational and safety limitations

In this section the operational and safety limitations on a vessel berthed at the ore-(off)loading quay in the Coega harbour are assessed in order to determine which of the ship motions is of importance in estimating the port's operation efficiency. The operation limitations are related to the loading and unloading of a berthed ship. The safety limitations concern the maximum mooring forces within the lines and the risk of the vessel touching the bottom. Reference is made to report: "Assessment of vessel motions at berth 1 based on a physical model study" (Moes, 1999).

Criteria

The criteria as given in PIANC (1995) are used to evaluate the allowable mooring conditions at berth. The criteria for dry bulk carriers are presented in Table 4.3. This table refers to the peak-to-peak motion of the vessel for all degrees of freedom except sway. For sway the zero to maximum movement away from the fender line is given. There are no criteria for heave, pitch and roll when using conveyor belt loading since these motions do not affect the equipment. Table 4.3 is considered as referring to the maximum allowable motion. Each of the six degrees of freedom is evaluated independently with no combinations being considered.

Table 4.3. Recommended motion criteria for safe working conditions for dry bulk carriers

Cargo handling equipment	Surge (m)	Sway (m)	Heave (m)	Yaw (°)	Pitch (°)	Roll (°)
Elevator / Bucket-wheel	1.0	0.5	1.0	2	2	2
Cranes	2.0	1.0	1.0	2	2	6
Conveyor belt	5.0	2.5		3		

Guidelines with regard to the allowable mooring forces in the mooring lines are given in OCIMF (1992). This publication limits the maximum mooring forces in each line to 55% of its minimum breaking strength. In the prototype mooring layout, mooring lines 1 and 6 consist of 3 lines while the other lines consist of two lines. Each line has a breaking strength of 1 MN thus the permissible load for lines 1 and 6 is 1.7 MN each and for lines 2, 3, 4 and 5 is 1.1 MN each.

The maximum permissible vertical ship motion at berth is 1.2 m during extreme events. If the vertical motion reaches 1.2 m the net underkeel clearance is 0.6 m. The vessel motion should not enter the 0.6 m allowance for net underkeel clearance during a one-yearly event. For more extreme events, the reduction of the net underkeel clearance is considered acceptable.

Extrapolation of the measured data

As mentioned in Chapter 4.2.3 the waves generated in the model are recorded at positions W1 near the vessel and W2 near the main breakwater. Position W2 is close to the location of the S4 buoy where the wave-measuring instrument in the prototype is deployed. The measured wave records at S4 consist of records of 3 hours duration, while the model measurements relate to the maximum measured in 40 minutes (4 minutes in model). To predict the maximum response of the vessel using the measured S4 data, the model measurements are extrapolated to represent a period of 3 hours (18.0 minutes in model). These extrapolations are undertaken only for the 160° direction. The results are presented in Table 4.4.

The recorded principal motions are a combination of low and high frequency responses. The maximum positive value combined with the maximum negative value is defined as the maximum peak-to-peak motion. This value (H_1) is larger than the maximum singular peak-to-peak motion and therefore conservative.

Table 4.4. Ratios for extrapolating measured data to represent a period of 3 hours

	Surge	Sway	Heave	Yaw	Pitch	Roll
$H1_{3\ hours}$ / $Hs_{40\ minutes}$	1.66	1.84	1.85	1.86	1.88	1.88

The factors as shown in Table 4.4 are applied to all the significant motions for all direction to produce response curves.

Also the mooring line forces are increased to allow for the 3-hour duration. Lines 1, 3, 4 and 6 respond mainly to the surge motion and, therefore, the factor 1.66 is used. Lines 2 and 5 respond mainly to roll, sway and yaw so a factor 1.86 is used.

The maximum measured vertical displacements of 6 keel points are not increased to be representative of 3 hourly values since the motions at berth are calculated for low astronomical tide. The occurrence of low tide is over durations less than one hour.

Operational limitations

Downtime is assessed on the basis of the wave data measured at S4 and the response curves obtained from the physical modelling. The total annual expected downtime for the various operations in days is presented in Table 4.5.

Table 4.5. Total expected downtime in a year

Equipment	Annual Expected Downtime
Elevator / Bucket wheel	39.8 days
Cranes	1.1 days
Conveyor Belts	0.0 days

The roll of the vessel is the critical motion with regard to continuous unloading systems (elevator / bucket wheel unloaders). Reducing the amount of the short wave penetration into the port can reduce the amount of roll. Extending the main breakwater affords more protection from the short wave penetration. This reduction of short wave penetration will not reduce the downtime resulting from surge and sway as these motions are driven by long wave action. The sway and surge motions also lead to the downtime to crane operations. By using a stiffer mooring system these motions can be reduced. Additional model testing is needed to assess the effectiveness of the solutions. No downtime is expected for conveyor belt loading operations.

Safety limitations

The safe mooring limitations relate to the risk of the mooring lines breaking or the vessel touching the bottom. The exceedance of the safety criteria is only permitted under extreme climatic conditions. The maximum measured significant wave height ($H_{S,max}$) per direction and peak period is presented in Table 4.6. These figures can be interpreted as one-yearly extreme events. The amount of recorded wave data at S4 is not sufficient to make predictions of wave heights with return periods of more than 1 year.

Table 4.8. Maximum measured significant wave heights (m) at S4

Direction (° TN)	T_P (s) 10	12	14	16	18
110	1.89	0.82	-	-	-
128	2.21	2.10	3.34	3.49	-
140	2.00	3.63	3.54	3.23	0.71
160	2.12	2.11	2.39	1.98	1.11

No events measured at S4 lead to the exceedance of the OCIMF guidelines for the mooring forces. The smallest ratio between the maximum allowable wave height and the maximum measured wave height at S4 is 1.2. This is for waves with a direction of 160° and a peak period of 12 s. Using additional lines to moor the vessel can reduce the individual mooring line forces.

5. Hypotheses

Derivation of hypotheses with regard to surge, sway and yaw

5.1. Introduction

After reviewing the theory of moored ships in general and the Coega model study, in this chapter hypotheses are derived for the moored ship in the Coega model. In order to acquire insight, some aspects are reviewed first. The waves in the model are treated in Section5.2. This section studies the development of waves from outside the harbour to the position of the moored ship. Special attention is paid to the long waves in the model. The ship's response is treated briefly in Section5.3; it deals with the response of the model ship during the Coega model tests, both free floating and moored.

The actual formulation of hypotheses is discussed in Section 5.4. Relevant conclusions from the theory are reviewed. It is investigated to what extent the theory applies to the model test results. Subsequently, hypotheses with regard to surge, sway and roll motions are derived. The choice for these three ship motions is based on the results of the Coega model tests See Section 4.3. In this section, it is concluded that surge, sway and roll are the only ship motions leading to operational downtime.

5.2. Waves in the model

To facilitate decent comprehension of the ship motions, understanding of the waves that cause the ship motions is necessary. The waves in the model are treated here.

A bank of wave generators generated irregular waves in the model in cycles of four minutes. The wave spectra have a JONSWAP spectral shape, with a spectral peak enhancement factor $\gamma = 3.3$. For the composition of the time series of the waves, the phases of the frequency components is chosen randomly.

The test conditions are simulated at W2. The results of the wave diffraction and refraction into the harbour are measured in the harbour at W1. Only the wave heights and periods are measured. The direction of the wave is estimated visually.

5.2.1. Propagation of waves from W2 to W1

The ship motions result directly from the waves as they are at the position of the ship. Hence, the ship motions should be studied in relation to the wave field at W1. This section describes the propagation of the waves from W2 to W1.

In order to study the propagation of waves from W2 (outside the harbour) to W1 (near the bow of the ship) the wave height transfer coefficient (WTC) is determined for all wave directions. The definition of the wave height transfer coefficient is: the ratio of the significant wave height at W1 (H_{mo}_W1) to the significant wave height at W2 (H_{mo}_W2).

This WTC can be determined for the significant wave heights of three different frequency ranges:

- Whole frequency range, H_{mo}
- Low frequency range, H_{lo}
- High frequency range, H_{hi}

The dividing line between high and low frequencies is taken at 0.03 Hz, that is, at 33.33 s. The whole frequency range is from 0 to 0.2 Hz.

Figure 5.1 shows the WTC calculated for waves over the whole frequency range [0-0.2 Hz]. Following can be concluded:

- For all wave heights, the WTC is largest for a wave direction 160°. The angle between the propagation direction of the waves and the approach channel is smallest for this direction. This explains the high values of the WTC.
- The WTC reaches its maximum of 0.27 for a wave period of 10 s and a wave height of 2m.
- For other wave directions the WTC is clearly lower; all values are around 0.1.
- The WTC value is higher for larger wave heights. This is true for all wave directions except for 160°. Especially the test condition with a wave period of 10 s and a wave height of 2 m shows irregularity. The reason for this is not clear. It is suspected that the reason can be found in a model effect. Further investigation in how the waves in the model are generated is needed in order to verify that this concerns a model effect.

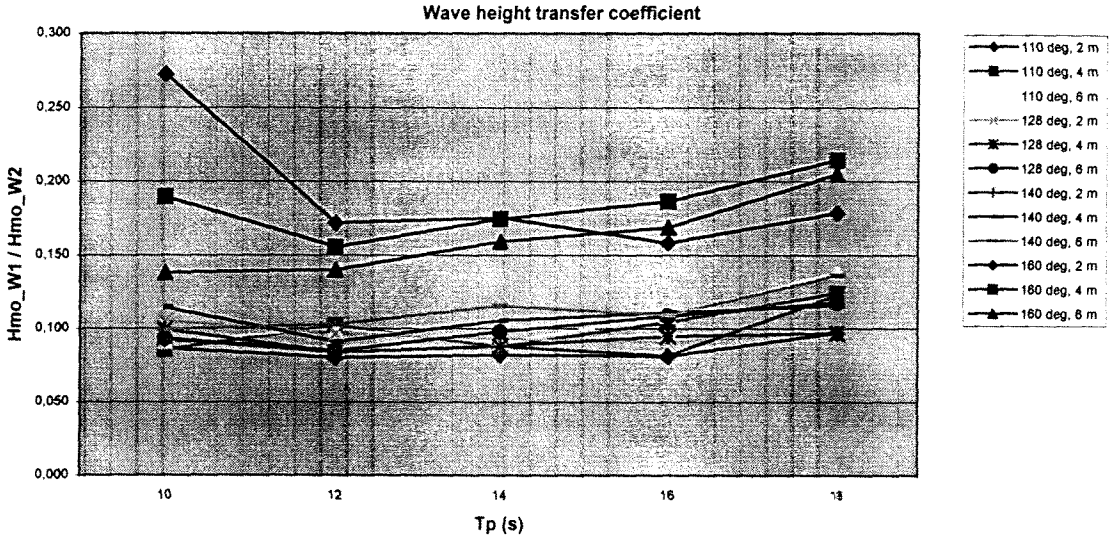

Figure 5.1. Wave height transfer coefficient [0-0.2 Hz]

Figure 5.2 shows the WTC calculated for waves over the high frequency range [0.03-0.2 Hz]. As can be expected, there is a striking resemblance with Figure 5.2. The values are of the same magnitude. Again the test condition with a wave period of 10 s, a wave height of 2 m and a wave direction of 160° shows a remarkable irregularity.

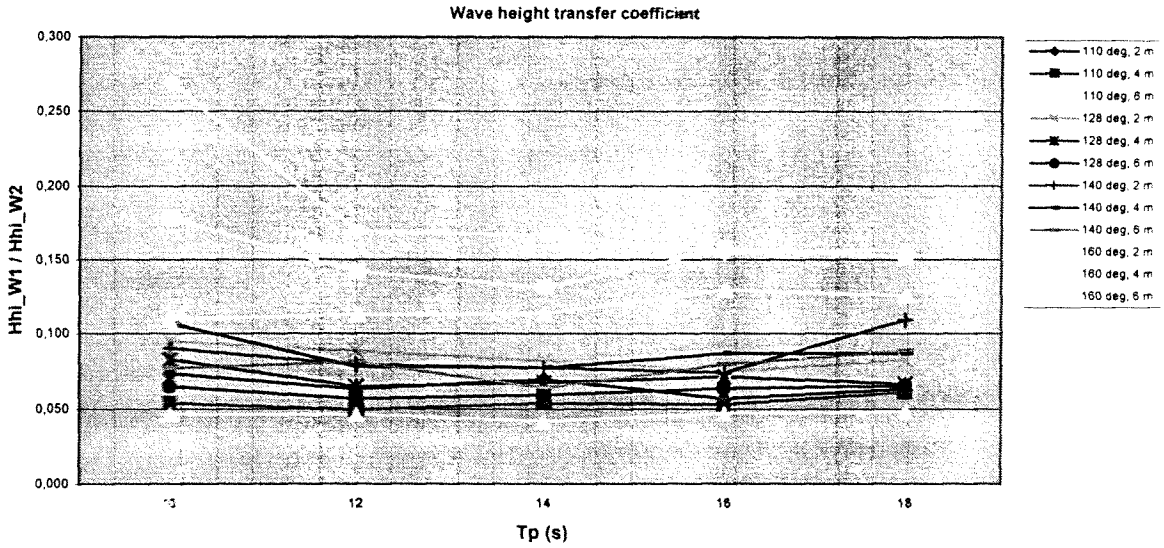

Figure 5.2. Wave height transfer coefficient [0.03-0.2 Hz]

Figure 5.3 shows the WTC calculated for waves over the low frequency range [0-0.03 Hz]. It can be seen that the values of the WTC are larger for the low frequency waves. For all wave directions the WTC values are between 0.3 and 0.7. The high values of H_{lo} inside the harbour can result from two different phenomena:

- The penetration of low frequency waves into the harbour is larger than of high frequency waves.
- Resonance in the harbour takes place leading to amplified wave heights near the position of W1.

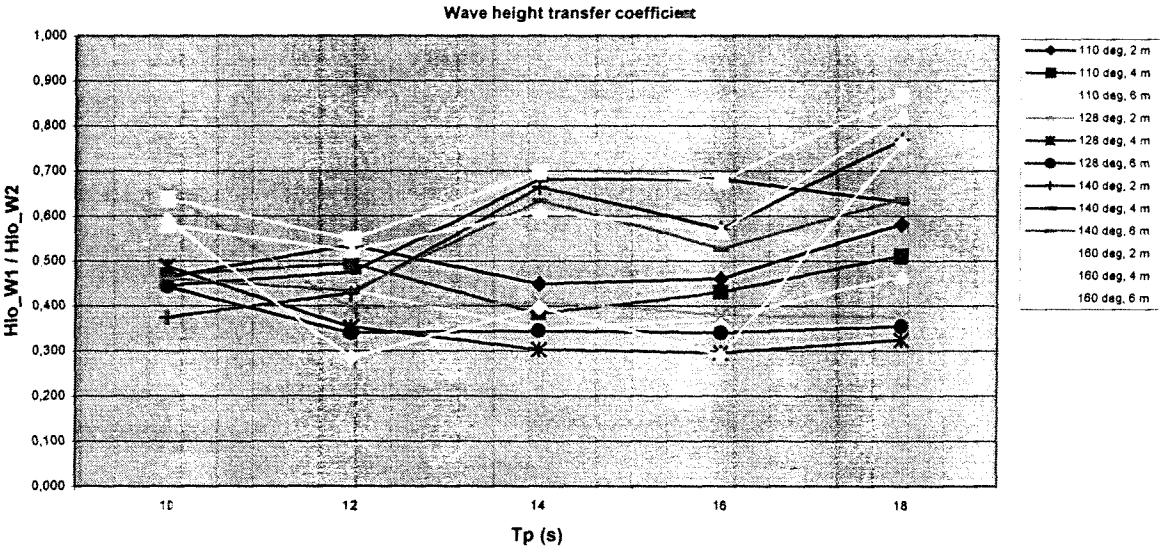

Figure 5.3. Wave height transfer coefficient [0-0.03 Hz]

In order to determine which phenomena play a significant role in the Coega model, occurrence of harbour basin resonance is investigated. The shape of a basin can lead to standing waves in this basin. Standing waves cause significant horizontal water motions near nodes and significant vertical water motions near antinodes. This resonance occurs when the natural period of the basin equals the period of the waves. For a basin with uniform depth and rectangular shape, the natural period of the basin can be calculated as follows:

- Closed basins: $T_n = \frac{2L_B}{n} * \frac{1}{\sqrt{gd}}$ with n = 1, 2, ..(5-1)
- One-sided open basins: $T_n = \frac{4L_B}{(1+2n)} * \frac{1}{\sqrt{gd}}$ with n = 0, 1, .. (5-2)

in which
T_n = natural period of the n^{th} harmonic
L_B = length of the basin
d = depth of the basin
g = gravitational force

For the Coega model tests the length of the basin is approximately 560 meter (see Figure 5.5.) and the depth of the basin is 17 meter. According to Equation 5-2 the natural period of the fundamental mode (first harmonic, n = 0) of the basin is equal to 172 seconds. For the second and third harmonic (see Figure 5.4) the natural period is 57 seconds and 34 seconds, respectively. The width of the basin is approximately 310 meter (see Figure 5.5.). The natural period of the fundamental mode for a standing wave in the transverse direction of the basin is, according to Equation 5-1, equal to 48 seconds.

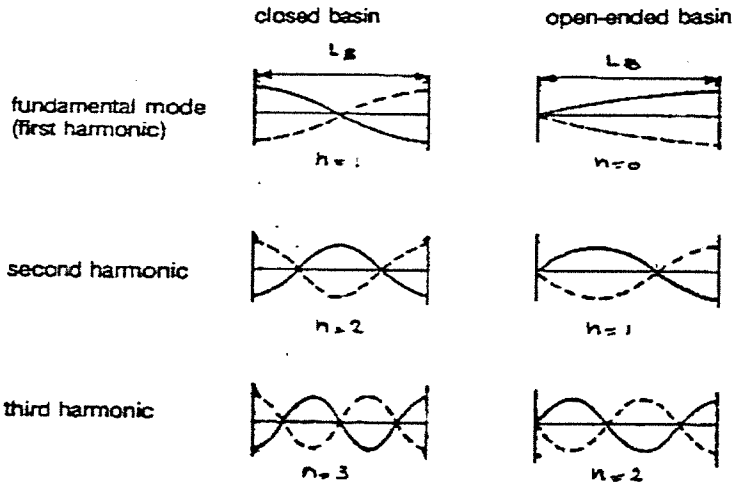

Figure 5.4. Basin oscillations of closed and open-ended basins

A standing wave in transverse direction initiates an antinode near the moored ship while a standing wave in longitudinal direction causes a node near the moored ship. Accordingly, significant vertical motions can be expected in case of standing waves in transverse direction and significant horizontal motions for standing waves in longitudinal direction.

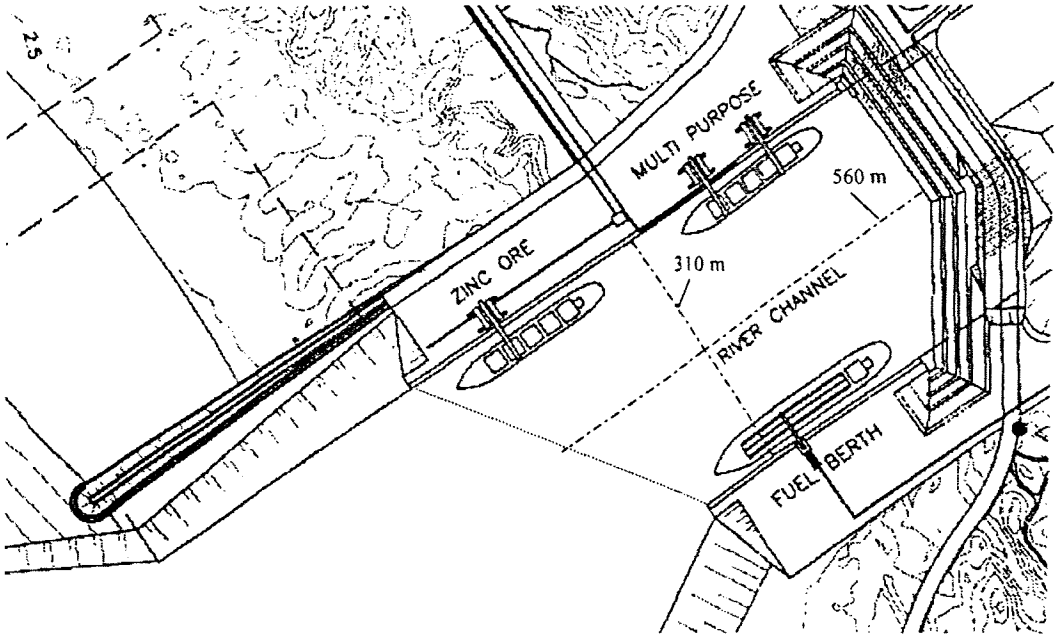

Figure 5.5. Layout of the Coega model basin

Appendix 9 shows the spectral density curves of the waves and the resulting ship motions for the model tests with the following five wave conditions:

- WC10: wave height is 6 m, wave direction is 160°, peak period is 10 s
- WC12: wave height is 6 m, wave direction is 160°, peak period is 12 s
- WC14: wave height is 6 m, wave direction is 160°, peak period is 14 s
- WC16: wave height is 6 m, wave direction is 160°, peak period is 16 s
- WC18: wave height is 6 m, wave direction is 160°, peak period is 18 s

By comparing the spectral density curves of the water motion at the entrance of the harbour (W2) and near the moored ship (W1) it can be investigated near which frequencies resonance takes place. According to wave conditions (WC) 10, 16 and 18 resonance occurs around a frequency of 0.006 Hz. This means around a period of 170 s, which is the same as the natural period of the fundamental mode of the basin. Harbour basin resonance seems to be the cause of the amplified water motion near this frequency.

Wave conditions (WC) 12 and 14 show a significant resonance near a period of 750 s. If harbour basin resonance is the cause of this, the length of the basin is around 2500 m. The distance between the harbour entrance and the end of the basin is approximately 2500 m. Hence the long wave action inside the basin could be due to a standing long wave over a distance of 2500 m. This would not lead to increased horizontal ship motions since the location of the moored ship is close to the antinode of this standing wave.

No apparent resonance can be detected near a frequency of 0.02 Hz (period of 50 s). Consequently, it is concluded that resonance in transverse direction does not take place. This also holds for resonance due to the second or third harmonic in longitudinal direction.

As described in Section 4.1 numerical harbour resonance modelling has been conducted by the C.S.I.R. for the long wave conditions in the Coega harbour. The harbour layout used in that investigation is not exactly the same as the harbour layout used during the model tests. Nonetheless, the results of this investigation present an indication of the resonance occurring in the harbour basins.

The mooring conditions for small craft in the corner just north of the jetty appear to be a problem, due to the presence of an anti-node. This is the location of the ore-(off)loading berth. It is concluded that resonance occurs near the jetty for a wave period of 120 seconds. The natural period of the fundamental mode of the Coega (physical) model basin is 172 seconds. Taking into account the slightly different layout of the harbour, the resonance discerned in the numerical model could be caused by the same phenomenon. This confirms the assumption that resonance occurs due to a stimulation of the first harmonic of the basin.

5.2.2. Long waves in the Coega model

With respect to the Coega model tests an investigation has been performed concerning the occurrence of long waves in the area of the Coega harbour (Moes, 1997). One of the findings of this investigation is that it appears justified to accept the values in Table 5.1 as realistic estimates of the long wave conditions at the entrance of the Coega harbour. The values in Table 5.1 follow from the theory of bound long waves developed by Barthel (1983) and applied to wave generation in physical models by van Tonder (1991).

Table 5.1. Estimated relations of the long wave conditions at W2

T_p (s)	H_{lo} / H^2_{mo} (m^{-1})
10	0.032
12	0.045
14	0.063
16	0.080
18	0.097

The relation between low frequency waves and the high frequency waves at W2 is presented in Figure 5.6. This figure shows that, for all wave directions, the waves stay below the estimated heights. Both the wave direction of 110° and 128° follow the theory of Barthel well. This is not the case for the wave directions 140° and 160°. Reason for this might be found in the plan of the model. However, it could be true that this phenomenon occurs in reality as well.

- Model layout

It could be so that the plan of the model influences the development of the waves in the basin. The back of the model tank is impervious and reflects incoming waves. This could lead to long waves that do not occur in reality. This effect is biggest for the wave direction of 110° and smaller for the wave direction of 160°. Since the sides of the tank do absorb wave energy the effect is smaller for oblique waves. It is noted that even if this reflection takes place it only results in a different value of the ratio H_{lo} / H_{hi} if low and high frequency waves reflect differently.

- Reality

In the report referred to above (Moes, 1997) the influence of the direction of long waves is not described. It is possible that, in reality, the wave heights of low frequency waves are smaller for wave directions of 140° and 160° than for wave directions of 128° and 110°. When entering more shallow water bound long waves refract earlier than the short long waves to which they are bound. The wave direction of the long waves changes while the wave direction of the short waves will not change until even more shallow water is reached. From that point the long waves are no longer bound to the short waves. From the bathymetry chart of the area (see Appendix 1) it can be seen that waves with a direction of 160° refract as they approach the harbour. This is also true for a wave direction of 140° but to a lesser extent. Waves with a direction of 110° and 128° approach the harbour almost parallel to the depth contours. Therefore, these waves are not likely to refract.

So as to confirm one of the abovementioned possibilities it is of importance to understand how the long waves are generated in the Coega model. It is essential to know how the long waves measured at W2 originate. It is possible that the wave generators create waves of low frequency. If there are no waves of low frequency generated this transfer of wave energy from the higher to the lower wave frequencies could be attributed to a real wave transformation process, associated with groupiness of the (generated) waves. In other words, the long waves are bound long waves generated by the short waves in the model.

It is also striking that the low frequency wave heights of waves with a direction of 140° are even lower than those of waves with a direction of 160°. This aspect cannot be explained by refraction in reality or reflection in the model. It could be attributed to the presence of the wave-guides. Further investigation in how the waves are generated could verify this assumption.

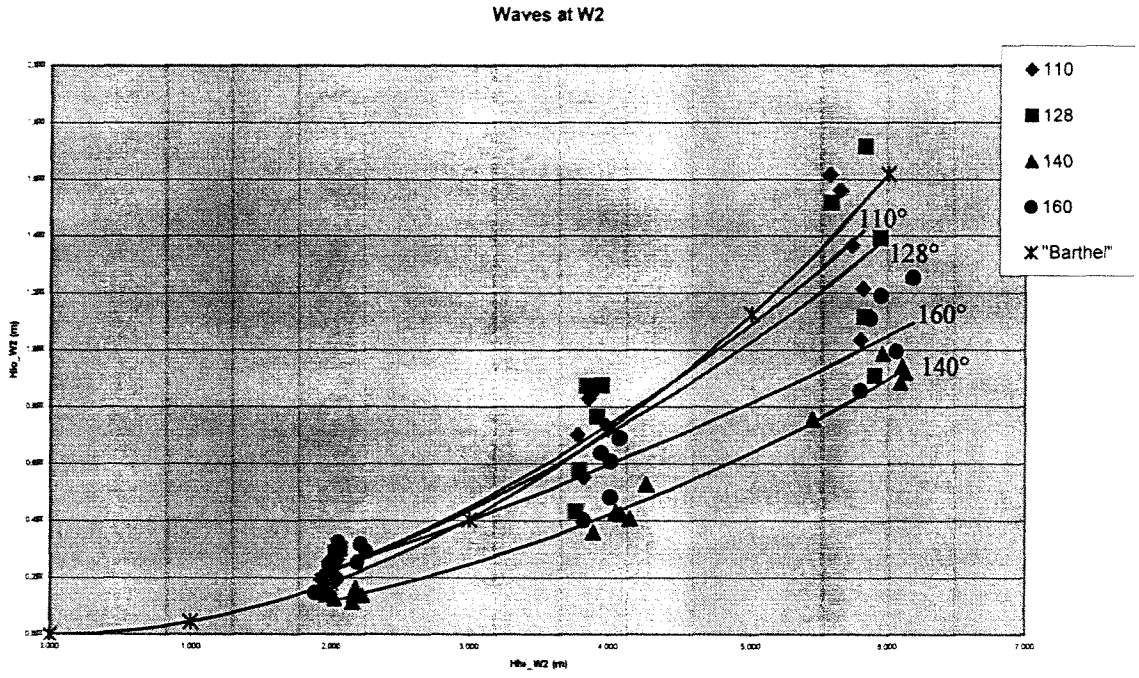

Figure 5.6. Waves in the model at W2

In view of the preceding, it appears important to know whether the waves at W2 are bound waves or not. According to several sources there should be a quadratic relation between the low frequency wave height and the significant wave height in case of bound long waves. The relation between H_{lo} and H^2_{mo} is examined for both the locations W1 and W2. When the long waves reach the location of W1 they can no longer be considered bound waves. Nonetheless, for this location the relation between the low frequency wave height and the significant wave height is also studied.

The relations are tested with the help of Excel. The different quantities are compared by means of a trendline and the R^2 values are determined. The R-value of a trendline is calculated as follows:

$$R = \frac{n(\Sigma XY) - (\Sigma X)(\Sigma Y)}{\sqrt{\left[n\Sigma X^2 - (\Sigma X)^2\right]\left[n\Sigma Y^2 - (\Sigma Y)^2\right]}} \tag{5-3}$$

The definition of R is such that the value of R^2 is always between 0 and 1. An R^2 value of 1 stands for a perfect match between the results of the model tests and the trendline through these measured data. In other words, the measured data completely satisfy the suggested relation. It is assumed that a R^2 value of 0.9 is sufficient to confirm a supposed relation. The results are shown in Figures 5.7 and 5.8. Table 5.2 gives the R^2 values for the different directions.

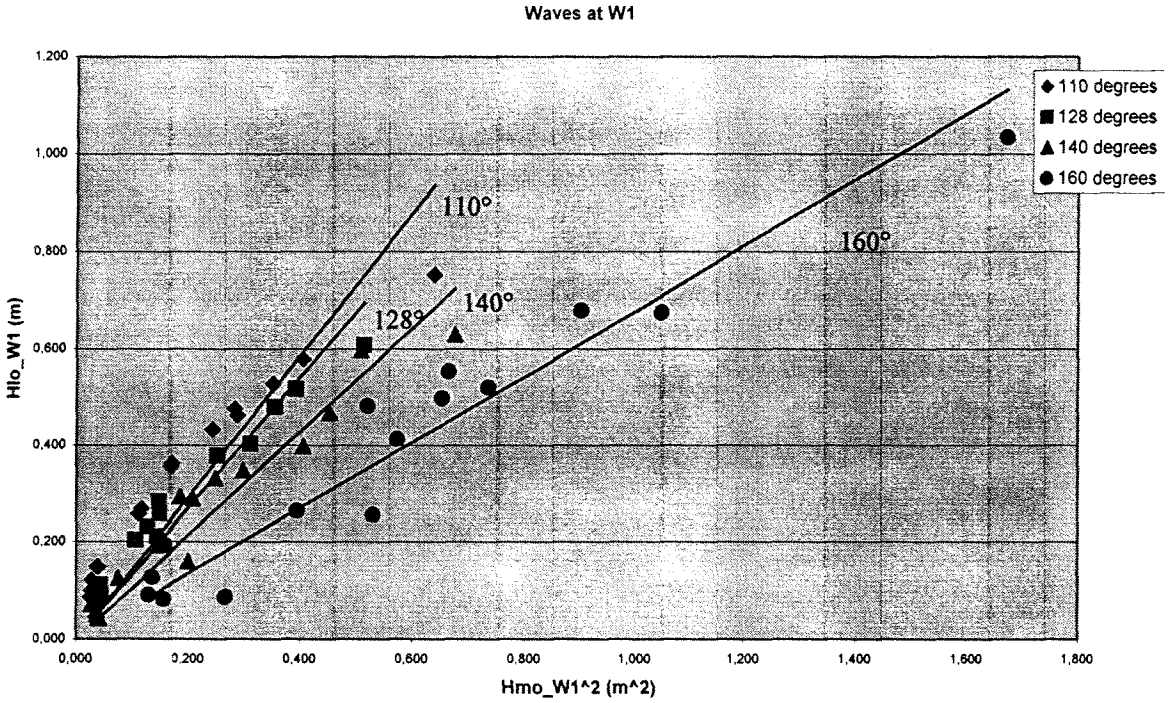

Figure 5.7. Long waves at W1

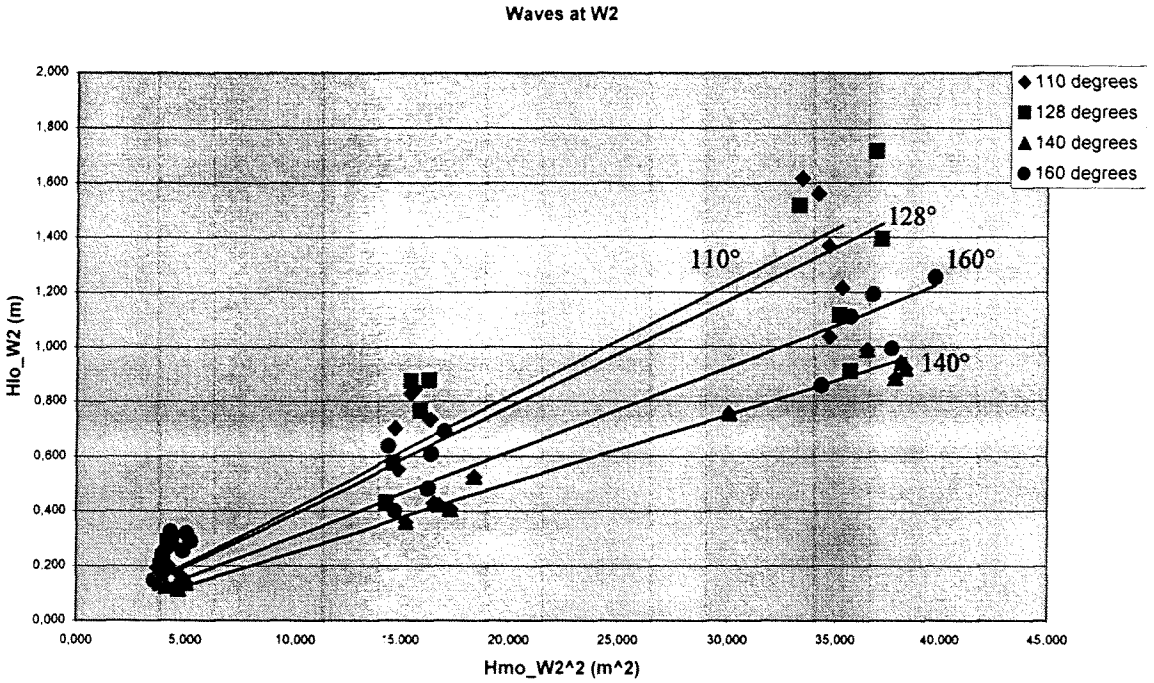

Figure 5.8. Long waves at W2

Table 5.2. R^2 and C (model) values for the relations between H_{lo} and H^2_{mo}

Direction at W2	$H_{lo\_W1} = C_1 \cdot H^2_{mo\_W1}$		$H_{lo\_W2} = C_2 \cdot H^2_{mo\_W2}$	
	R^2 value(-)	C_1 (1/cm)	R^2 value (-)	C_2 (1/cm)
110°	0.8046	1.4663	0.8854	0.0409
128°	0.9028	1.3562	0.8273	0.0389
140°	0.9137	1.0712	0.9871	0.0250
160°	0.9280	0.6773	0.8715	0.0308

From Table 5.2 it can be concluded that the waves in the model agree well with the assumed quadratic relation between the low frequency wave height and the significant wave height. The values of C are not dimensionless. A C-value of, for instance, 0.04 1/cm in the model corresponds to a value of C of 0.04 1/m in prototype.

Waves with a direction of 160° show a striking irregularity in Figures 5.7 and 5.8. Outside the harbour (W2) the long waves with a direction of 160° are, generally, higher than the long waves with a direction of 140°. Inside the harbour (W1) the opposite is the case. As mentioned before, further investigation in this respect is required.

5.2.3. Direction of the waves near the quay

The deepwater waves that approach the harbour entrance will diffract around the breakwater and approach the moored ship at a different angle. Other phenomena like refraction and reflection also influence the direction of the waves.

The waves that affect the moored ship propagate into the harbour and diffract around the SE'ly tip of the quay. The wave direction at the location of the bow of the vessel is visually estimated to be between about 130° and 150° relative to the longitudinal axis of the moored ship (see Figure 5.9).

In case of surge motions the force of the waves on the ship in longitudinal direction is of importance. For the roll and sway motions, the forces of the waves perpendicular to the ship play an important role.

During the verification of the hypotheses the direction of the waves is not taken into account. All ship motions are assessed as if they are caused by waves that approach the ship from a constant direction. This assumption can influence the results.

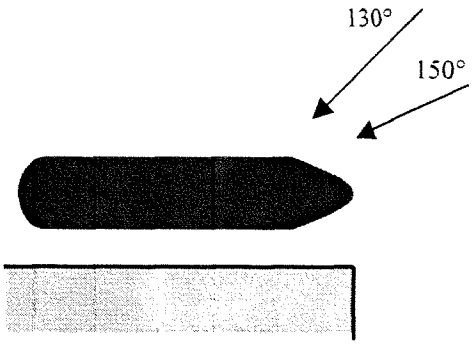

Figure 5.9. Wave direction near the ship

5.3. Response of the model ship to the waves

5.3.1. Response amplitude operator of the model ship

The response amplitude operator (RAO) is an indication of how a free-floating ship responds to waves. In case of a moored ship the mooring system partly determines the reaction of the ship to the waves. For that reason the ship motions in the model cannot be predicted solely by the RAO. Nonetheless, the RAO gives a good impression of how the free-floating model ship reacts. This, in turn, can increase comprehension of the reaction of the moored ship.

Horizontal ship motions are more influenced by the mooring system than vertical ship motions. As a result, the RAO is not very helpful when investigating the surge and sway motions of the moored model ship. On the other hand, the RAO can be of help when the roll motions are studied.

Using the computer programme "DELFRAC", the RAO of the model ship is determined. The response of the ship is calculated for waves that encounter the ship from different directions. The following directions are used: 90°, 100°, 110°, 120°, 130°, 140°, 150°, 160°, 170° and 180° (90° being off portside and 180° being forward). Appendix 11 shows the RAO of a free-floating ship for respectively surge, sway and roll. The following conclusions can be made from this:

Surge

- The RAO of the surge motion of the ship has, more or less, the same shape for all wave directions apart from 90°. There is no response for frequencies higher than 0.1 Hz. For frequencies lower than 0.1Hz the response increases with lower frequencies.

- For a wave direction of 180° the RAO reaches its maximum value of 15. This maximum per wave direction decreases for larger wave angles between the ship and the waves. In other words, the surge motion is biggest for waves approaching the ship aftward. The more the wave direction deviates, the smaller the surge motion becomes. This is in accordance with the theory of Section 5.1.3.
- Beam waves (wave direction of 90°) result in a totally different RAO for surge. This is understandable since there is, theoretically, no force acting in longitudinal direction of the ship. This results in a different form of the RAO with very small values (maximum of 0.07).

Sway

- The shape of the RAO for sway is the same as for surge. There is no response for frequencies higher than 0.1 Hz and for lower frequencies the response increases.
- For a wave direction of 90° the RAO reaches its maximum of 16. This maximum per wave direction decreases for increasing angles between the ship and the waves. In other words, the sway motion is biggest for beam waves. The more the wave direction deviates from this 90°, the smaller the sway motion becomes. This is, as expected, exactly the opposite of the response for surge.
- Waves approaching the ship aftward result in no response for the sway motion. This is due to the same principle as described for surge. There is no force acting in the transverse direction of the ship resulting in no motion in this direction.
- The shape of the RAO shows for all the directions a slight irregularity for 0.08 Hz. This is probably due to coupling with the roll motion.

Roll

- There is a peak in the RAO at 0.08 Hz. This peak is present for all wave directions and reaches its maximum of 22.5 deg/m for a wave direction of 90°. According to the reports of the CSIR, the natural roll period, T_ϕ, of the model ship is 11.92 s or 0.08 Hz (see Appendix 3). Hence, it can be concluded that, for the roll motion, the DELFRAC computer programme represents the model ship sufficiently.
- Just like with the sway motion, there is no roll motion for a wave direction of 180°. With a wave direction changing from 180° to 130° the roll motion first increases and than decreases again. It reaches its minimum for a wave direction of 130°. With a wave direction changing from 130° to 90° the roll amplitude increases again until it reaches its maximum at 90°.
- For frequencies lower than 0.07 Hz there is a second peak in the RAO. This peak is only present for wave direction between 130° and 180°. For all wave directions the second peak is small compared to the first peak. Except for a wave direction of 130°, here the second peak reaches its maximum of 1.05 deg/m, which is almost as high as the first peak. The cause of this second peak could be the coupling between roll and sway.

5.3.2. Examination of the ship motions

The three ship motions are analysed in order to see if the theory is in accordance with the Coega model tests. Figures 5.10, 5.11 and 5.12 show the relation between the wave field and the significant values of the ship motions. The generated wave directions, significant wave heights and peak periods at W2 are used to describe the wave field. For the sake of clarity, these wave parameters are expressed in prototype values.

- Surge

The surge motion is largest for wave heights of 6 m and periods of 18 s. This is true for all wave directions. In general there is an increase in the surge motion with an increase of both the wave height and the wave period. The wave direction does not seem to be of importance for the surge motion. The response of the ship is, more or less, the same for all for wave directions.

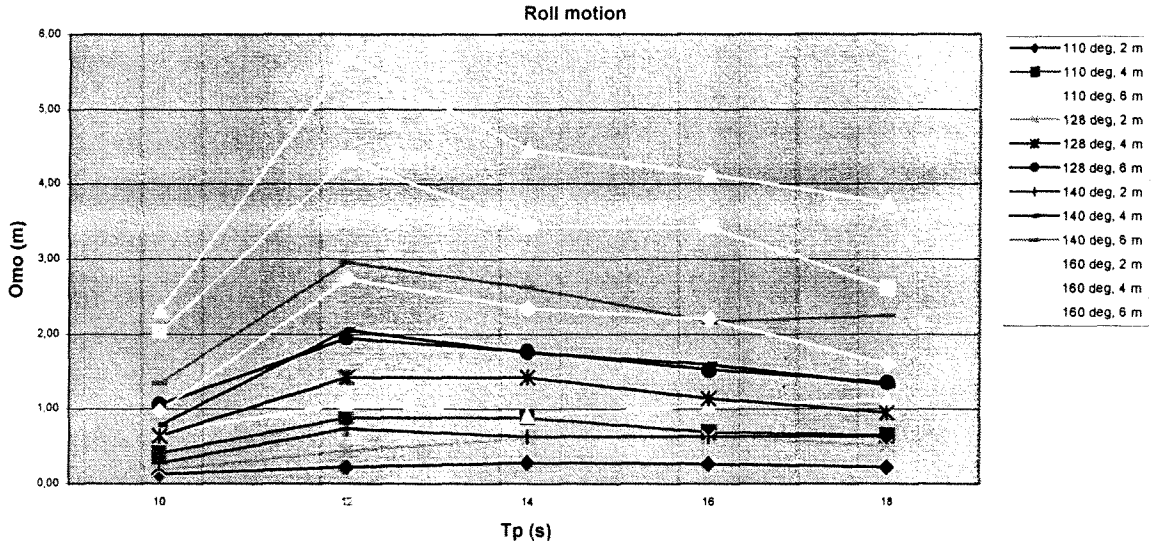

Figure 5.10. Surge motion

- Sway

For all wave directions, the largest sway motion is for wave heights of 6 m. For wave directions of 110° and 140° this occurs at a wave period of 18 s. For wave directions of 128° and 160° this occurs at a wave period of 16 s. Therefore, the wave direction does seem to matter for sway motions, especially for wave heights of 6 m. In general, there is an increase in the sway motion with an increase of both the wave height and the wave period.

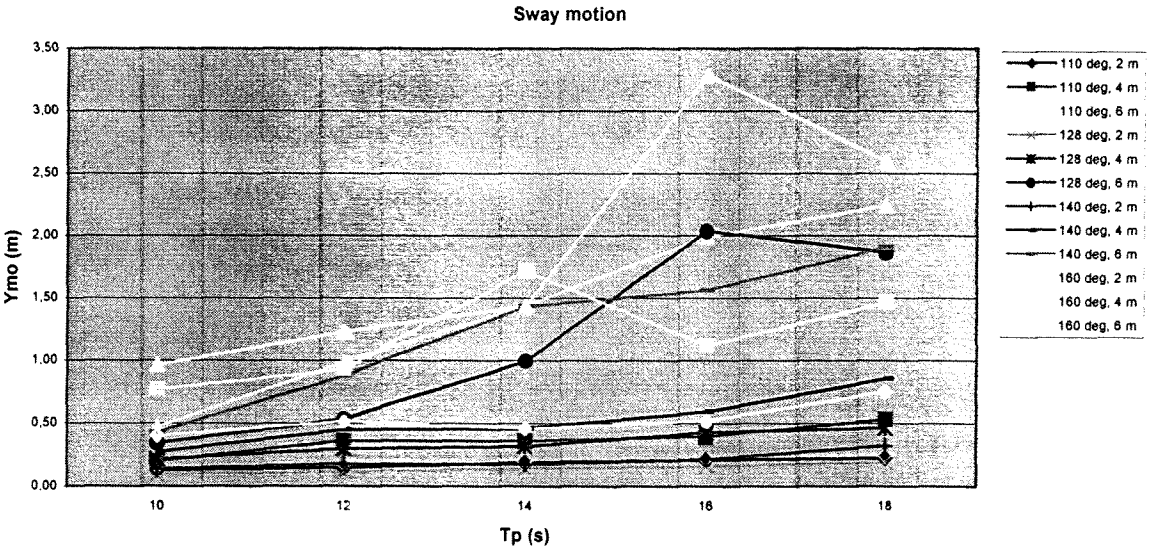

Figure 5.11. Sway motion

- Roll

For all wave directions, the roll motion is largest for wave heights of 6 m and a wave period of 12 s. Here the direction of the wave is definitely of importance; de roll motion is largest for a wave direction of 160°, smaller for a direction of 140°, even smaller for 128° and the smallest for 110°.

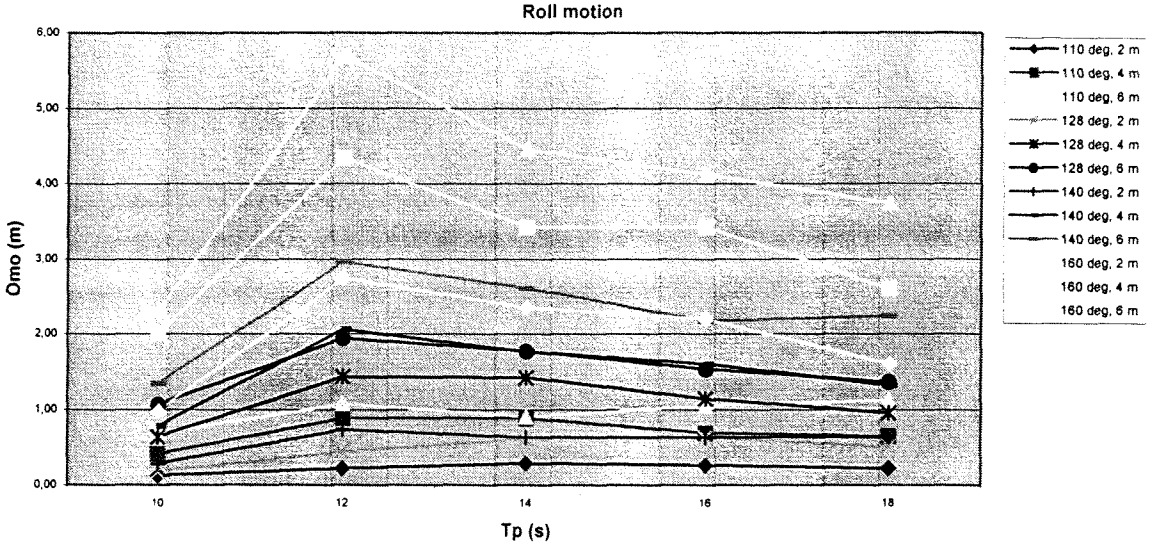

Figure 5.12. Roll motion

5.4. Formulation of hypotheses

With the information presented in the previous sections formulation of hypotheses takes place in this section. In order to formulate sensible hypotheses, the general findings from the literature are summarized and applied to the Coega model tests. This includes the empirical relations as described in Section.

5.4.1. Conclusions from the literature

From the literature the following conclusions according to the surge, roll and sway motion can be made:

- Surge and sway are both horizontal motions while roll is a vertical motion. In general, this means that the roll motion is mainly in the wave frequency range and that long wave phenomena play an important role regarding surge and sway.

- Especially for surge the motions seem to be almost completely in the low frequency range. For that reason, it is assumed that the surge motion is caused only by low frequency waves.

- In the sway motion of the ship both harmonic and subharmonic response occurs. Hence, both low frequency and high frequency phenomena are taken into account. High frequency response is caused by the coupling between the sway and the roll motion. The effects of low and high frequency waves are assumed to be independent and, therefore, superposition can be applied.

- Also in the roll motion response occurs in the whole frequency range. The harmonic roll motion is caused by resonance between the ship's natural period of roll and the waves. The subharmonic response of the roll motion is caused by the coupling with the sway motion through mooring lines and fenders. For this reason it is supposed that the subharmonic part of the roll motion can be expressed in relation to the sway motion.

The mooring system and the ship characteristics both determine the natural period of the ship in the various modes. Since these features are not varying in the case of the Coega model tests, the natural periods are constant.

The natural periods in turn determine the response of the ship. For instance, the surge motion of a ship moored in a stiff mooring system (steel wires and/or pretensioned) can respond harmonically. This implies a linear relation between the surge motion and the wave height. For softer line systems the natural period for surge increases, resulting into more subharmonic response. The mooring system in the model tests consists of polypropylene lines that are tight but not pretensioned. Therefore it is expected that the response is subharmonic.

Not only the natural period of the motion determines the response of the ship. The relationship between the natural period and the peak period of the wave spectrum is also an important factor. For instance the roll motions become very profound when the peak period approaches the natural period of the roll motion.

The response amplitude operator (RAO) describes, per mode, the reaction of the ship to the waves (see section 5.2.1). This is, so to speak, the translator between the wave spectrum and the ship motion spectrum. Unfortunately, this RAO can only be determined for a free-floating ship in shallow water. This means that the subharmonic response due to the mooring system cannot be included. As a result, the ROA can only be used to determine surge motions or sway motions due to low-frequency waves. The RAO of a free-floating ship can be applied for the roll motions of the ship, since this is mainly a harmonic phenomenon.

5.4.2. Hypotheses with regard to surge, roll and sway

On the basis of previous sections hypotheses are derived for the three ship motions. These hypotheses only concern the relation between the significant motions and the significant wave heights. The wave periods are not included in the hypotheses because no explicit relation can be derived from the theory. It is clear that the wave period is of importance to the ship's response but not to what extent. The influence of the wave period is examined further in Chapter 6.

Hypotheses with relation to surge

The relations with regard to the surge motion are discussed extensively in the previous sections. It is clear that surge is a horizontal motion, thus reacts mainly to the low frequency part of the wave spectrum. For waves approaching the ship with a direction of 130° to 150° the influence of the wave direction is small. The influence of the period is significant. In view of the theory and the empirical relations the hypothesis for the surge motion becomes:

- $X_{mo} = C * H_{lo}$ (H-1)

Hypotheses with relation to roll

Three aspects come forward from the theory. Firstly, the harmonic part of the roll motion is dominant. The roll motions of the ship seem to react to the high frequency waves. Secondly, there exists a coupling between the roll motion and the sway motion. Sway is just like surge a horizontal motion and responds mainly to the low frequency part of the wave field. Therefore, the sway motions occur more slowly than the roll motions. The influence of the coupling to the roll motion is negligible.

The third aspect that comes forward from the theory is the strong dependence of the roll motion on the peak period. It is clear that, for roll, the response of the ship is not the same for all values of the peak period. If the peak period of the wave field comes near to the natural period of the moored ship resonance takes place. This effect is expressed in a period dependent coefficient, C (T_P).

Considering the abovementioned aspects, the following hypothesis is developed:

- $\Phi_{mo} = C\ (T_P) * H_{hi}$ **(H-2)**

in which C (T_P) is a function of the peak period. This function depends on the natural roll period.

Hypotheses with relation to sway

Sway is just like surge a horizontal motion reacting mainly to the low frequency part of the wave spectrum. However, in case of the sway motion there is another aspect as well, namely the coupling between the roll motion and the sway motion. The roll motion relates to the high frequency part of the wave field. As a result of the coupling, the sway motion also relates to this high frequency part. Consequently, it appears logical to represent the sway motion as a superposition of two parts:

1. Low frequency $Y_{mo} = C_{lo} \cdot H_{lo}$
2. Coupling with roll $Y_{mo} = C_{hi}\ (T_P) \cdot H_{hi}$

With due observance of both phenomena the hypothesis for the sway motion becomes:

- $Y_{mo} = C_{hi}\ (T_P) * H_{hi} + C_{lo} * H_{lo}$ **(H-3)**

in which C_{hi} (T_P) is a function of the peak period and C_{lo} is constant.

It could be so that superposition of the two phenomena cannot be applied. In that case the hypothesis for the sway motion is:

- $Y_{mo} = C\ (T_P) * H_{mo}$ **(H-4)**

in which C_{hi} (T_P) is a function of the peak period. The shape of this function depends on both the natural period of roll and the natural period of sway.

6. Verification

Verification of the hypotheses and application to the model ship

6.1. Introduction

After the formulation of hypotheses in Chapter 5 these hypotheses are studied further in this chapter. The main goal is to confirm or reject the assumed relations between the wave field and the ship motions. It is desirable that the relations are expressed in such a manner that the coefficients are dimensionless. In that case, the coefficient is valid for both model and prototype.

The relations are tested with the help of Excel. The different quantities are compared by means of a trendline and the R^2 values are determined. The R^2 value of a trendline is calculated with Equation 5-3. The definition of R is such that the value of R^2 is always between 0 and 1. An R^2 value of 1 stands for a perfect match between the results of the model tests and the trendline through these measured data. In other words, the measured data completely satisfy the suggested relation. It is assumed that a R^2 value of 0.9 is sufficient to confirm a hypothesis.

Beside the validation of the hypotheses this chapter also looks into the role of the wave period. It is tried to include the wave period in the relations. This is done by trial an error but of course with the theory as basis.

Lastly, the characteristics of the model ship and the mooring system are taken into account. It is investigated whether the coefficients are representative for these characteristics. By means of the "DELFRAC" computer programme it is tried to reproduce the data measured during the physical model tests. This calculated data is then compared to the measured data.

6.2. Surge motion

6.2.1. Verification of hypotheses

In Section 5.4.2 the following hypothesis is developed with regard to the surge motion of a ship:

- $X_{mo} = C_X * H_{lo}$ (6-1)

For the sake of completeness and as a comparison, more equations are considered than just the hypothesis. The following relations between the ship motion and the wave field are taken into account:

1) $X_{mo} = C_{X1} * H_{mo}$
2) $X_{mo} = C_{X2} * H^2_{mo}$
3) $X_{mo} = C_{X3} * H_{lo}$
4) $X_{mo} = C_{X4} * H^2_{lo}$

Table 6.1 shows the values of R^2 and C_X that are found for the above-mentioned relations. From the R^2 values it is concluded that relation 3 is the only one that can be considered valid. This is in agreement with hypothesis H-1. Figure 6.1.illustrates the relation. The low value of R^2 (0.57) for relation 2 confirms that low frequency wave heights inside the harbour are not proportional to H^2_{mo} inside the harbour.

Table 6.1. Values of R^2 and C_X for the different relations

Relation	C_X (prototype)	R^2
1	6.8803 (-)	0.7193
2	8.6475 (1/m)	0.5761
3	10.17 (-)	0.9348
4	15.602 (1/m)	0.6301

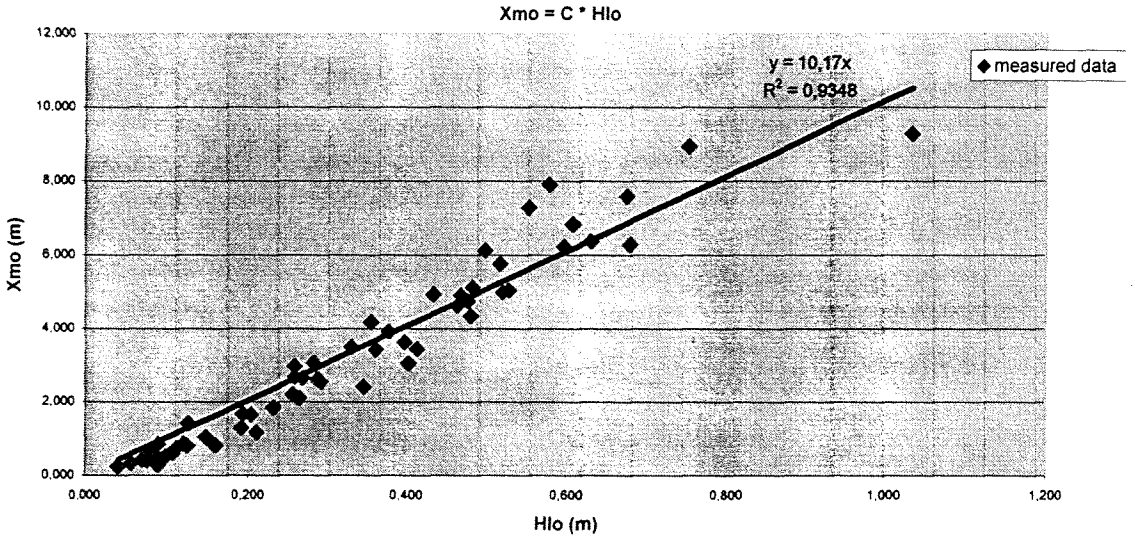

Figure 6.1. Surge motion versus wave field, $X_{mo} = C_{X3} * H_{lo}$

There is no unambiguous relation gathered from the theory concerning the influence of the wave period on the ship motions. Van Oorschot (1976) concludes that the low frequency part of the motion increases with increasing peak period of the wave spectrum, but he does not reveal to what extent. Deelen (1984) also confirms the dependency of the surge motion on the peak period.

In order to examine the peak period influence, the following relations are tested:

1) $X_{mo} = C_X * H_{lo}$
2) $X_{mo} = C_X * H_{lo} * T_P$
3) $X_{mo} = C_X * H_{lo} * T_P^2$

The result is shown in Table 6.2. This table gives the values of R^2 for each of the three relations. The validity of the relation decreases significantly with the inclusion of T_P. The R^2 value of the relation including T_P^2 is low to such an extent that the relation cannot be considered valid at all.

Table 6.2. Values of R^2 for relations including peak periods

	$X_{mo}=C_X*H_{lo}$	$X_{mo}=C_X*H_{lo}*T_P$	$X_{mo}=C_X*H_{lo}*T_P^2$
R^2 value	0.9348	0.8498	0.5116

It is concluded that the accuracy decreases with the inclusion of the peak period in the relation. A relation with dimensionless coefficient is preferred. Consequently, the relation for the surge motion becomes:

- $X_{mo} = 10 * H_{lo}$ (6-2)

The surge motion relates linearly to the low frequency significant wave height with a value that is not varying significantly with the peak period of the incident short wave spectrum.

6.2.2. Application to model ship

Linear mass-spring system

Since the surge motion relates linearly to the low frequency significant wave height it is assumed that the system of the moored ship can be represented by a linear mass-spring system. The representation of the moored model ship by a mass-spring system is discussed in Appendix 12. To verify if the assumed representation is valid the energy spectrum of the surge motion is calculated and compared to the measured energy spectrum.

A surge energy spectrum is calculated by multiplying a measured wave energy spectrum (at W1) with the square of the response amplitude operator (RAO) of the moored ship (see Appendix 12). This is done for five different wave fields that are characterized by the peak period of the overall wave field (WC10, WC12, WC14, WC16 and WC18). Since the direction of the waves near the ship is visually estimated between 130° and 150°, all calculation are performed for three wave directions (130°, 140° and 150°).

Initially the surge motion is calculated for a stiffness of the mooring system parallel to the quay of k_X = 472 kN/m (prototype). This leads to overestimation of the surge motion. Furthermore, the calculated surge shows, for all wave conditions, a peak near frequencies lower than the peak frequency of the measured surge motion (see Appendix 12). Since the natural frequency results from the choice of the spring coefficient, the stiffness is increased to k_x = 1 550 kN/m (prototype). Table 6.3 shows the calculated significant surge motions for all five wave fields and for all three wave directions near the ship. Both the absolute value and the percentage of the measured value are presented.

Table 6.3. Calculated and measured significant surge motion (k_X = 1550 kN/m, prototype)

	Measured	Calculated 150°		Calculated 140°		Calculated 130°	
T_P (s)	X_{mo} (m)	X_{mo} (m)	X_{mo} (%)	X_{mo} (m)	X_{mo} (%)	X_{mo} (m)	X_{mo} (%)
10	13.8	6.4	46	5.8	42	5.0	36
12	6.6	9.6	145	8.7	132	7.5	114
14	6.2	11.0	177	10.0	161	8.7	140
16	12.8	11.0	86	9.9	77	8.6	67
18	12.8	15.9	124	14.5	113	12.6	98

It can be concluded that the calculated surge motion is of the same magnitude as the measured surge motion. The ratio of the calculated and the measured significant surge motion is between 0.4 and 1.8 for all considered wave fields and directions.

Empirical relation

In their investigation, Mol et al. (1985) also schematised the moored ship as a linear damped mass spring system with one degree of freedom. The following empirical relation was found on the basis that the dynamic motion is the static value multiplied by a coefficient that represents the dynamic influence:

$$X_S = C_X \cdot H_{SI} \cdot \sqrt{\frac{g \cdot M}{d \cdot k_t}} \qquad (6\text{-}3)$$

in which
X_S = significant surge motion
C_X = coefficient
H_{SI} = long period significant wave height
g = gravitational force
M = mass of the ship
k_t = stiffness of the mooring system in parallel to the quay
d = water depth

In Section 6.2.1 the following relation is found:

$$X_{mo} = 10 \cdot H_{lo} \qquad (6\text{-}4)$$

With substitution of:
g = 10 m/s^2
m = 80.7·10^6 kg
k_X = 472 kN/m
d = 17 m
Relation 6-4 can be rewritten as:

$$X_{mo} = C_X \cdot H_{lo} \cdot \sqrt{\frac{g \cdot m}{d \cdot k_X}} = 1.0 \cdot C_X \cdot H_{lo} \qquad (6\text{-}5)$$

According to Equation 6-5 the value of C_X is 10. Mol et al. found C_X values ranging between 1 and 3, with an average of 1.7.

As described in Appendix 12, a mooring stiffness of 472 kN/m leads to a peak in the surge spectrum at lower frequencies than the peak in the measured surge spectrum. In order to equal the natural period of the calculated data to the natural period of the measured data the mooring stiffness is altered. With a stiffness of the mooring system parallel to the quay of k_X = 1 550 kN/m the value of C_X becomes 1.8.

If the assumed stiffness of k_X = 1 550 KN/m is a correct representation of the stiffness of the mooring system in the physical model, it can be concluded that the measured data show a value of C_X that is equivalent to the values found by Mol et al. (1985).

Gradient in water level

As mentioned in Section 5.1 standing waves occur in harbour basins when the natural period of oscillation of the basin equals the period of incident waves. For the Coega model tests this phenomenon occurs near a frequency of 0.006 Hz. In that case a node is present near the position of the moored ship. This node brings about large horizontal water motions possibly leading to large horizontal ship motions.

It is expected that the gradient of the water level near the node can also produce surge motion. The gradient in the water level creates a harmonic force on the moored ship that can be the cause of surge motion of the moored ship. This phenomenon is discussed in Appendix 14.

The amplitude of the surge motion as calculated in Appendix 14 is 2.1 m. The measured significant surge at that frequency band is 4m. In other words, the ratio of the calculated and the measured surge motion is 0.5. This indicates that the gradient of the water level can lead to surge motion. However, the magnitude of the calculated surge is only 50% of the measured surge.

It is noted that the calculations in Appendix 14 apply to one particular wave condition; wave height 6m, wave direction 160° and peak period 18 s. The energy spectrum of this condition (see Appendix 9e) shows significant surge motion near the period T_1 = 172 s. For other wave conditions this might not be as clear. Consequently, this section merely shows that the gradient of the water level could lead to surge motions. It does not show that all measured surge motion in the Coega model tests is due to this phenomenon.

Drift forces

In Section 6.2.1 it is concluded that the surge motion relates linearly to the low frequency significant wave. Consequently, the application to the model ship has been on the basis of this linear relation. The surge motion has been calculated by means of a linear relation with the low frequency wave forces. In order to investigate to whole frequency range, the surge motion is calculated by means of a linear relation with the wave frequency drift forces in Appendix 13. The drift forces relate quadratically to the wave elevation. As a result, the surge motion in relation to the square of the wave height is investigated.

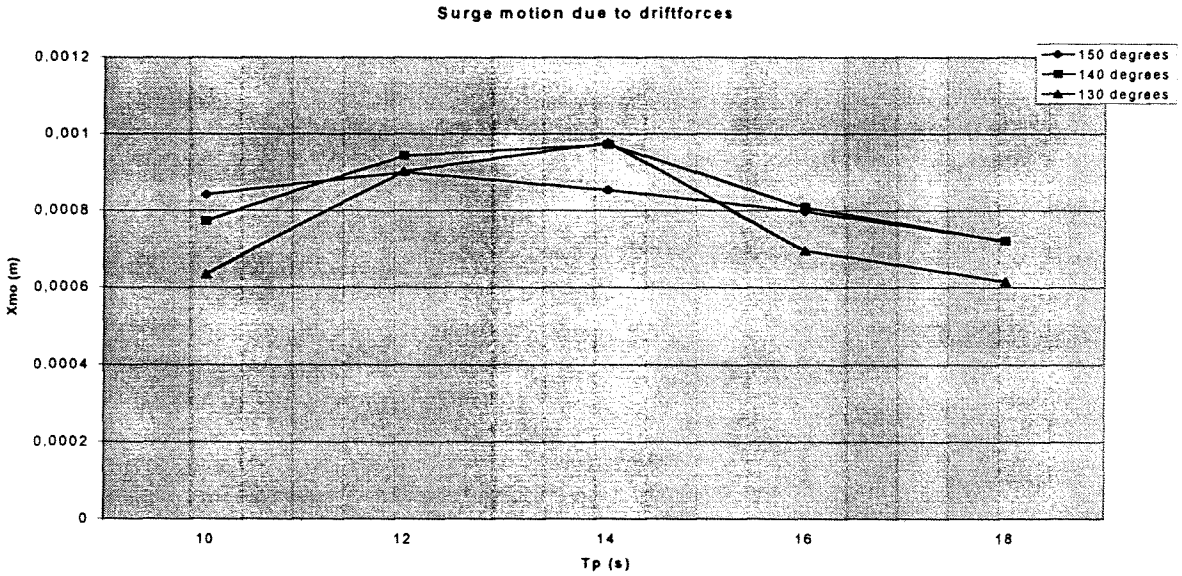

Figure 6.2. Calculated surge motion due to drift forces

Figure 6.2. shows the surge motion calculated by means of a linear relation of the surge motion to the drift forces over the whole frequency range. As expected, the surge motion due to the drift forces is of negligible magnitude compared to the measured surge motion in the Coega model tests. This conclusion is in agreement with the hypothesis that the surge motion is mainly due to the low frequency wave forces.

6.3. Roll motion

6.3.1. Verification of hypotheses

The hypothesis regarding the roll motions as developed in Chapter 5 is:

- $\Phi_{mo} = C_{\phi}(T_P) * H_{hi}$ (6-6)

in which $C_{\phi}(T_P)$ is a function of the peak period. The shape of this function depends on the natural period of roll.

For the sake of completeness and as a comparison, more equations are considered than just this hypothesis. All the measured data are divided into five groups of, more or less, constant wave period in order to increase insight in the influence of the natural period of roll. For the five groups separately it is investigated to what extent they fulfil the relations. The result is shown in Appendix 15. This appendix gives an overview of the R^2 values for all the relations that are taken into account. The following conclusions result from these R^2 values:

- There is an unmistakable relation between the high frequency wave height, H_{hi}, and the roll motion, Φ_{mo}. This is in accordance with the hypothesis for roll.
- A relation between the low frequency part of the wave height, H_{lo}, and the roll motion is not found despite the coupling between roll and sway. This was expected, as mentioned in Section 5.4.2.
- The significant wave height is, as expected, not of importance. For some peak periods there is a relation between H_{mo} and Φ_{mo}. However, the R^2 value for those peak periods is again and again higher for the relation between H_{hi} and Φ_{mo}. Therefore, an expression with H_{mohi} is preferred over an expression with H_{mo}.

Considering the abovementioned conclusions, the parameters H_{lo} and H_{mo} are left out of consideration. Table 6.4 gives an overview of the values of R^2 and C_{ϕ} found for the relations regarding the high frequency significant wave height, H_{hi}.

In connection with the important influence of the natural period of roll, all relations are tested for both the whole frequency range and for specific bandwidths of the wave spectrum. As a result each group of constant period contains less measured data. Whenever there is a group in which the measured data consist of less than three points, this period is not taken into account.

Table 6.4. Values of R^2 and C_ϕ (in model values) for relations with H_{hf}

Relation :	$\Phi_{ma} = C_{\phi 1} * H_{hf}$		$\Phi_{ma} = C_{\phi 2} * H_{hf} * T_P$		$\Phi_{ma} = C_{\phi 3} * H_{hf} * T^2_P$	
T_P (s)	R^2	$C_{\phi 1}$(°/m)	R^2	$C_{\phi 2}$(°/ms)	R^2	$C_{\phi 3}$(°/ms²)
10	0.8081	2.7043	0.8080	0.2664	0.8076	0.0262
12	0.8249	6.0382	0.8072	0.5081	0.7809	0.0427
13	**0.8514**	7.2255	0.8156	0.5562	0.7632	0.0427
14	**0.8639**	4.6629	**0.8723**	0.3339	**0.8793**	0.0239
16	**0.9000**	5.3746	**0.9104**	0.3394	**0.9188**	0.0214
17	**0.9564**	4.5454	**0.9591**	0.2640	**0.9613**	0.0153
18	**0.9309**	4.6851	**0.9175**	0.2604	**0.9025**	0.0145
All T_P	0.7084	4.8574	0.6516	0.3334	0.4086	0.0202

The values of Table 6.4 lead to the following conclusions:

- The R^2 values of the relations over the whole range of periods are very low. Definitely not sufficient to confirm a relation. Consequently, no unambiguous relation (valid for all wave periods) can be derived for the roll motion.
- Per group of constant peak period the R^2 values are sufficiently high. The groups with peak periods 10 s and 12 s do not fulfil the requirement of 0.9. But the R^2 values are high enough to consider the relation valid.
- Per group of constant period, the relative difference between the R^2 values of the three relations is small.

Figure 6.3 shows the $C_{\phi 1}$ values, which are not constant but depend on the peak period. This is in accordance with the hypothesis for roll in which $C_\phi(T_P)$ (= $C_{\phi 1}$) is a function of the peak period. The form of this function is supposed to be influenced by the natural period of roll (T_ϕ = 12 s). Accordingly, the $C_\phi(T_P)$ function shows a peak for T_P values of 12s and 13s.

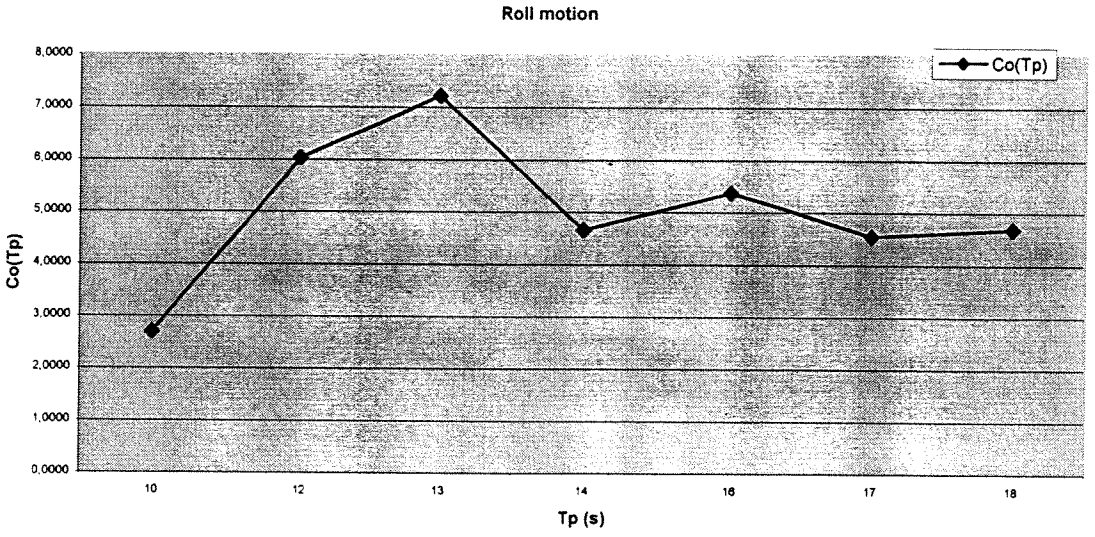

Figure 6.3. Values $C_{\phi 1}$ versus peak period of wave field

There is a proportionality between the roll motion and the high frequency significant wave height. The ratio between the ship motions and the wave height is a function of the peak period. This function appears to be influenced by the natural period of roll.

6.3.2. Application to model ship

In this section the ratio between the roll motion and the wave height is investigated. It is tried to the reproduce the measured function $C_\phi(T_p)$ by means of the response amplitude operator of a free-floating ship. The energy spectrum of the roll motion is calculated with the following equation:

$$S_\phi(\omega) = \left[\frac{\hat{\phi}}{\hat{\zeta}}(\omega)\right]^2 \cdot S_\zeta(\omega) \tag{6-7}$$

From this energy spectrum the significant roll motion can be calculated.

According to Equation 6-6 a wave field with a significant wave height of 1 m and a specific peak period leads to a significant roll motion equal to the $C_\phi(T_p)$ value for that peak period. By determining the significant roll motion for several peak periods a number of values of $C_\phi(T_p)$ can be calculated and compared to the $C_\phi(T_p)$ function as found in Section 6.3.1. Figure 6.4 shows the $C_\phi(T_p)$ function calculated for wave directions 130°, 140° and 150° together with the measured $C_\phi(T_p)$ function.

The JONSWAP wave spectrum is calculated with Equation 6-8.

$$S_\zeta(\omega) = \frac{320 \cdot H_{1/3}^2}{T_p^4} \cdot \omega^{-5} \cdot \exp\left\{\frac{-1950}{T_p^4} \cdot \omega^{-4}\right\} \cdot \gamma^4 \tag{6-8}$$

in which
S_ζ = JONSWAP wave spectrum
$H_{1/3}$ = significant wave height (1 m)
T_p = peak period of the wave spectrum (10 s, 12 s, 14 s, 16 s and 18 s)
ω = angular frequency
γ = peakedness factor (3.3)

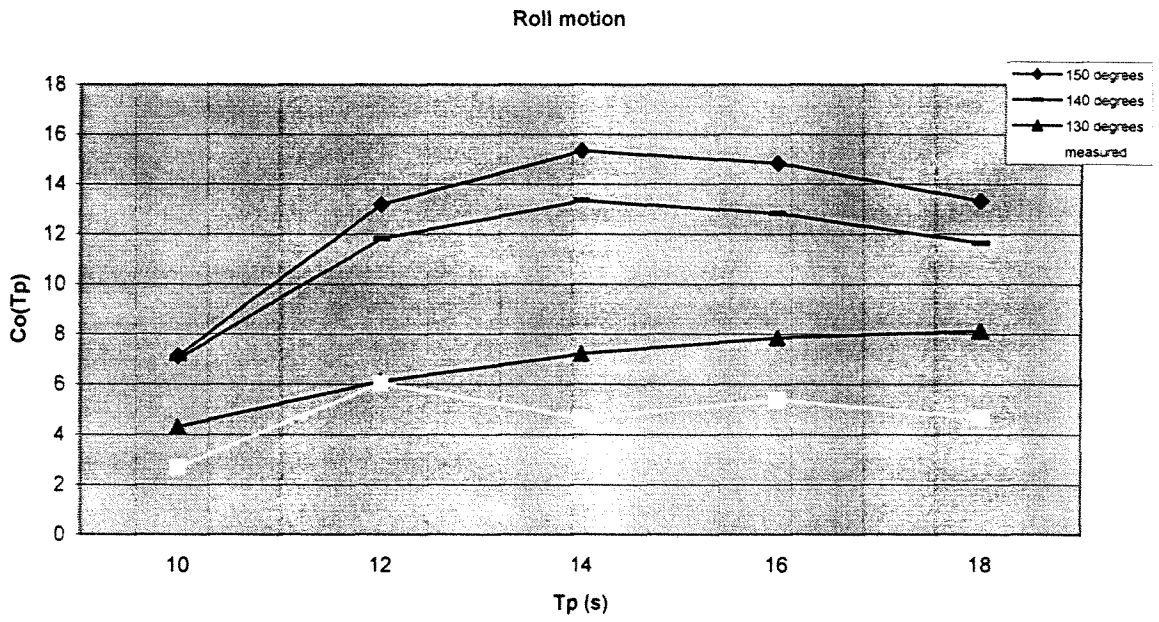

Figure 6.4. Comparison of the calculated and measured $C_\phi(T_p)$ function

Figure 6.4 shows that the calculated values are higher than the measured values. This is as expected since the values are calculated for a free floating ship while the measured values represent a moored ship. The calculated $C_\phi(T_p)$ function shows a peak for a period of 14 s. The peak in the measured $C_\phi(T_p)$ function is around 12 s. This, too, can be explained by the difference between moored and free-floating roll motions. The natural roll period of a moored ship is lower than that of a free-floating ship.

It can be concluded that the $C_\phi(T_p)$ function calculated for a free-floating ship overestimates the roll motions of a moored ship.

6.4. Sway motion

6.4.1. Verification of hypotheses

The hypotheses regarding the sway motions as developed in Chapter 5 are:

- $Y_{mo} = C_{hi}(T_P) * H_{hi} + C_{lo} * H_{lo}$ (6-9)

in which $C_{hi}(T_P)$ is a function of the peak period and C_{lo} is constant

- $Y_{mo} = C(T_P) * H_{mo}$ (6-10)

in which $C(T_P)$ is a function of the peak period The shape of this function depends on both the natural period of roll and the natural period of sway.

For the sake of completeness and as a comparison, more equations are considered than just the hypotheses. The result is shown in Appendix 15. This appendix gives an overview of the R^2 values for all the relations that are taken into account. The following conclusions result from these R^2 values:

- Despite the coupling between the roll motion and the sway motion no relation is found between the high frequency part of the wave field, H_{hi}, and the sway motion. This implies that the first part of the right-hand side of formula 6-6 does not correspond with the measured data. Consequently this part is not included during further investigation.
- The low frequency significant wave height (H_{lo}) is not of importance. For specific peak periods there is a relation between H_{lo} and Y_{mo}. However, the R^2 value for those peak periods is again and again higher for the relation between H_{mo} and Y_{mo}. Therefore, an expression with H_{mo} is preferred over an expression with H_{lo}.
- The R^2 values of the relations with the significant wave height, H_{mo}, are indeed higher than those of other relations but they do not fulfil the requirement of 0.9. So for the sway motion the condition of 0.9 is lowered to 0.8.

In view of the preceding conclusions Relation 6-9 is not investigated further. This hypothesis is dismissed. Relation 6-10 is investigated further in order to determine the influence of the peak period.

Table 6.5 contains an overview of the values of R^2 and C_X found for relations including the peak period. The function $C_Y(T_P)$ in Relation 6-10 is supposed to be influenced by the natural periods of both roll and sway. In order to investigate this assumed influence, all relations are tested for both the whole frequency range and for specific bandwidths of the wave spectrum. There are seven groups of constant peak period. The groups with a period of 11 s, 15 s, and 17 s do not exist because there are not enough measured data for these periods.

Table 6.5. Values of R^2 and C_Y (in model values) for relations with H_{mo}

Relation:	$Y_{mo} = C_{Y1} * H_{mo}$		$Y_{mo} = C_{Y2} * H_{mo} * T_P$		$Y_{mo} = C_{Y3} * H_{mo} * T^2_P$	
T_P (s)	R^2	C_{Y1} (-)	R^2	C_{Y2} (1/s)	R^2	C_{Y3} (1/s²)
10	**0.8008**	0.8816	**0.7960**	0.0867	**0.7906**	0.0085
12	0.5330	1.7173	0.5474	0.1449	0.5588	0.0122
13	0.6012	1.6672	0.5463	0.0989	0.4817	0.0098
14	**0.8478**	1.3845	**0.8496**	0.1280	**0.8509**	0.0071
16	0.7018	1.9570	0.6916	0.1227	0.6796	0.0077
17	**0.8690**	1.9071	**0.8721**	0.1107	**0.8745**	0.0064
18	**0.8100**	2.4010	**0.7883**	0.1330	**0.7657**	0.0074
All T_P	0.6669	1.7033	**0.7584**	0.1187	0.7013	0.0074

The values of Table 6.5 lead to the following conclusions:

- The R^2 values of the relations over all peak periods are low. Only the relation $Y_{mo} = C_{s2} * H_{mo} * T_P$ fulfils the condition of 0.8.
- The groups with constant peak periods of 10 s, 14 s, 17 s and 18 s show R^2 values higher than 0.8. This goes for all three relations.
- Opposite applies to the groups with peak periods of 12 s, 13 s and 16 s.
- The difference of the R^2 values is small between the three relations.

Perhaps the deviation of the R^2 values for the peak periods of 12 s and 13 s can be attributed to the coupling between the sway motion and the roll motion. For these periods resonance takes place because of correspondence of the wave period to the natural roll period of the ship. The high values of C_{s1} confirm this. Normally, without coupling of roll and sway, these values would be between 0.9 and 1.4. The value of 1.7 is clearly higher and indicates larger sway motions.

The deviation of the R^2 value of the group with constant peak period of 16 s cannot be explained this way. These R^2 values do not deviate as much as those for 12 s and 13 s. Probably this deviation is due to an accidental irregularity in the measured data.

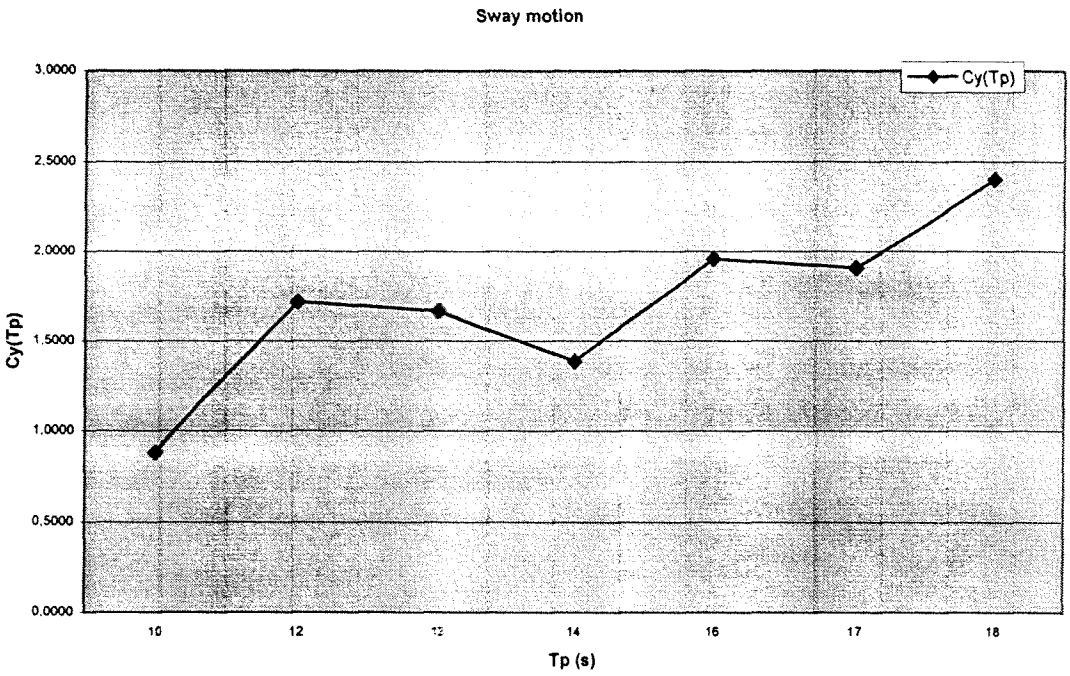

Figure 6.5. Values C_{YI} versus peak period of wave field

Figure 6.5 shows that the C_Y values are not constant but depend on the peak period. This is in accordance with the hypothesis for sway in which $C_Y(T_P)$ (= C_{YI}) is a function of the peak period. The form of this function is supposed to be influenced by the natural period of roll. In general the $C_Y(T_P)$ function increases with increasing peak period. Near a peak periods of 12 s a discontinuity is present. This indicates coupling of the sway motion to the roll motion.

There is a proportionality between the sway motion and the significant wave height. The ratio between the ship motion and the wave field is a function of the peak period. This function increases whit increasing peak period and appears to be influenced by the natural period of roll.

6.4.2. Application to model ship

The ratio between the sway motion and the wave height is investigated in the same way as the roll motion in section 6.3.2. It is tried to the reproduce the measured function $C_Y(T_p)$ by means of the response amplitude operator of a free-floating ship. Figure 6.6 shows the $C_Y(T_p)$ function calculated for wave directions 130°, 140° and 150° together with the measured $C_Y(T_p)$ function.

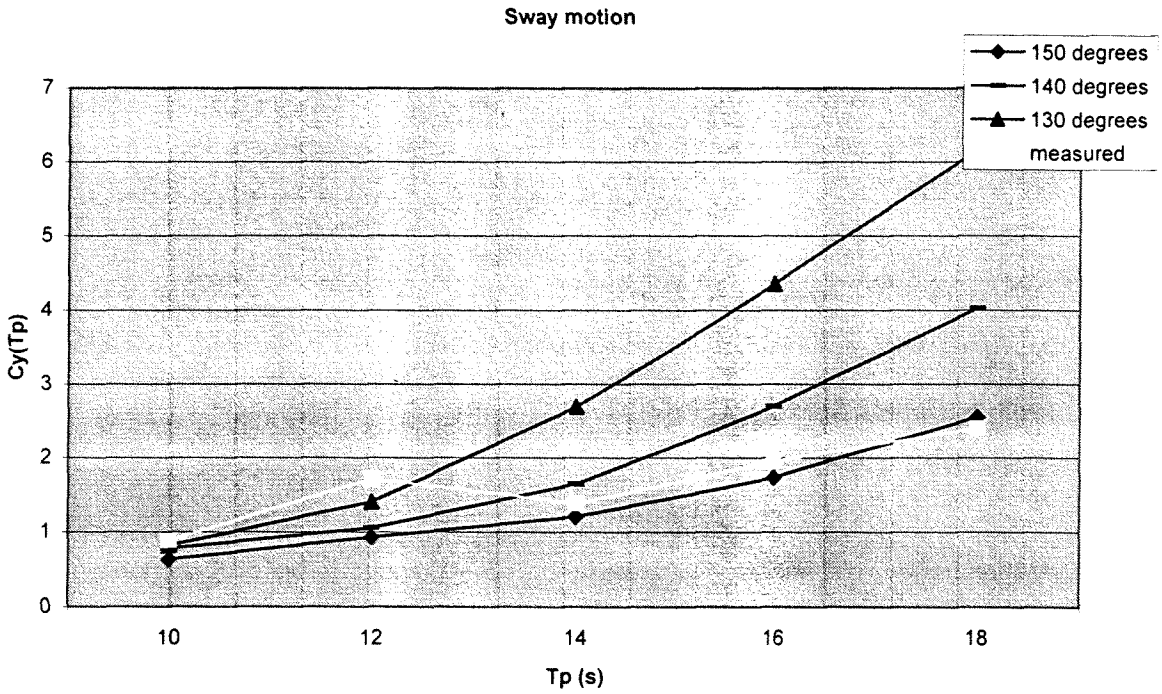

Figure 6.6. Comparison of the calculated and measured $C_Y(T_p)$ function

Figure 6.6 shows that the calculated values for a wave direction of 150° represent the measured values to a large degree. At a peak period of 12 s the calculated value is smaller than the measured value. Here, larger sway motions occur for a moored ship than for a free floating ship, due to coupling with the roll motion.

It can be concluded that the $C_Y(T_p)$ function calculated for a free-floating ship can represent the $C_Y(T_p)$ function of a moored ship. Only around the natural roll period this function underestimates the sway motion of a ship since the coupling with the roll motion is not taken into account.

7. Conclusions and recommendations

7.1. Introduction

The aim of the project described in this report is to come to straightforward relationships to describe the behaviour of moored ships. In other words, to derive simple relations between motions of a moored ship and the wave field near the ship. It is emphasized that this project is limited to one type of ship moored with one type of mooring system inside one specific harbour. Consequently, the conclusions of this project do not contain general validity. Nonetheless, the results of this project present tools that contribute to the understanding of the response of a moored ship to incident waves.

7.2. Conclusions

Hypotheses with regard to the surge, sway and roll motion are derived from the theory on the behaviour of a moored ship. These hypotheses are verified using the data measured in the physical model. The following conclusions result from validation of the hypotheses:

- The surge motion relates linearly to the low frequency significant wave height with a value that is not varying significantly with the peak period of the incident short wave spectrum.
- The roll motion is proportional to the high frequency significant wave height. The ratio between the ship motions and the wave height is not constant for different wave fields. The ratio is a function of the peak period that appears to be influenced by the natural period of roll.
- For the sway motion a proportionality between this ship motion and the significant wave height is observed. The ratio between the ship motion and the wave field is a function of the peak period. This function increases with increasing peak period and appears to be influenced by the natural period of roll.

Because of the linear relation between the surge motion and the low frequency wave field it is assumed that the system of the moored ship can be represented by a linear mass-spring system. To verify the assumed representation, the energy spectrum of the surge motion is calculated and compared to the measured energy spectrum. This comparison shows that the calculated surge motion is of the same magnitude as the measured surge motion. The ratio of the calculated and the measured significant surge motion is between 0.4 and 1.8 for all considered wave fields and directions.

Mol et al. (1985) also schematised the moored ship as a linear damped mass spring system with one degree of freedom. They formulated an empirical relation on the basis that the dynamic motion is the static value multiplied by a coefficient (C_X) that represents the dynamic influence. Mol et al. (1985) found C_X values ranging between 1 and 3, with an average of 1.7. The value of C_X found for the measured data of the Coega model tests is 1.8, which is within the range found by Mol et al. (1985).

Standing waves occur in harbour basins when the natural period of oscillation of the basin equals the period of incident waves. For the Coega model tests this phenomenon occurs near a frequency of 0.006 Hz. In that case a node is present near the position of the moored ship. It is estimated that the gradient of the water level near the node can produce surge motion. The ratio of the surge motion calculated by means of the gradient force and the measured surge motion is 0.5. This indicates that the gradient of the water level can lead to surge motion but it does not show that all measured surge motion in the Coega model tests is due to this phenomenon.

In order to investigate to whole frequency range, the surge motion is calculated by means of a linear relation with the wave frequency drift forces. The drift forces relate quadratically to the wave elevation. As a result, the surge motion in relation to the square of the wave height is investigated. As expected, the surge motion due to the drift forces is of negligible magnitude compared to the measured surge motion in the Coega model tests. This conclusion is in agreement with the hypothesis that the surge motion is mainly due to the low frequency wave forces.

The ratio between the ship motion and the wave height, $C(T_p)$, is investigated for both roll and sway. The ship motion spectrum is calculated by multiplying the square of the response amplitude operator of a free-floating ship with a wave spectrum of which the significant wave height is 1 m. The JONSWAP wave spectrum is calculated for several peak periods. Since the significant wave height is 1 m, the significant ship motion is equal to the C value for each specific peak period. By determining the significant ship motion for several peak periods the $C(T_p)$ function can be calculated and compared to the $C(T_p)$ function as found from the measured data.

The $C_\phi(T_p)$ function calculated for a free-floating ship overestimates the roll motions of a moored ship. The natural roll period of a moored ship is lower than that of a free-floating ship. Consequently, the calculated $C_\phi(T_p)$ function shows a peak at a higher value of T_p than the measured $C_\phi(T_p)$ function.

The $C_Y(T_p)$ function calculated for a free-floating ship represents the $C_Y(T_p)$ function of a moored ship to a large degree. Around the natural roll period this function underestimates the sway motion of a ship since the coupling with the roll motion is not taken into account.

7.3. Recommendations

The physical model study of the Coega harbour was not conducted in order to investigate the behaviour of moored ships in general. The data used in this MSc-project is limited to the results of this model study in which type of ship, mooring system and harbour layout are not varied. The conclusions resulting from this project are limited to the investigated conditions. In order to come to relations of general validity more investigation is needed. It is recommendable to conduct a physical model study of which the research objective is primarily to derive relations describing the ship's behaviour.

This study should investigate more than the ships response to incident waves. The mooring system and ship characteristics should be varied in order to investigate their influence on the ship's behaviour. It should be kept in mind that the objective is to develop a simple model that provides a valuable design tool to be used in an early stage of the port development process. During the planning phase of new harbour detailed information is not available. The recommended investigation can be set up accordingly. For instance the type of ships can be divided roughly in three categories each represented by one model ship. Due attention should be paid to the mooring system since the choice of the mooring stiffness determines the ship motions to a high degree.

It is concluded that the surge motion relates linearly to the low frequency significant wave height. Schematisation of the Coega model ship as a linear damped mass spring system with one degree of freedom results in a C_X value within the range found by Mol et al. (1985). Consequently, it is suggested that future investigation continues with this concept.

Roll motions calculated for a free-floating ship overestimate the motions of a moored ship. It is advised to include the mooring system in order to derive more accurate results. Sway motions calculated for a free-floating ship provide a fairly accurate representation of the moored ship motions. By taking into account the coupling with the roll motion the calculations can be improved.

The results of this physical model study should be compared to prototype measurements in order to validate the conclusions of the study. It is this writer's opinion that a simple computer (spreadsheet) programme can be developed after the conduction of a comprehensive physical model study.

References

Barthel, V., Mansard, E.P.D., Sand, S.E., Vis, F.C. (1983), "Group bounded long waves in physical models", Ocean Engineering, vol. 10, no. 4, pp 261-294

Barthel, V., Mansard, E. (1994), "Influences of long waves on ship motions in a lagoon harbour", Coastal Engineering 1994, vol. 1, pp 791-805

Bingham, H.B. (1999), "A hybrid Boussinesq-panel method for predicting the motion of a moored ship", Coastal Engineering 40, vol. 1

Blevins R.D. (1995), "Formulas for natural frequency and mode shape", Malubar, Krieger, pp 492

Bowers, E.C. (1977), "Harbour resonance due to set-down beneath wave groups", J. Fluid Mech., vol. 70, part 1, pp 71-92

Burcharth, H.F. (1980), "Comparison of nature waves and model waves with special reference to wave grouping", 17th International Conference on Coastal Engineering, Sydney, pp 169-201

Bruun Per (1989), "Port Engineering: Harbour Planning, Breakwaters, and Marine Terminals", vol. 1, 4th edition, Houston, Gulf, pp 1461

DiCastro, F., Drimer, N., Glozman, M., Harari, P., Keren, Y., Radomir, M., Sheremet, A., Stiassnie, M., Zwamborn, J.A. (undated),"A numerical model for studying the motion of berthed ships in harbours" CAMERI, Coastal and Marine Engineering Research Institute, Technion City, Israel, pp 335-341

Deelen, C. (1984), "Port of Sines, ship motion study, part 5, report on model study", Delft Hydraulics Laboratory, Delft Soil Mechanics Laboratory

Headland, J.R., Ying-Keung Poon, P.E. (1998), "Numerical modeling of long wave ship motions", Coastal Engineering 1998, pp 1337-1349

Journée, J.M.J., Massie W.W. (2000), "Offshore hydromechanics", Delft University of Technology, 1st edition

Keith, J.M. (1973), "Ship's response to quartering seas", Papers presented at Nato advanced study institute on analytical treatment of problems in the berthing and mooring of ships, Wallingford, England, pp 217-220

Kilner, F.A. (1960), "Model tests on the motion of moored ships placed on long waves", Proceedings of seventh conference on Coastal Engineering, The Hague, Netherlands, pp 723-745

Lean, G.H. (1971), "Subharmonic motions of moored ships subjected to wave action", Transactions of the Royal Institute of Naval Architects, London, vol. 113, pp 387-399

Massie, W.W. (1973), "Non-linear surge motion of a moored ship", Papers presented at Nato advanced study institute on analytical treatment of problems in the berthing and mooring of ships, Wallingford, England, pp 299-329

McGehee, D.D. (1991), "Measured response of moored ships to long period waves at Los Angles and Long Beach harbors", P.I.A.N.C.- A.I.P.C.N., Bulletin 1991, N° 75, pp 7-15

Moes, H., Hough, G. (undated), "Measurement of moored ship motions using video imaging technology", South-Africa, pp 281-290

Moes, (1999), "Assessment of vessel motions at berth 1 based on a physical model study" *(proprietary document)*

Moes, Van Aswegen (1999), "Coega harbour: Model tests of moored ship motions at the ore quay", progress report no 1 *(proprietary document)*

Moes, Van Aswegen (1999), "Coega harbour: Model tests of moored ship motions at the ore quay", progress report no 2 *(proprietary document)*

Moes (1997), "Coega harbour: Long-wave conditions in the harbour" *(proprietary document)*

Mol, A., Ligteringen, H., Waanders, A.J. (1985), "Motions of moored vessels, a statistical approach"

Muckle, W. (1987), "Muckle's Naval Architecture", London, Butterworths, pp 461

Nagai, T., Hashimoto, N., Asai, T., Tobiki, I., Ito, K., Toue, T., Kobayashi, A., Shibata, T. (1994), "Relationship of a moored vessel in a harbour and a long wave caused by wave groups", Coastal Engineering 1994, vol. 1, pp 847-860

O'Brien, W.T. (1985), "The slow drift oscillations of moored vessels: field measurement, model calibration and parametric analyses", International Conference of Numerical and Hydraulic Modelling of Port and Harbours, Birmingham, England, pp 195-210

Raichlen, F., Lee, J.J., Walker, J.R. (undated), "Physical modelling of harbour resonance", pp 193-207

Rawson, K.J., Tupper, F.C. (1983), "Basic ship theory: Ship design and construction", vol. 1, London, Longman, pp 701

Russell, R.C.H. (1959), "A study of the movement of moored ships subjected to wave action", Proceedings of the institution of civil engineers, London, vol. 12, paper No. 6341, pp 379-398

Sand, S.E. (1982), "Long wave problems in laboratory models", J. Waterway Port Coastal and Ocean, div. 108, pp 492-503

Shiraishi, S., Kubo, M., Ueda, S., Sakakibara, S. (undated), "A countermeasure by mooring system for moored ship motion under long period waves", Japan, pp 207-216

Shiraishi, S., Yoneyama, H., Sakakibara, S., Sasa, K. (undated), "Numerical estimation of low-frequency ship oscillations in harbours and its applications to port facility design", Report of the port and harbour research institute, vol. 37, No. 4, pp 37-77

Shiraishi, S. (1998), "Low-frequency ship motions due to long-period waves in harbors, and modifications to mooring systems that inhibit such motions", Japan, pp 389-398

Shiraishi, S., Nagamatsu, K., Umihara, T. (1999), "Analysis on the fender deformation by moored ship motions due to wave actions at ocean facing port", Proceedings of the Ninth International Offshore and Polar Engineering Conference, Brest, France, pp 582-589

Schneekluth, H. (1987), "Ship design for efficiency and economy", London. Butterworth, pp 266

Ueda, S. (1987), "Analytical method of ship motions moored to quay walls and application to port planning", Coastal Zone '87, WW Div., A.S.C.E., Seattle WA, pp 1545-1559

Ueda, S., Shiraishi, S. (1988), "The allowable ship motions for cargo handling at wharves", Report of the port and harbour research institute, vol. 27, nr. 4, pp 3-61

Ueda, S., Shiraishi, S. (1989), "Ship motions moored at quay walls and their effects to wharf operation efficiency", Proceeding of sixth symposium on coastal and ocean management ASCE, Charleston, SC, pp 2271-2285

Van den Bunt, J.D. (1973), "Model study on mooring forces due to regular and irregular waves", Papers presented at Nato advanced study institute on analytical treatment of problems in the berthing and mooring of ships, Wallingford, England, pp 251-265

Van Oorschot, J. H. (1976), "Subharmonic components in hawsers and fender forces", paper presented at the 15th international conference on coastal engineering, Honolulu

Van Tonder, A (1991), "A hydraulic model wave synthesis package for 2-D flume studies, phase 1" CSIR Technical report, Stellenbosch

Vis, F.C., Keuning, P.J. (1979), "Yanbu industrial complex port, hydraulic studies, part 4, technical design study on ship motion", Yanbu industrial complex port, Delft Hydraulics Laboratory *(proprietary document)*

Wilson, B.W. (1973), "Progress in the study of ships moored in waves", Papers presented at Nato advanced study institute on analytical treatment of problems in the berthing and mooring of ships, Wallingford, England, pp 143-213

THE ANALYSIS OF MODEL MEASUREMENTS CONCERNING THE BEHAVIOUR OF MOORED SHIPS IN LONG WAVES

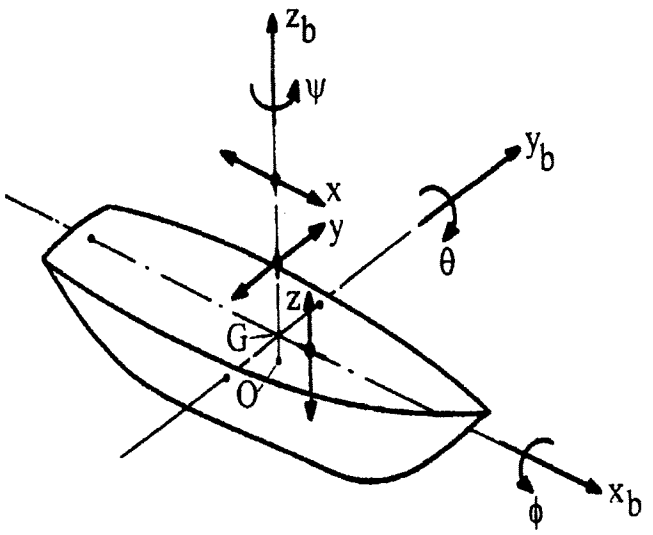

APPENDICES

Jadwiga Sarneel
728182

DECEMBER 2000

MSc PROJECT

DELFT UNIVERSITY OF TECHNOLOGY, FACULTY OF CIVIL ENGINEERING AND GEOSCIENCES, SECTION OF HYDRAULIC ENGINEERING

COMMITTEE:

- PROF. IR. H. LIGTERINGEN
- PROF. DR. IR. J.A. BATTJES
- IR. R. GROENVELD
- IR. H. MOES
- PROF. DR. IR. J.A. PINKSTER

List of Appendices

Appendix 1 Bathymetric charts

1.a Bathymetric chart of Algoa Bay

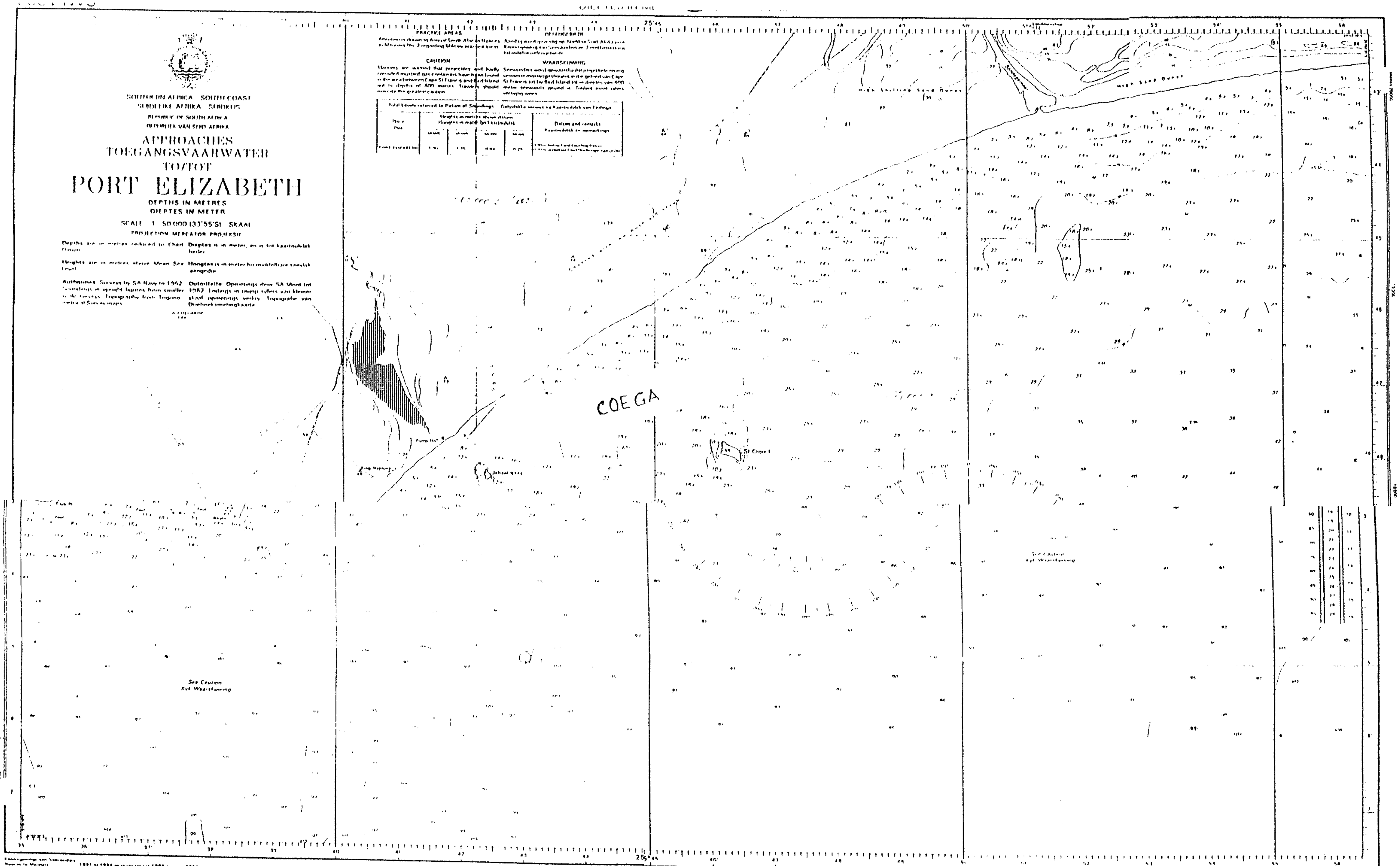

Published at Cape Town on 26 Sep 1980 under the Superintendence of Captain C.J.H. Wagenfeld, Hydrographer, SA Navy
1980 onder toesig van Kaptein C.J.H. Wagenfeld, Hidrograaf, SA Vloot

SAN 1024

Appendix 1 Bathymetric charts

1.b Bathymetric chart of Coega Harbour

SALT WORKS
RAIL ROAD
BERTH 1
TUG BERTH
SILT TRAP
RIVER CHANNEL
FUEL BERTH
CHANNEL DEVIATION
RECLAMATION
0 MSL
0 MSL
-10
-11
-12
-13
-14

Appendix 2 Form coefficients

Source: Rawson and Tupper (1983)

Form coefficients are used in defining the ship form. They express the fatness or slimness of the hull of the ship.

- Block coefficient, C_B $$C_B = \frac{\nabla}{L \times B \times d} \quad \text{(A-1)}$$

in which
∇ = actual volume of the underwater form (m^3)
L = length (m)
B = breath (m)
d = draught (m)

Fast ships require low values of block coefficients while in slow ships high values of the block coefficient are permissible. Mean values of block coefficient might be 0.88 for a large oil tanker, 0.60 for an aircraft carrier and 0.50 for a yacht.

- Prismatic coefficient, C_P $$C_P = \frac{\nabla}{A_M \times L} \quad \text{(A-2)}$$

in which
A_M = midship area (m^2)

This coefficient has its use in dealing with ship resistance. Expected values generally exceed 0.55.

- Midship area coefficient, C_M $$C_M = \frac{A_M}{B \times d} \quad \text{(A-3)}$$

This coefficient is used to express the fullness of the midship. Its value usually exceeds 0.85 for ships other than yachts.

- Water plane area coefficient, C_W $$C_W = \frac{A_W}{L \times B} \quad \text{(A-4)}$$

in which
A_W = water plane area (m^2)

This coefficient expresses the fineness of the water plane. It varies from about 0.70 for ships with unusually fine ends to about 0.90 for ships with more blunt forms.

- Vertical prismatic coefficient, C_{VP} $$C_{VP} = \frac{\nabla}{A_W \times d} \quad \text{(A-5)}$$

A large value of the vertical prismatic coefficient indicates body sections of U-form while a small value of this coefficient is associated with V-shaped sections.

Between the different coefficients the following two relations exist:

- $C_B = C_P * C_M$ (A-6)
- $C_B = C_W * C_{VP}$ (A-7)

Appendix 3 Ship characteristics

Description	Symbol	Prototype ship (in prototype values)	Model ship (in prototype values)
Ship dimensions			
Deadweight tonnage	Dwt	65 000 tonnes	65 000 tonnes
Length overall	L_{oa}	253.0 m	253.0 m
Length between perpendiculars	L_{pp}	243.4 m	243.4 m
Beam	B	32.2 m	32.2 m
Depth	H	17.5 m	17.5 m
Design draught	D	12.5 m	12.5 m
Volume of displacement	V	78 600 m^3	78 600 m^3
Displacement in salt water	Δ	80 700 tonnes	80 700 tonnes
Transverse metacentric height above keel	KM_T	13.2 m	13.2 m
Longitudinal metacentric height above keel	KM_L	358.9 m	358.9 m
Loading conditions			
Height of centre of gravity (CG) above keel	KG	9.4 m	9.76 m
Transverse metacentric height above keel	GM_T	3.8 m	2.87 m
Longitudinal metacentric height above keel	GM_L	349.5 m	-
Longitudinal distance of CG from aft perpendicular	LCG	134 m	118.9 m
Transverse radius of gyration	k_{xx}	11.3 m	9.954 m
Longitudinal radius of gyration	k_{yy}	68.2 m	65.383 m
Natural roll period	T_ϕ	11.6 s	11.92 s
Natural pitch period	T_θ	9.7 s	-

Appendix 4 Scale factors

Source: Journée and Massie (2000)

Generally speaking, a model is some form of representation of an object. Usually it is a more convenient representation of an actual or proposed situation. Physical models require similarity between the prototype and the model. Three similarities are needed:

- Geometric similarity (physical dimensions)
- Kinematic similarity (velocities)
- Dynamic similarity (forces and accelerations)

Table A4.1 shows several scale factors. This scale factor is a number larger than 1 that denotes the ratio between the prototype value and the model value. With the scale factors of Table A5.1 other scale factors (area, volume, mass and mass moment of inertia) can be determined:

Table A.1. Principal scale factors

	Scale factor	Relationship
Length	α_L	$L_p = \alpha_L * L_m$
Velocity	α_V	$V_p = \alpha_V * V_m$
Acceleration of gravity	α_g	$g_p = \alpha_g * g_m$
Density of fluid	α_ρ	$\rho_p = \alpha_\rho * \rho_m$
Fluid kinematic viscosity	α_ν	$\nu_p = \alpha_\nu * \nu_m$
Fluid dynamic viscosity	α_η	$\eta_p = \alpha_\eta * \eta_m$

Various forces are scaled differently in a model. This can be seen from Table A4.2. Modelling will involve inertia forces whenever velocities and accelerations are involved. Gravity forces are involved for flow situations in which a free water surface is involved. These two types of forces play a significant role in a physical model study of waves in an open channel (basin).

Table A.2. Force scale factors

	Scale factor
Inertia	$\alpha_\rho * \alpha^2_V * \alpha^2_L$
Gravity	$\alpha_\rho * \alpha_g * \alpha^3_L$
Viscous	$\alpha_\eta * \alpha_V * \alpha_L$
Surface tension	$\alpha_\sigma * \alpha^2_L$
Internal stresses	$\alpha_\rho * \alpha_g * \alpha_L$

Since not all forces are identically reproduced some forces will become relatively more important in the model than they are in the prototype. For that reason the ratio of the two most important forces should be the same in the model as they are in the prototype. Such ratios are dimensionless and provide additional information in modelling.

The ratio between inertia force and gravity force is expressed in the Froude number, Fn.

$$Fn = \sqrt{\frac{Inertia\ \ Force}{Gravity\ \ Force}} \qquad \text{(A-8)}$$

An equal Froude number in the model as in the prototype results in the following relation for the scale factors:

$$\alpha_\rho \cdot \alpha_V^2 \cdot \alpha_L^2 = \alpha_\rho \cdot \alpha_g \cdot \alpha_L^3 \qquad \text{(A-9)}$$

Since $\cdot \alpha_V = \frac{\alpha_L}{\alpha_T}$ and $\alpha_g = 1$ the following relation can be derived from A-9:

$$\frac{\alpha_L}{\alpha_T^2} = 1 \qquad \text{(A-10)}$$

Consequently, when Froude scaling is applied the length scale determines the time scale, $\alpha_T = \sqrt{\alpha_L}$. In case of a length scale of 100 (one meter in prototype corresponds to one centimetre in the model) the time scale is 10. This means that one second in the model represents 10 seconds in the prototype.

Note: in a distorted model the geometric similarity is not fulfilled. For example, the length scale for vertical dimensions is smaller than for horizontal dimensions in order to reduce the viscous influence in an open channel model.

Appendix 5 Measured significant wave height at W1 and W2

5.a Direction 110°

W2	110		W1	110	
Filename	Avg.Hmo (m)	Avg.Tp (s)	Filename	Avg.Hmo (m)	Avg.Tp (s)
Ship161s	2,09	10	Ship161b	0,16	10,3
Ship171s	2,07	12	Ship171b	0,17	11,2
Ship183s	1,98	14,4	Ship183b	0,15	14,1
Ship191s	2,1	16	Ship191b	0,16	16
Ship202s	2,03	18,1	Ship202b	0,2	18,4
Ship212s	3,98	10	Ship212b	0,35	10,1
Ship221s	4,14	12,3	Ship221b	0,42	11,6
Ship233s	3,92	14,5	Ship233b	0,35	15,3
Ship242s	3,99	16	Ship242b	0,4	16,7
Ship253s	4	18,5	Ship253b	0,47	17,3
Ship263s	6,11	9,9	Ship263b	0,54	10,9
Ship272s	6,01	12,4	Ship272b	0,59	11,6
Ship281s	6,06	15	Ship281b	0,53	12,3
Ship292s	6	15,9	Ship292b	0,64	12
Ship302s	5,93	19	Ship302b	0,75	25,6

5.b Direction 128°

W2	128		W1	128	
Filename	Avg.Hmo (m)	Avg.Tp (s)	Filename	Avg.Hmo (m)	Avg.Tp (s)
Ship13s	2,06	10,1	Ship13b	0,18	10,1
Ship23s	2,09	12	Ship23b	0,19	12,3
Ship32s	2,09	14,2	Ship32b	0,2	13,6
Ship42s	2,1	15,9	Ship42b	0,23	16,04
Ship52s	2,07	17,7	Ship52b	0,2	18,27
Ship62s	3,95	10,4	Ship62b	0,35	10,12
Ship72s	3,99	12,2	Ship72b	0,36	11,87
Ship83s	4,11	14,5	Ship83b	0,39	14,15
Ship91s	4,09	15,9	Ship91b	0,41	15,94
Ship102s	3,96	18,5	Ship102b	0,39	18,27
Ship111s	5,89	9,8	Ship111b	0,53	10,39
Ship121s	5,76	12,2	Ship121b	0,6	12,07
Ship131s	6,05	14,9	Ship131b	0,62	14,01
Ship143s	5,91	15,8	Ship143b	0,64	15,54
Ship153s	6,05	19,1	Ship153b	0,71	20,74

Appendix 5 Measured significant wave height at W1 and W2

5.c Direction 140°

W2	140		W1	140	
Filename	Avg.Hmo (m)	Avg.Tp (s)	Filename	Avg.Hmo (m)	Avg.Tp (s)
Ship461s	2,09	10,19	Ship461b	0,21	10,18
Ship471s	2,12	12,1	Ship471b	0,22	12,11
Ship482s	2,06	14,23	Ship482b	0,22	13,69
Ship491s	1,98	15,59	Ship491b	0,19	16,08
Ship501s	2,15	17,98	Ship501b	0,26	18,28
Ship512s	3,95	10,01	Ship512b	0,39	10,14
Ship522s	4,04	12,13	Ship522b	0,43	12,46
Ship532s	3,97	14,5	Ship532b	0,47	14,54
Ship541s	3,98	15,9	Ship541b	0,51	15,46
Ship552s	4,21	17,98	Ship552b	0,52	19,21
Ship562s	5,78	10,03	Ship562b	0,56	10,15
Ship572s	6,21	12,28	Ship572b	0,69	11,91
Ship581s	6,13	14,5	Ship581b	0,75	16,4
Ship592s	6,07	15,9	Ship592b	0,73	17,03
Ship601s	6,01	18,22	Ship601b	0,85	19,3

5.d Direction 160°

W2	160		W1	160	
Filename	Avg.Hmo (m)	Avg.Tp (s)	Filename	Avg.Hmo (m)	Avg.Tp (s)
Ship311s	1,99	9,99	Ship311b	0,56	10,11
Ship322s	2,19	11,83	Ship322b	0,55	11,51
Ship332s	2,01	13,93	Ship332b	0,46	13,45
Ship342s	2,11	16,24	Ship342b	0,49	16,03
Ship352s	2,16	18,21	Ship352b	0,48	18,13
Ship362s	3,85	10,16	Ship362b	0,82	10,13
Ship371s	3,92	12	Ship371b	0,83	11,55
Ship382s	3,99	14,26	Ship382b	0,89	12,6
Ship392s	4,03	16	Ship392b	0,89	15,66
Ship402s	3,99	18,5	Ship402b	0,88	18,29
Ship411s	6	10,2	Ship411b	0,99	10,13
Ship422s	6,03	12,09	Ship422b	1,06	12,71
Ship431s	5,9	15,21	Ship431b	1,17	13,34
Ship443s	6,07	15,96	Ship443b	1,18	17,58
Ship452s	6,34	18,63	Ship452b	1,43	17,33

Appendix 6 Mooring layout

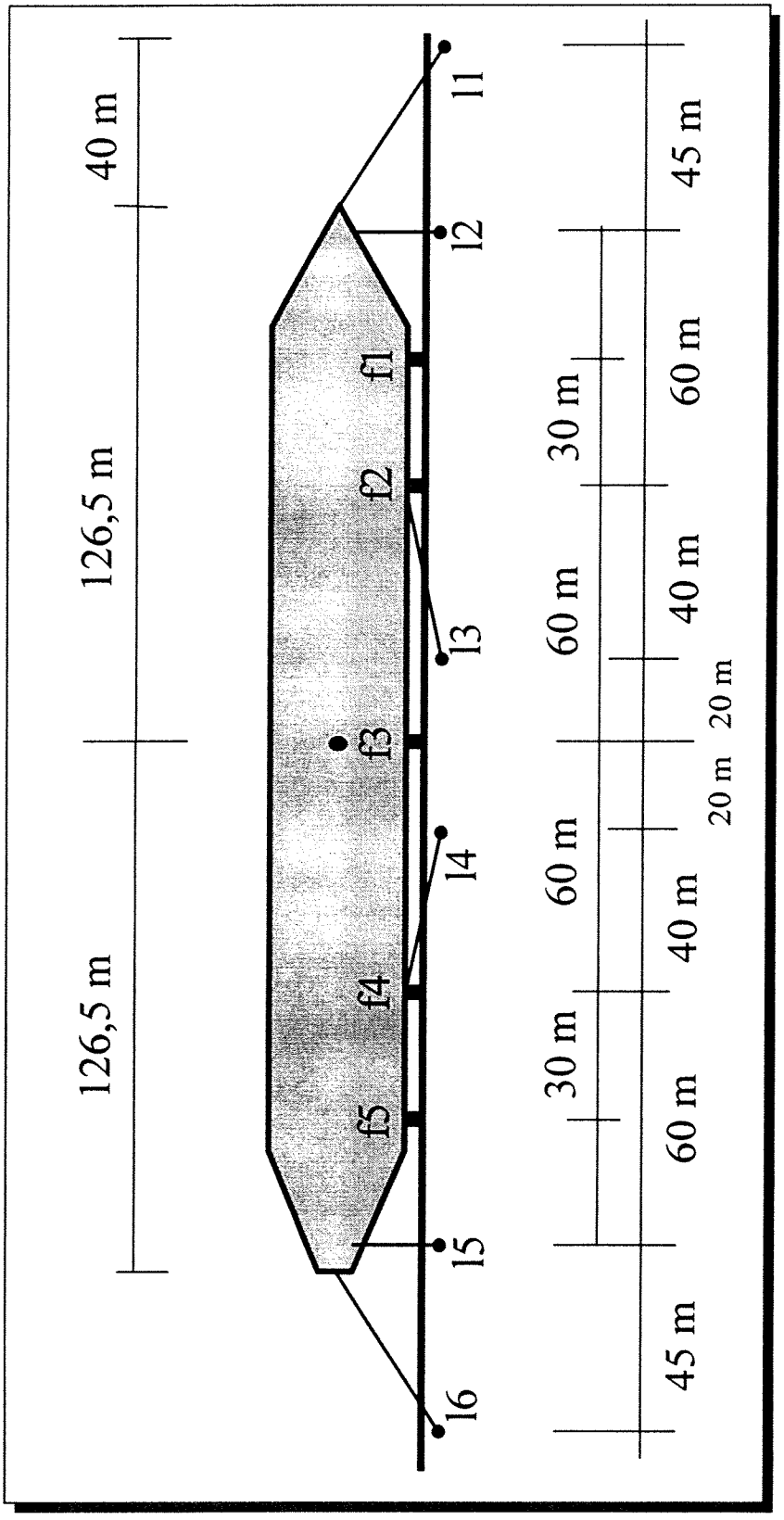

Appendix 7 Fender and mooring line characteristics

7.a Load-deflection characteristics of model fenders (in prototype values)

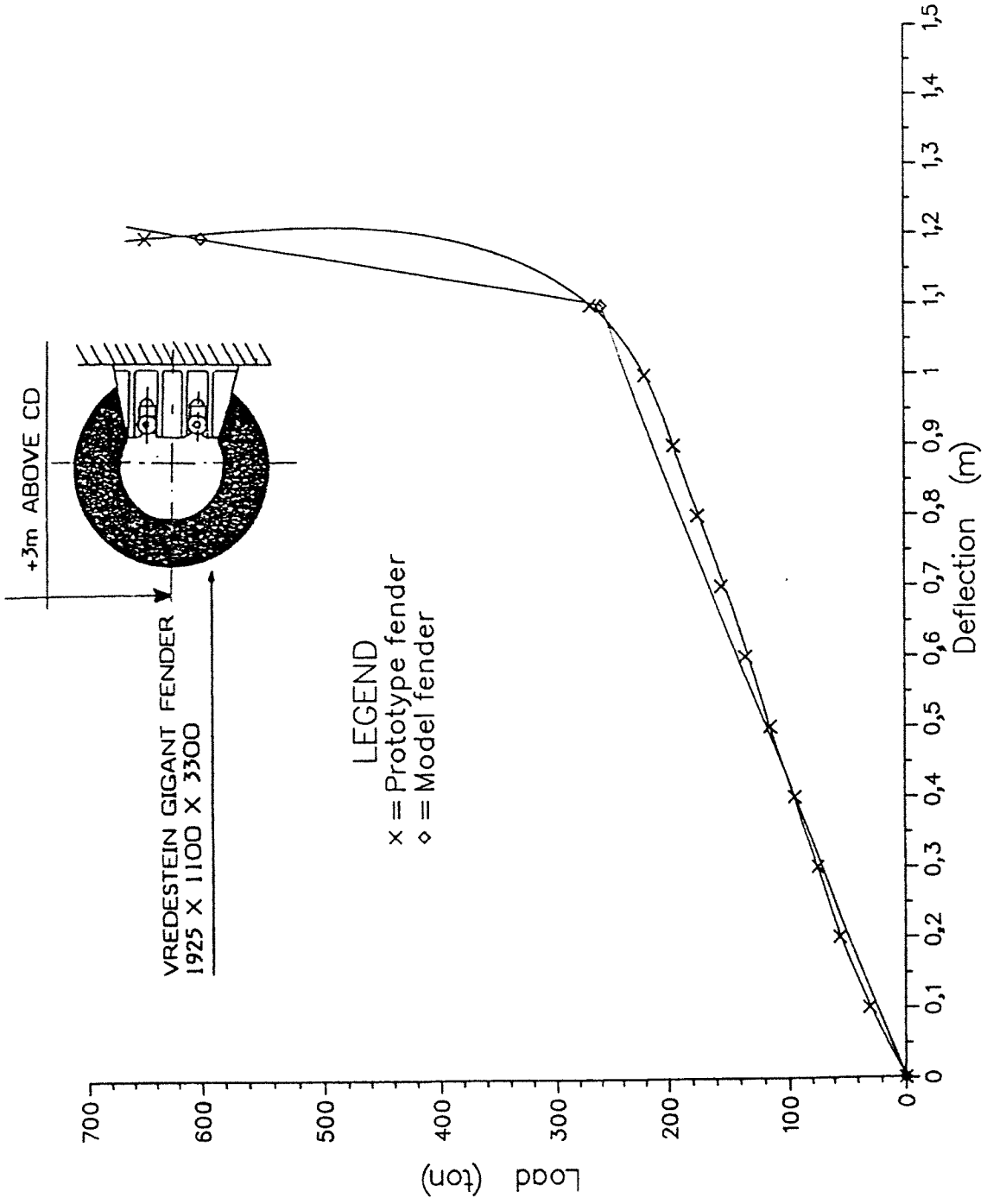

Appendix 7 Fender and mooring line characteristics

7.b Load-elongation characteristics of model mooring lines (in prototype values)

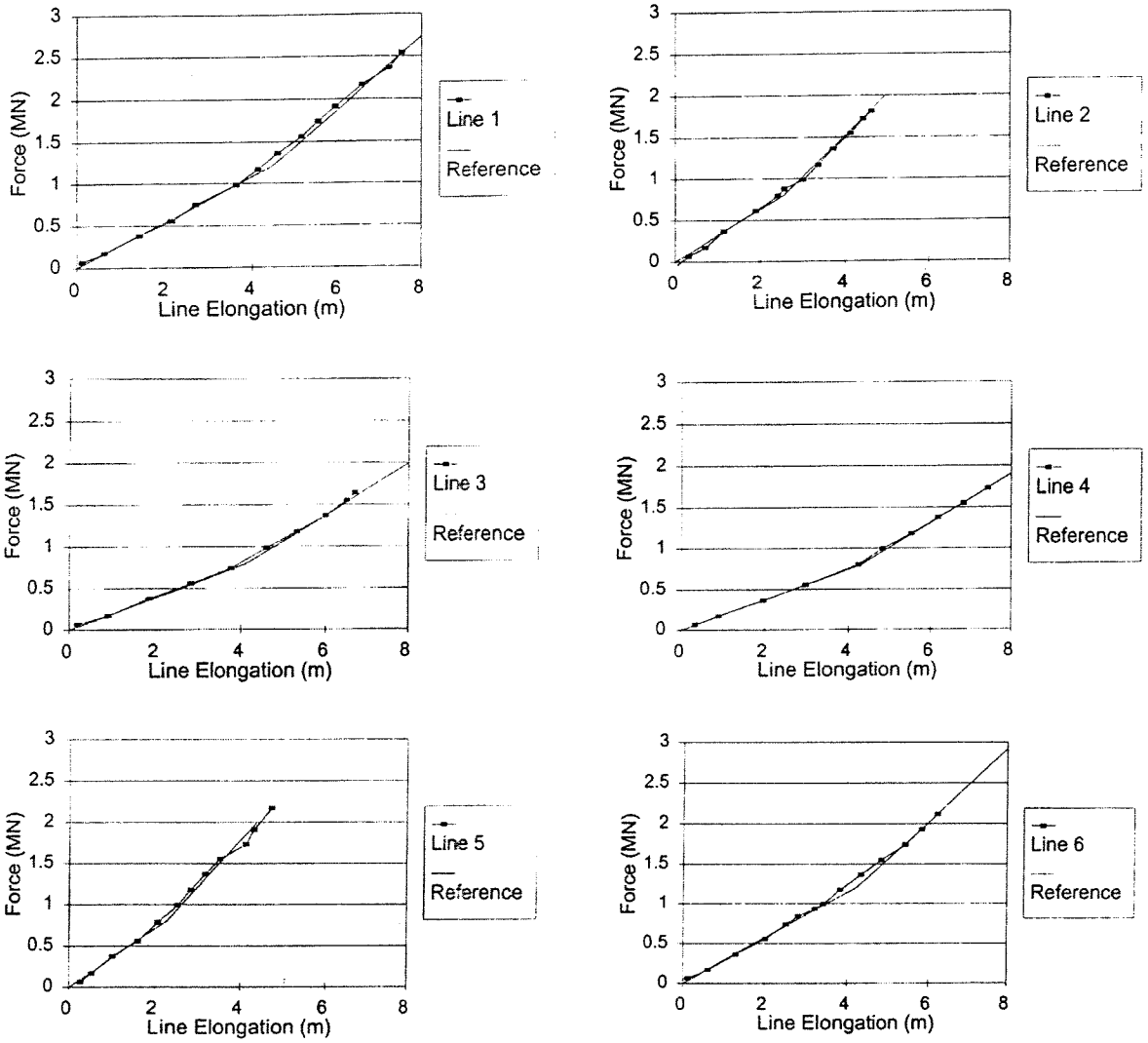

Appendix 8 Example of a keogram

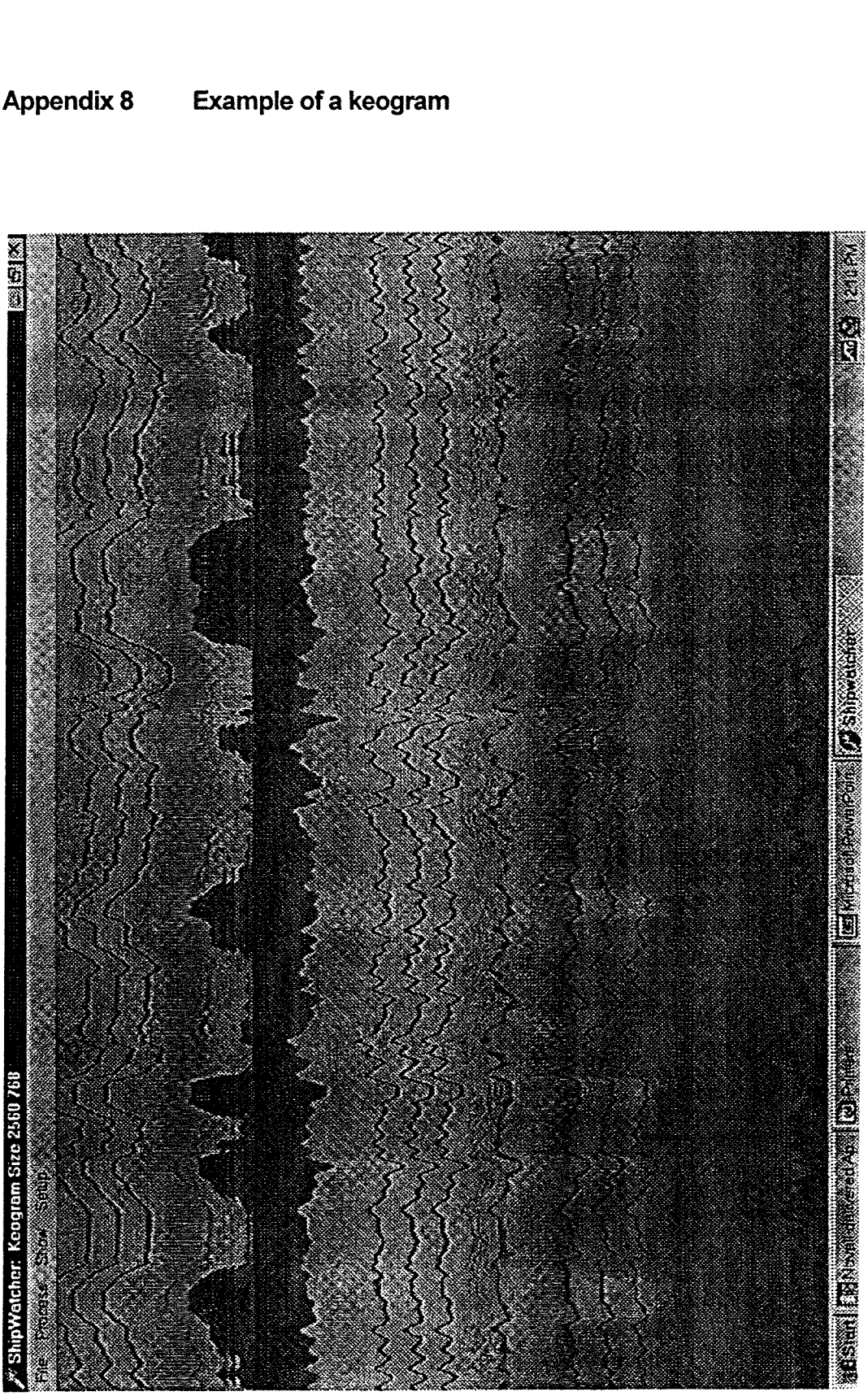

Appendix 9 Output of spectral analysis

9.a Wave condition: H_{mo} = 6 m, T_p = 10 s, wave direction = 160°

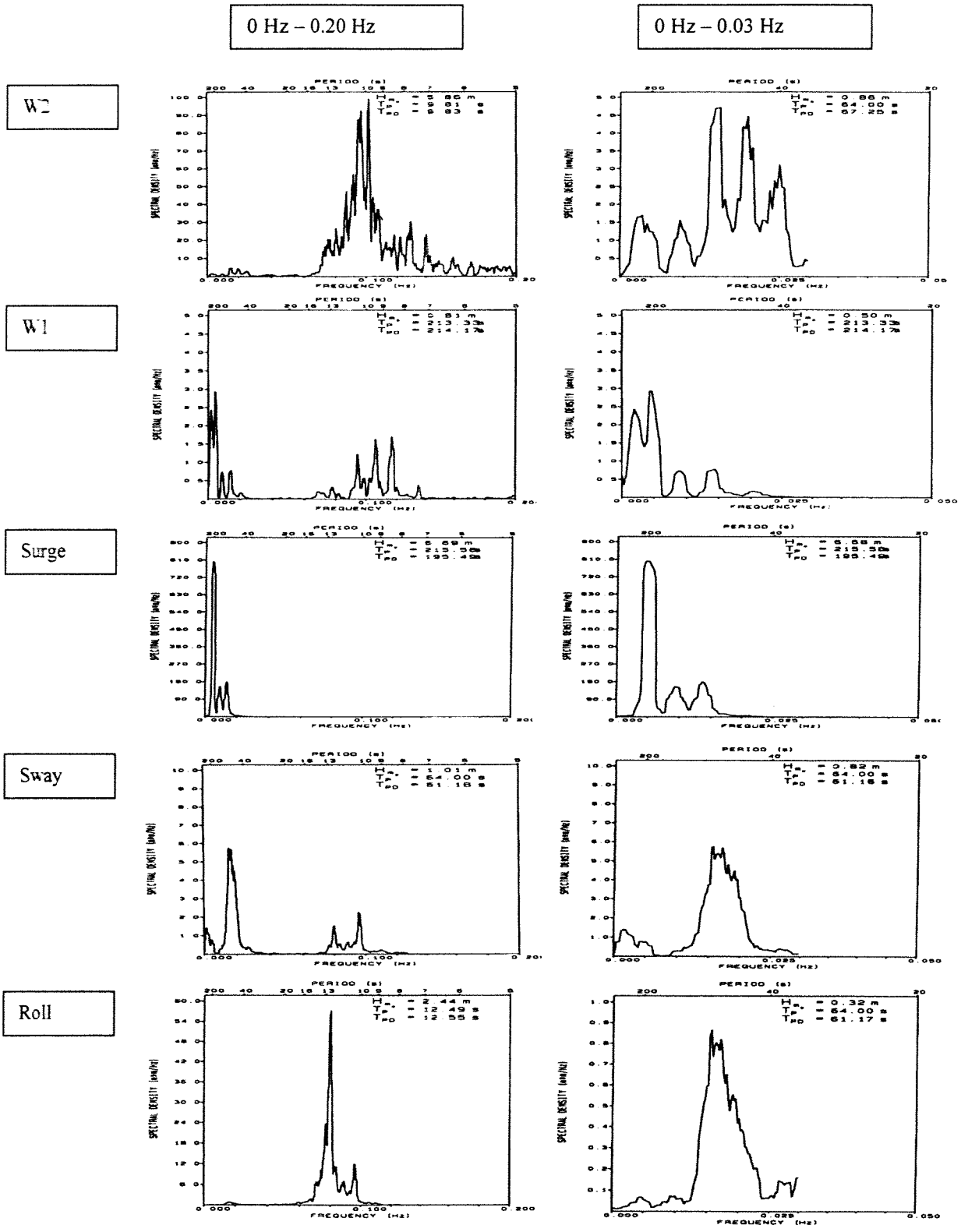

Appendix 9 Output of spectral analysis

9.b Wave condition: H_{mo} = 6 m, T_p = 12 s, wave direction = 160°

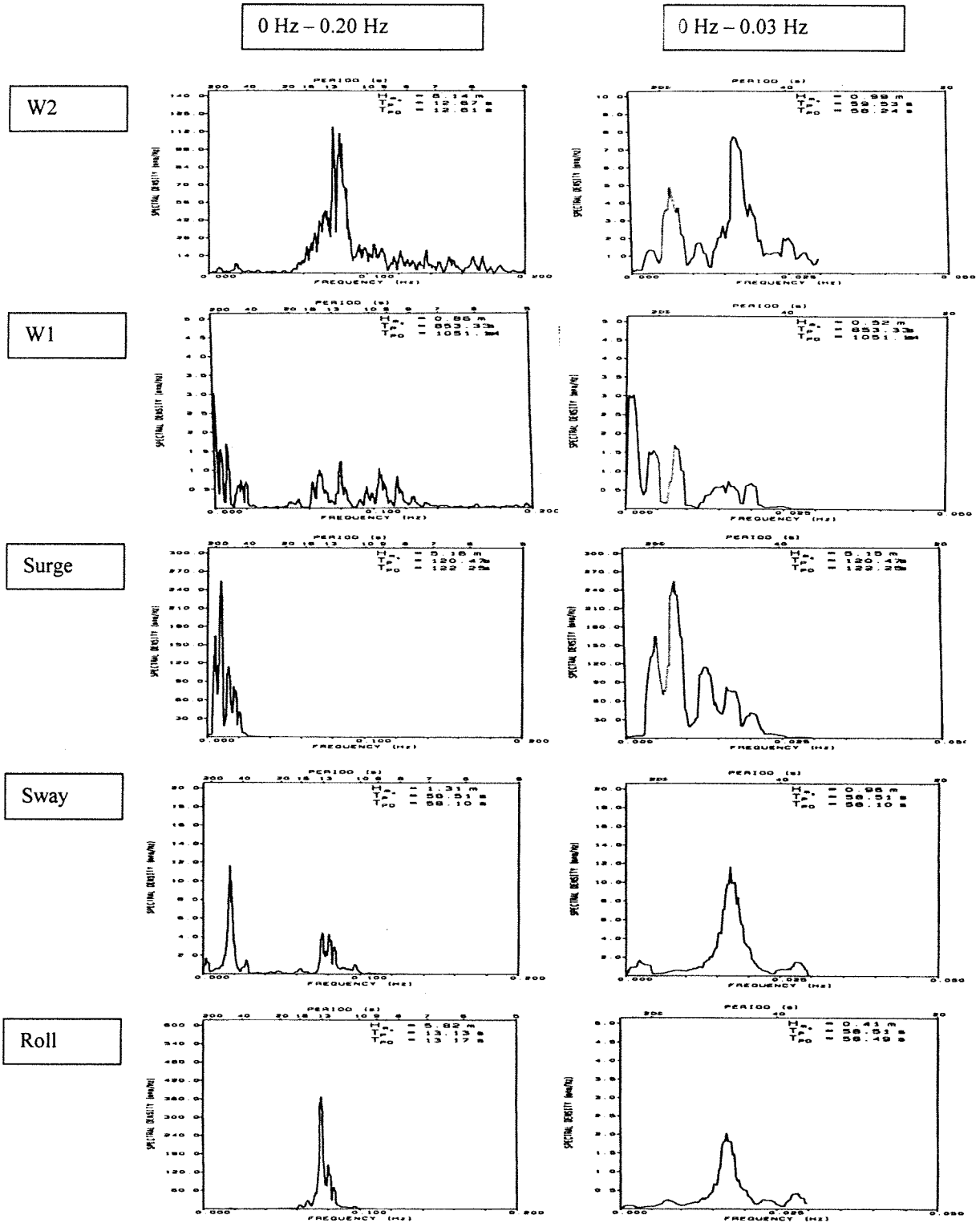

Appendix 9 Output of spectral analysis

9.c Wave condition: H_{mo} = 6 m, T_p = 14 s, wave direction = 160°

	0 Hz – 0.20 Hz	0 Hz – 0.03 Hz
W2	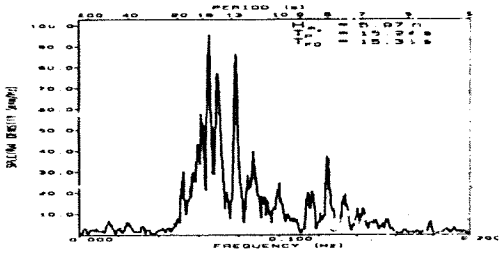	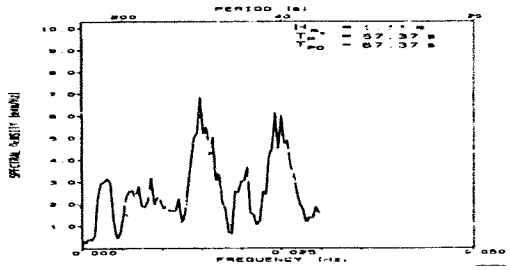
W1	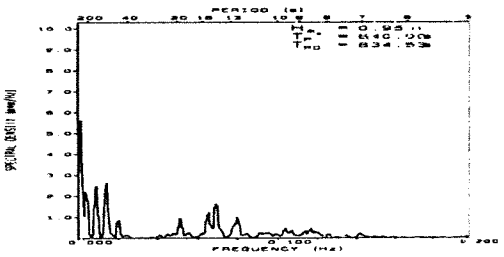	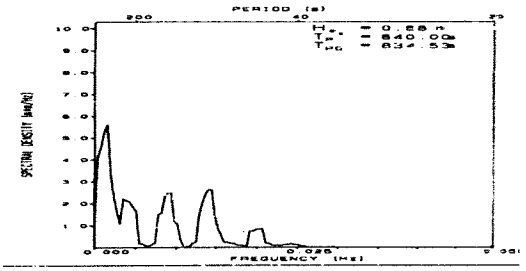
Surge	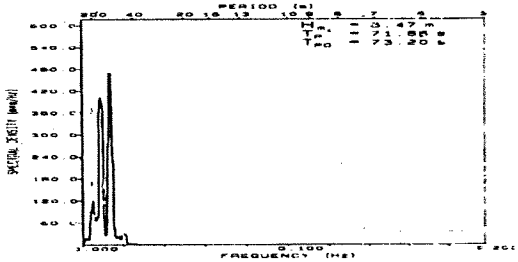	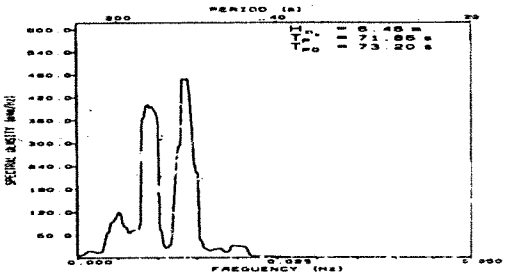
Sway	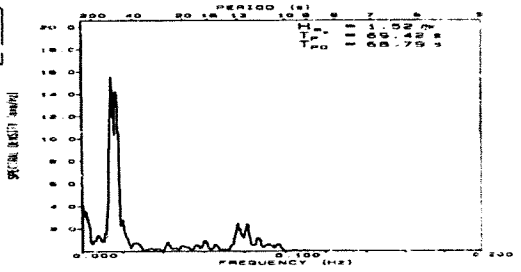	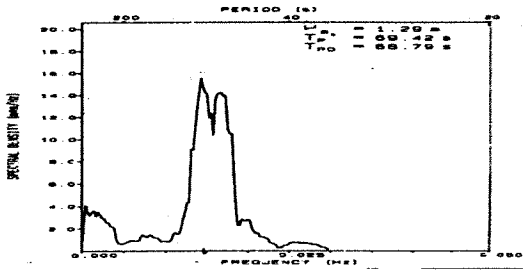
Roll	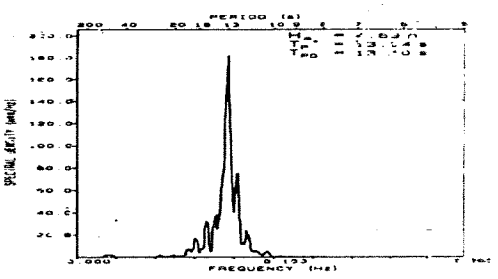	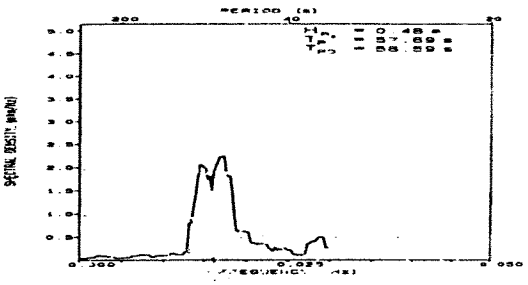

Appendix 9 Output of spectral analysis

9.d Wave condition: H_{mo} = 6 m, T_p = 16 s, wave direction = 160°

	0 Hz – 0.20 Hz	0 Hz – 0.03 Hz
W2	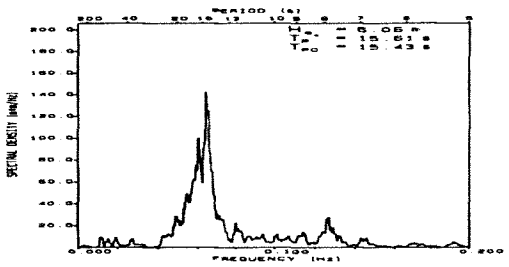	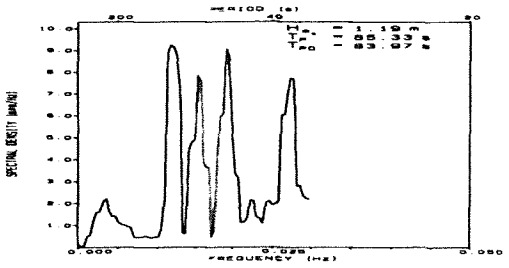
W1	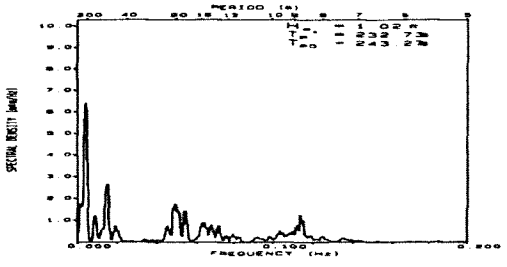	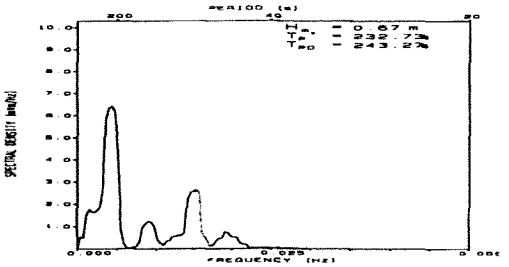
Surge	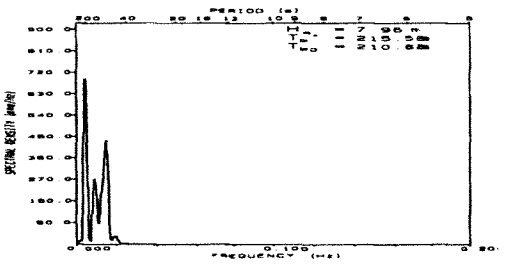	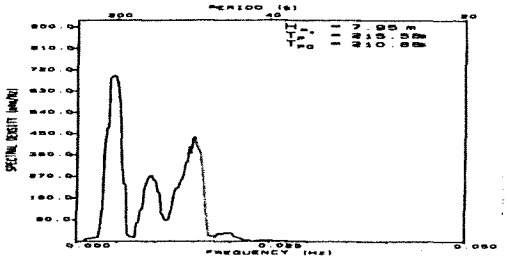
Sway	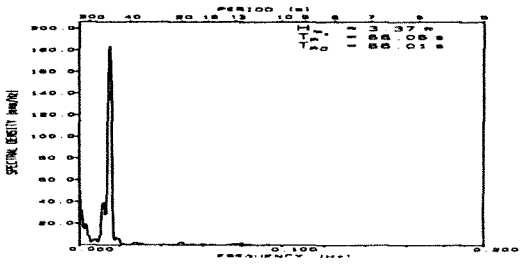	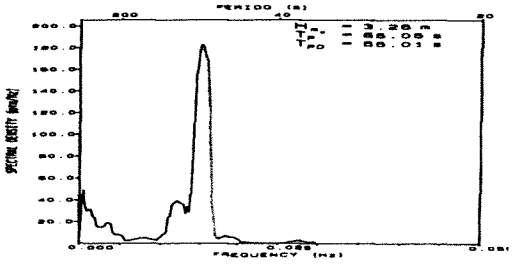
Roll	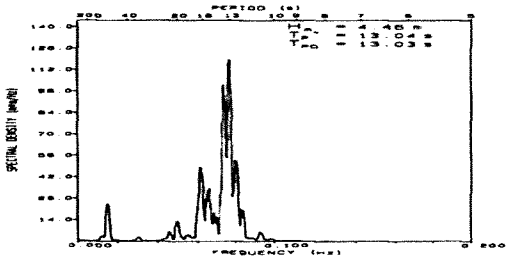	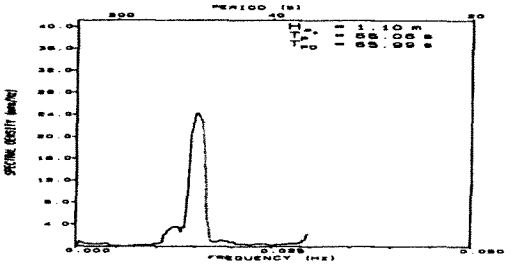

Appendix 9 Output of spectral analysis

9.e Wave condition: H_{mo} = 6 m, T_p = 18 s, wave direction = 160°

	0 Hz – 0.20 Hz	0 Hz – 0.03 Hz
W2	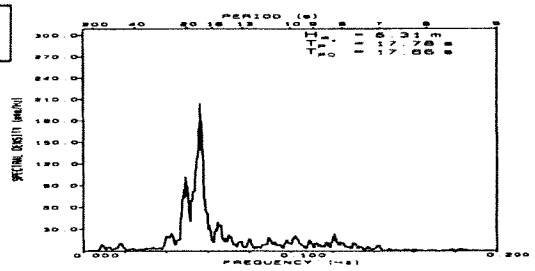	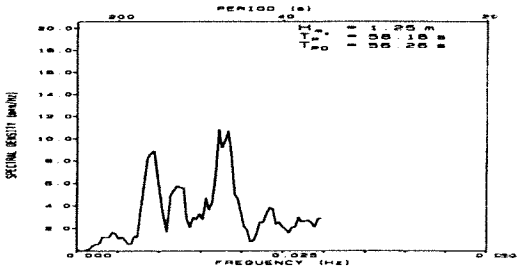
W1	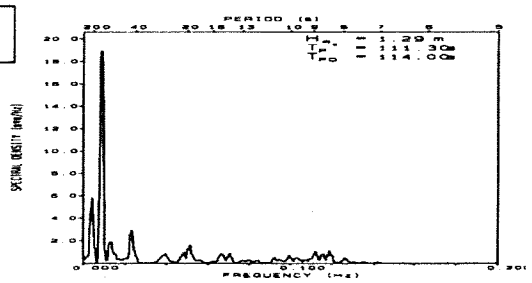	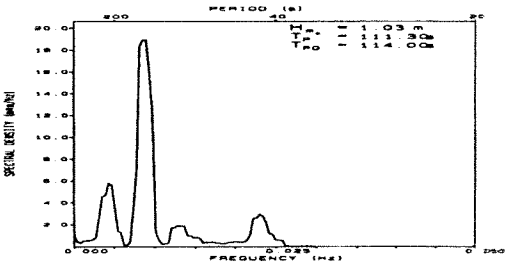
Surge	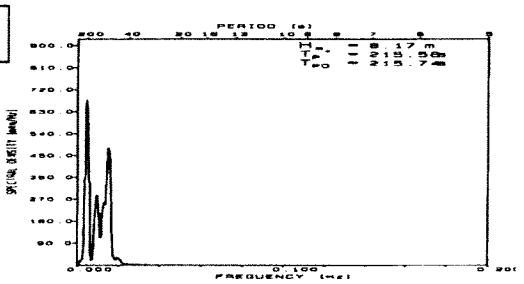	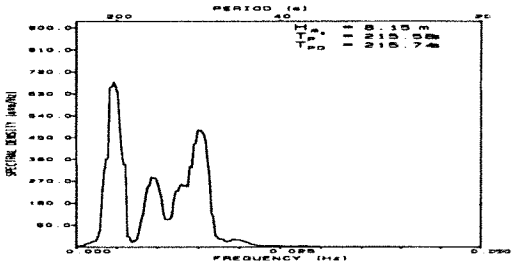
Sway	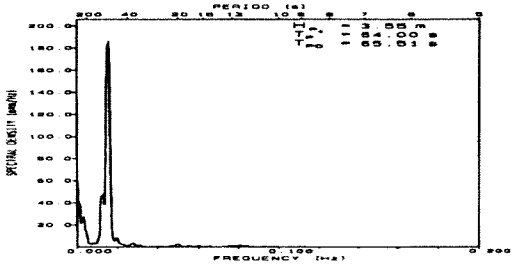	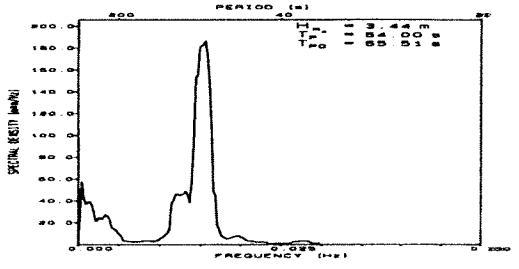
Roll	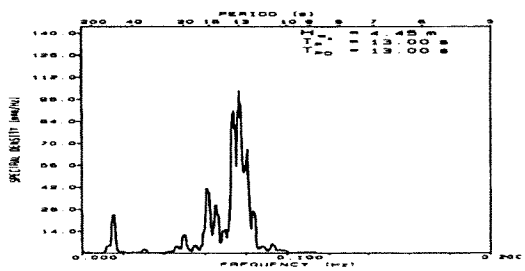	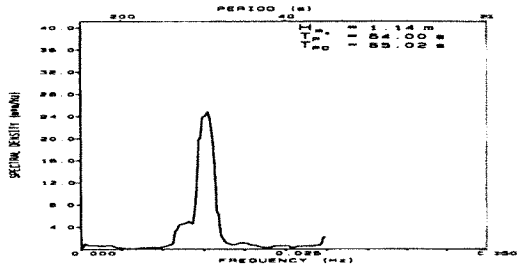

Appendix 10 Ship motion response

10.a Wave direction 110°

SHIP MOTION RESPONSE FOR 2 m WAVES FROM 110 deg

Mean (m)	surge	sway	yaw	heave	roll	pitch
Tp = 10 s	0.020	0.078	0.010	0.036	0.018	0.000
Tp = 12 s	0.065	0.051	0.012	0.030	0.040	0.012
Tp = 14 s	0.099	0.041	0.013	0.004	0.007	0.011
Tp = 16 s	0.003	0.073	0.012	0.038	0.011	0.000
Tp = 18 s	0.022	0.029	0.028	0.011	0.002	0.003

H1 (m)	surge	sway	yaw	heave	roll	pitch
Tp = 10 s	0.59	0.19	0.16	0.18	0.25	0.07
Tp = 12 s	0.76	0.29	0.21	0.22	0.44	0.10
Tp = 14 s	0.73	0.34	0.24	0.20	0.57	0.09
Tp = 16 s	1.29	0.35	0.28	0.27	0.53	0.11
Tp = 18 s	1.44	0.41	0.31	0.29	0.44	0.12

Hmax (m)	surge	sway	yaw	heave	roll	pitch
Tp = 10 s	0.48	0.16	0.14	0.12	0.20	0.05
Tp = 12 s	0.75	0.25	0.17	0.17	0.41	0.07
Tp = 14 s	0.62	0.30	0.20	0.15	0.48	0.08
Tp = 16 s	1.28	0.32	0.25	0.17	0.43	0.08
Tp = 18 s	1.33	0.37	0.30	0.26	0.38	0.08

Hmo (m)	surge	sway	yaw	heave	roll	pitch
Tp = 10 s	0.39	0.13	0.10	0.11	0.13	0.04
Tp = 12 s	0.55	0.15	0.12	0.15	0.23	0.06
Tp = 14 s	0.45	0.19	0.15	0.13	0.29	0.06
Tp = 16 s	0.86	0.21	0.16	0.17	0.26	0.06
Tp = 18 s	1.04	0.23	0.17	0.20	0.22	0.07

Tp (s)	surge	sway	yaw	heave	roll	pitch
Tp = 10 s	212.0	69.5	69.5	215.6	12.4	217.2
Tp = 12 s	208.4	67.9	67.5	220.4	12.5	220.4
Tp = 14 s	201.5	66.4	66.8	208.4	13.4	201.5
Tp = 16 s	198.3	67.1	67.5	209.1	16.1	195.0
Tp = 18 s	201.5	65.7	68.7	201.5	66.2	201.5

Hmolo	surge	sway	yaw	heave	roll	pitch
Tp = 10 s	0.39	0.11	0.09	0.11	0.05	0.03
Tp = 12 s	0.54	0.13	0.10	0.14	0.09	0.04
Tp = 14 s	0.44	0.17	0.12	0.12	0.10	0.03
Tp = 16 s	0.86	0.19	0.14	0.16	0.10	0.05
Tp = 18 s	1.04	0.20	0.15	0.19	0.11	0.05

Tplo	surge	sway	yaw	heave	roll	pitch
Tp = 10 s	212.0	69.5	69.5	215.6	71.9	217.2
Tp = 12 s	208.4	67.9	67.5	220.4	1463.6	220.4
Tp = 14 s	201.5	66.4	66.8	208.4	1409.7	201.5
Tp = 16 s	198.3	67.1	67.5	209.1	66.8	195.0
Tp = 18 s	201.5	65.7	68.7	201.5	66.2	201.5

Hmohl	surge	sway	yaw	heave	roll	pitch
Tp = 10 s	0.07	0.06	0.05	0.04	0.11	0.03
Tp = 12 s	0.09	0.08	0.07	0.07	0.21	0.04
Tp = 14 s	0.09	0.09	0.08	0.06	0.27	0.05
Tp = 16 s	0.09	0.10	0.08	0.06	0.24	0.04
Tp = 18 s	0.10	0.11	0.08	0.06	0.20	0.04

Tphi	surge	sway	yaw	heave	roll	pitch
Tp = 10 s	5.7	10.4	10.1	10.4	12.4	10.3
Tp = 12 s	13.7	12.1	11.6	12.1	12.5	11.6
Tp = 14 s	14.7	14.5	14.6	13.2	13.4	14.6
Tp = 16 s	18.2	16.0	14.7	17.2	16.1	14.7
Tp = 18 s	21.0	20.0	17.7	19.9	15.9	17.7

SHIP MOTION RESPONSE FOR 4 m WAVES FROM 110 deg

Mean (m)	surge	sway	yaw	heave	roll	pitch
Tp = 10 s	0.003	0.056	0.007	0.038	0.035	0.012
Tp = 12 s	0.040	0.086	0.023	0.002	0.032	0.010
Tp = 14 s	0.030	0.049	0.006	0.021	0.016	0.003
Tp = 16 s	0.052	0.050	0.005	0.013	0.004	0.003
Tp = 18 s	0.052	0.049	0.007	0.019	0.022	0.001

H1 (m)	surge	sway	yaw	heave	roll	pitch
Tp = 10 s	3.93	0.38	0.27	0.49	0.81	0.15
Tp = 12 s	4.93	0.53	0.40	0.64	1.30	0.19
Tp = 14 s	3.75	0.51	0.43	0.62	1.63	0.18
Tp = 16 s	6.43	0.59	0.45	0.68	1.15	0.22
Tp = 18 s	6.47	0.81	0.57	0.78	1.22	0.25

Hmax (m)	surge	sway	yaw	heave	roll	pitch
Tp = 10 s	3.07	0.29	0.23	0.37	0.69	0.11
Tp = 12 s	3.96	0.47	0.34	0.46	1.22	0.13
Tp = 14 s	3.05	0.46	0.31	0.60	1.42	0.14
Tp = 16 s	5.39	0.58	0.33	0.63	0.99	0.20
Tp = 18 s	5.57	0.76	0.48	0.78	1.15	0.24

Hmo (m)	surge	sway	yaw	heave	roll	pitch
Tp = 10 s	2.68	0.20	0.15	0.38	0.41	0.10
Tp = 12 s	3.43	0.36	0.25	0.45	0.88	0.12
Tp = 14 s	2.65	0.36	0.25	0.39	0.88	0.11
Tp = 16 s	4.18	0.40	0.26	0.51	0.69	0.14
Tp = 18 s	4.93	0.53	0.33	0.59	0.65	0.15

Tp (s)	surge	sway	yaw	heave	roll	pitch
Tp = 10 s	208.4	55.1	148.9	212.0	12.2	208.4
Tp = 12 s	201.5	53.7	37.8	232.0	12.2	201.5
Tp = 14 s	204.8	52.3	36.8	212.0	13.9	204.8
Tp = 16 s	212.0	55.6	37.1	212.0	14.6	212.0
Tp = 18 s	209.1	55.9	39.8	212.7	12.1	209.1

Hmolo	surge	sway	yaw	heave	roll	pitch
Tp = 10 s	2.67	0.17	0.12	0.37	0.13	0.08
Tp = 12 s	3.43	0.33	0.23	0.44	0.24	0.09
Tp = 14 s	2.65	0.33	0.21	0.38	0.24	0.08
Tp = 16 s	4.18	0.36	0.23	0.50	0.27	0.12
Tp = 18 s	4.93	0.50	0.30	0.57	0.31	0.14

Tplo	surge	sway	yaw	heave	roll	pitch
Tp = 10 s	208.4	55.1	148.9	212.0	55.1	208.4
Tp = 12 s	201.5	53.7	37.8	232.0	54.1	201.5
Tp = 14 s	204.8	52.3	36.8	212.0	51.9	204.8
Tp = 16 s	212.0	55.6	37.1	212.0	55.6	212.0
Tp = 18 s	209.1	55.9	39.8	212.7	57.3	209.1

Hmohl	surge	sway	yaw	heave	roll	pitch
Tp = 10 s	0.09	0.11	0.08	0.08	0.39	0.08
Tp = 12 s	0.10	0.15	0.11	0.12	0.85	0.08
Tp = 14 s	0.12	0.15	0.14	0.11	0.85	0.08
Tp = 16 s	0.11	0.16	0.12	0.11	0.64	0.07
Tp = 18 s	0.12	0.18	0.13	0.12	0.56	0.07

Tphi	surge	sway	yaw	heave	roll	pitch
Tp = 10 s	21.6	10.4	9.9	10.4	12.2	10.0
Tp = 12 s	17.0	12.0	14.6	12.1	12.2	13.2
Tp = 14 s	19.5	12.1	14.6	12.7	13.9	14.5
Tp = 16 s	19.7	16.7	15.2	19.7	14.6	14.8
Tp = 18 s	19.7	19.8	19.8	19.6	12.1	19.9

SHIP MOTION RESPONSE FOR 6 m WAVES FROM 110 deg

Mean (m)	surge	sway	yaw	heave	roll	pitch
Tp = 10 s	0.020	0.080	0.017	0.040	0.002	0.00
Tp = 12 s	0.014	0.146	0.041	0.056	0.023	0.00
Tp = 14 s	0.123	0.247	0.054	0.015	0.037	0.00
Tp = 16 s	0.045	0.294	0.049	0.043	0.047	0.00
Tp = 18 s	0.078	0.330	0.061	0.050	0.037	0.00

H1 (m)	surge	sway	yaw	heave	roll	pitch
Tp = 10 s	6.02	0.82	0.52	0.89	1.76	0.25
Tp = 12 s	6.40	1.46	0.82	0.84	1.92	0.2
Tp = 14 s	7.18	2.40	0.88	0.92	1.85	0.2
Tp = 16 s	9.55	2.90	1.01	1.36	2.03	0.4
Tp = 18 s	11.32	2.79	1.10	1.42	1.98	0.4

Hmax (m)	surge	sway	yaw	heave	roll	pitch
Tp = 10 s	5.49	0.75	0.52	0.73	1.67	0.1
Tp = 12 s	5.89	1.46	0.72	0.82	1.63	0.1
Tp = 14 s	6.23	2.36	0.78	0.91	1.29	0.2
Tp = 16 s	8.28	2.79	0.88	1.31	1.64	0.2
Tp = 18 s	11.10	2.78	1.04	1.34	1.59	0.3

Hmo (m)	surge	sway	yaw	heave	roll	pitch
Tp = 10 s	4.83	0.47	0.34	0.68	0.68	0.1
Tp = 12 s	5.05	0.98	0.57	0.70	1.07	0.1
Tp = 14 s	4.75	1.44	0.59	0.67	0.91	0.1
Tp = 16 s	7.91	1.99	0.69	0.97	1.05	0.2
Tp = 18 s	8.94	2.24	0.79	1.09	1.12	0.2

Tp (s)	surge	sway	yaw	heave	roll	pitch
Tp = 10 s	205.1	69.0	69.0	216.0	12.9	205
Tp = 12 s	204.8	68.3	67.9	212.0	12.8	208
Tp = 14 s	198.3	69.8	70.2	216.0	68.3	201
Tp = 16 s	201.5	67.2	68.7	208.4	67.2	201
Tp = 18 s	201.5	68.7	43.6	208.4	68.7	201

Hmolo	surge	sway	yaw	heave	roll	pitch
Tp = 10 s	4.63	0.44	0.33	0.67	0.21	0.1
Tp = 12 s	5.05	0.96	0.55	0.69	0.42	0.1
Tp = 14 s	4.75	1.42	0.58	0.66	0.50	0.1
Tp = 16 s	7.91	1.98	0.67	0.96	0.67	0.2
Tp = 18 s	8.93	2.23	0.77	1.08	0.73	0.2

Tplo	surge	sway	yaw	heave	roll	pitch
Tp = 10 s	205.1	69.0	69.0	216.0	68.7	205
Tp = 12 s	204.8	68.3	67.9	212.0	67.1	208
Tp = 14 s	198.3	69.8	70.2	216.0	68.3	201
Tp = 16 s	201.5	67.2	68.7	208.4	67.2	201
Tp = 18 s	201.5	68.7	43.6	208.4	68.7	201

Hmohl	surge	sway	yaw	heave	roll	pitch
Tp = 10 s	0.10	0.16	0.10	0.11	0.65	0.0
Tp = 12 s	0.12	0.20	0.13	0.15	0.98	0.0
Tp = 14 s	0.16	0.18	0.13	0.12	0.76	0.0
Tp = 16 s	0.22	0.24	0.15	0.16	0.81	0.0
Tp = 18 s	0.23	0.24	0.16	0.16	0.85	0.1

Tphi	surge	sway	yaw	heave	roll	pitch
Tp = 10 s	25.1	12.2	11.4	12.2	12.9	10.4
Tp = 12 s	24.6	12.6	14.5	12.1	12.8	14.
Tp = 14 s	24.1	14.8	14.7	12.2	12.2	14
Tp = 16 s	24.0	22.3	19.9	19.9	14.5	20.4
Tp = 18 s	24.8	23.4	19.0	23.5	13.9	18.5

Appendix 10 Ship motion response

10.b Wave direction 128°

SHIP MOTION RESPONSE FOR 2 m WAVES FROM 128 deg

Mean (m)	surge	sway	yaw	heave	roll	pitch
Tp = 10 s	0.007	0.035	0.000	0.021	0.025	0.006
Tp = 12 s	0.003	0.023	0.003	0.017	0.041	0.006
Tp = 14 s	0.003	0.054	0.007	0.032	0.031	0.005
Tp = 16 s	0.007	0.003	0.006	0.006	0.014	0.003
Tp = 18 s	0.007	0.004	0.002	0.008	0.013	0.003

H1 (m)	surge	sway	yaw	heave	roll	pitch
Tp = 10 s	0.56	0.20	0.15	0.12	0.42	0.12
Tp = 12 s	0.77	0.26	0.15	0.14	0.81	0.15
Tp = 14 s	0.70	0.28	0.19	0.20	1.15	0.15
Tp = 16 s	1.10	0.33	0.20	0.22	1.25	0.11
Tp = 18 s	1.42	0.34	0.22	0.25	0.91	0.11

Hmax (m)	surge	sway	yaw	heave	roll	pitch
Tp = 10 s	0.43	0.18	0.13	0.10	0.38	0.11
Tp = 12 s	0.89	0.20	0.13	0.11	0.75	0.15
Tp = 14 s	0.55	0.22	0.18	0.14	1.10	0.15
Tp = 16 s	1.07	0.27	0.17	0.14	1.09	0.09
Tp = 18 s	1.42	0.32	0.18	0.18	0.86	0.09

Hmo (m)	surge	sway	yaw	heave	roll	pitch
Tp = 10 s	0.30	0.10	0.07	0.06	0.18	0.05
Tp = 12 s	0.41	0.12	0.09	0.08	0.44	0.09
Tp = 14 s	0.41	0.14	0.13	0.10	0.61	0.10
Tp = 16 s	0.62	0.17	0.12	0.12	0.83	0.07
Tp = 18 s	0.75	0.19	0.12	0.13	0.51	0.06

Tp (s)	surge	sway	yaw	heave	roll	pitch
Tp = 10 s	208.7	10.3	10.0	212.0	11.4	11.2
Tp = 12 s	120.5	12.3	11.7	830.4	12.5	12.4
Tp = 14 s	4096.0	45.5	14.3	2457.6	13.9	14.2
Tp = 16 s	72.7	45.0	15.0	208.4	15.0	14.4
Tp = 18 s	99.8	45.7	19.5	219.6	18.2	19.0

Hmo/o	surge	sway	yaw	heave	roll	pitch
Tp = 10 s	0.29	0.05	0.03	0.04	0.07	0.02
Tp = 12 s	0.41	0.06	0.03	0.05	0.08	0.02
Tp = 14 s	0.39	0.08	0.04	0.06	0.09	0.02
Tp = 16 s	0.61	0.11	0.05	0.08	0.13	0.02
Tp = 18 s	0.74	0.14	0.06	0.09	0.13	0.03

Tp/o	surge	sway	yaw	heave	roll	pitch
Tp = 10 s	208.7	45.4	45.5	212.0	208.7	1228.8
Tp = 12 s	120.5	1396.7	43.1	830.4	201.9	351.1
Tp = 14 s	4096.0	45.5	40.5	2457.6	2155.8	2457.6
Tp = 16 s	72.7	45.0	46.7	208.4	44.8	218.2
Tp = 18 s	99.8	45.7	46.7	219.6	45.9	114.9

Hmo/H1	surge	sway	yaw	heave	roll	pitch
Tp = 10 s	0.07	0.08	0.06	0.05	0.18	0.05
Tp = 12 s	0.08	0.11	0.08	0.07	0.44	0.09
Tp = 14 s	0.10	0.12	0.12	0.08	0.61	0.10
Tp = 16 s	0.10	0.12	0.11	0.09	0.62	0.06
Tp = 18 s	0.11	0.14	0.11	0.09	0.50	0.06

Tp/H1	surge	sway	yaw	heave	roll	pitch
Tp = 10 s	12.0	10.3	10.0	10.3	11.4	11.2
Tp = 12 s	11.1	12.3	11.7	12.4	12.5	12.4
Tp = 14 s	14.4	12.8	14.3	14.2	13.9	14.2
Tp = 16 s	19.3	17.2	15.0	17.2	15.0	14.4
Tp = 18 s	19.5	19.4	19.5	19.4	18.2	19.0

SHIP MOTION RESPONSE FOR 4 m WAVES FROM 128 deg

Mean (m)	surge	sway	yaw	heave	roll	pitch
Tp = 10 s	0.008	0.095	0.003	0.052	0.055	0.006
Tp = 12 s	0.021	0.047	0.012	0.007	0.048	0.006
Tp = 14 s	0.012	0.053	0.008	0.017	0.019	0.000
Tp = 16 s	0.019	0.079	0.009	0.004	0.003	0.003
Tp = 18 s	0.019	0.080	0.002	0.027	0.010	0.001

H1 (m)	surge	sway	yaw	heave	roll	pitch
Tp = 10 s	1.84	0.41	0.23	0.40	1.18	0.14
Tp = 12 s	2.55	0.58	0.35	0.46	2.26	0.19
Tp = 14 s	3.31	0.54	0.36	0.47	2.08	0.19
Tp = 16 s	5.07	0.75	0.47	0.57	2.07	0.21
Tp = 18 s	5.44	0.79	0.55	0.57	1.80	0.21

Hmax (m)	surge	sway	yaw	heave	roll	pitch
Tp = 10 s	1.74	0.36	0.20	0.30	1.10	0.13
Tp = 12 s	2.54	0.51	0.27	0.35	2.20	0.16
Tp = 14 s	3.19	0.52	0.32	0.31	1.96	0.17
Tp = 16 s	4.44	0.68	0.43	0.41	2.03	0.18
Tp = 18 s	4.92	0.75	0.48	0.50	1.74	0.18

Hmo (m)	surge	sway	yaw	heave	roll	pitch
Tp = 10 s	1.18	0.21	0.14	0.23	0.64	0.08
Tp = 12 s	1.66	0.30	0.19	0.27	1.43	0.11
Tp = 14 s	1.86	0.32	0.22	0.27	1.43	0.12
Tp = 16 s	2.96	0.43	0.28	0.32	1.14	0.13
Tp = 18 s	3.06	0.46	0.30	0.33	0.95	0.13

Tp (s)	surge	sway	yaw	heave	roll	pitch
Tp = 10 s	201.9	47.3	36.2	828.4	12.5	72.5
Tp = 12 s	148.5	45.9	36.4	223.6	13.1	13.3
Tp = 14 s	72.3	46.9	21.8	248.7	13.1	14.3
Tp = 16 s	126.3	55.9	38.3	212.0	13.3	209.1
Tp = 18 s	115.9	57.7	37.8	205.1	13.9	149.9

Hmo/o	surge	sway	yaw	heave	roll	pitch
Tp = 10 s	1.18	0.15	0.09	0.20	0.18	0.04
Tp = 12 s	1.66	0.21	0.12	0.21	0.18	0.05
Tp = 14 s	1.85	0.25	0.13	0.22	0.21	0.05
Tp = 16 s	2.96	0.37	0.22	0.28	0.26	0.07
Tp = 18 s	3.06	0.40	0.24	0.28	0.26	0.08

Tp/o	surge	sway	yaw	heave	roll	pitch
Tp = 10 s	201.9	47.3	36.2	828.4	2746.5	201.9
Tp = 12 s	148.5	45.9	36.4	223.6	48.4	205.1
Tp = 14 s	72.3	46.9	37.0	248.7	47.1	195.3
Tp = 16 s	126.3	55.9	38.3	212.0	52.8	209.1
Tp = 18 s	115.9	57.7	37.8	205.1	57.7	149.9

Hmo/H1	surge	sway	yaw	heave	roll	pitch
Tp = 10 s	0.08	0.15	0.10	0.11	0.61	0.07
Tp = 12 s	0.11	0.21	0.15	0.17	1.42	0.10
Tp = 14 s	0.11	0.20	0.17	0.15	1.41	0.11
Tp = 16 s	0.16	0.22	0.18	0.16	1.11	0.10
Tp = 18 s	0.18	0.24	0.18	0.16	0.92	0.10

Tp/H1	surge	sway	yaw	heave	roll	pitch
Tp = 10 s	16.1	10.3	11.2	11.0	12.5	11.2
Tp = 12 s	14.6	12.6	13.4	12.6	13.1	13.3
Tp = 14 s	14.4	12.8	14.4	12.8	13.1	14.3
Tp = 16 s	20.6	16.0	15.9	16.0	13.3	14.8
Tp = 18 s	19.9	19.0	19.1	19.0	13.9	17.0

SHIP MOTION RESPONSE FOR 6 m WAVES FROM 128 deg

Mean (m)	surge	sway	yaw	heave	roll	pitch
Tp = 10 s	0.026	0.138	0.008	0.063	0.018	0.010
Tp = 12 s	0.019	0.127	0.016	0.003	0.133	0.002
Tp = 14 s	0.031	0.162	0.018	0.004	0.018	0.007
Tp = 16 s	0.099	0.367	0.036	0.036	0.050	0.001
Tp = 18 s	0.052	0.305	0.038	0.037	0.053	0.000

H1 (m)	surge	sway	yaw	heave	roll	pitch
Tp = 10 s	4.28	0.53	0.49	0.80	2.05	0.27
Tp = 12 s	6.02	0.86	0.57	0.85	3.12	0.30
Tp = 14 s	7.08	1.86	0.67	0.84	2.95	0.30
Tp = 16 s	11.18	2.38	1.03	0.94	2.69	0.44
Tp = 18 s	10.96	2.56	1.30	1.08	2.57	0.47

Hmax (m)	surge	sway	yaw	heave	roll	pitch
Tp = 10 s	4.18	0.48	0.43	0.48	1.92	0.19
Tp = 12 s	5.15	0.76	0.46	0.66	3.05	0.23
Tp = 14 s	6.53	1.81	0.51	0.48	2.85	0.23
Tp = 16 s	6.46	2.28	0.78	0.62	2.27	0.28
Tp = 18 s	9.97	2.48	1.13	0.78	1.98	0.34

Hmo (m)	surge	sway	yaw	heave	roll	pitch
Tp = 10 s	3.05	0.35	0.22	0.47	1.06	0.13
Tp = 12 s	3.92	0.53	0.32	0.49	1.94	0.17
Tp = 14 s	4.35	0.99	0.39	0.52	1.77	0.17
Tp = 16 s	5.76	2.04	0.59	0.58	1.53	0.20
Tp = 18 s	6.84	1.87	0.73	0.68	1.36	0.24

Tp (s)	surge	sway	yaw	heave	roll	pitch
Tp = 10 s	195.0	48.6	39.4	208.4	12.4	195.0
Tp = 12 s	153.7	59.4	38.8	213.6	12.6	195.3
Tp = 14 s	72.7	68.3	40.6	315.1	13.0	175.5
Tp = 16 s	201.5	69.0	44.4	208.4	31.7	201.5
Tp = 18 s	177.0	68.7	42.7	219.6	68.7	205.1

Hmo/o	surge	sway	yaw	heave	roll	pitch
Tp = 10 s	3.05	0.27	0.17	0.45	0.21	0.09
Tp = 12 s	3.92	0.45	0.26	0.44	0.29	0.10
Tp = 14 s	4.34	0.96	0.33	0.48	0.42	0.10
Tp = 16 s	5.76	2.01	0.55	0.54	0.75	0.15
Tp = 18 s	6.83	1.83	0.69	0.63	0.67	0.19

Tp/o	surge	sway	yaw	heave	roll	pitch
Tp = 10 s	195.0	48.6	39.4	208.4	48.8	195.0
Tp = 12 s	153.7	59.4	38.8	213.6	57.2	195.3
Tp = 14 s	72.7	68.3	40.6	315.1	67.6	175.5
Tp = 16 s	201.5	69.0	44.4	208.4	68.7	201.5
Tp = 18 s	177.0	68.7	42.7	219.6	68.7	205.1

Hmo/H1	surge	sway	yaw	heave	roll	pitch
Tp = 10 s	0.10	0.22	0.14	0.15	1.04	0.10
Tp = 12 s	0.13	0.28	0.20	0.21	1.92	0.14
Tp = 14 s	0.16	0.28	0.21	0.21	1.72	0.14
Tp = 16 s	0.20	0.30	0.22	0.22	1.34	0.13
Tp = 18 s	0.25	0.36	0.24	0.25	1.19	0.15

Tp/H1	surge	sway	yaw	heave	roll	pitch
Tp = 10 s	25.1	10.4	10.1	12.1	12.4	10.1
Tp = 12 s	17.2	12.5	13.8	12.5	12.6	13.8
Tp = 14 s	21.9	12.1	14.7	12.0	13.0	14.0
Tp = 16 s	23.8	23.6	15.8	23.7	12.9	16.7
Tp = 18 s	23.1	23.1	19.6	23.2	13.6	19.6

Appendix 10 Ship motion response

10.c Wave direction 140°

SHIP MOTION RESPONSE FOR 2 m WAVES FROM 140 deg

Mean (m)	surge	sway	yaw	heave	roll	pitch
Tp = 10 s	0.028	0.092	0.001	0.066	0.021	0.001
Tp = 12 s	0.079	0.038	0.004	0.024	0.015	0.002
Tp = 14 s	0.027	0.038	0.005	0.020	0.024	0.000
Tp = 16 s	0.034	0.042	0.013	0.032	0.038	0.001
Tp = 18 s	0.044	0.059	0.024	0.036	0.043	0.004

H1 (m)	surge	sway	yaw	heave	roll	pitch
Tp = 10 s	0.462	0.246	0.158	0.158	0.537	0.087
Tp = 12 s	0.612	0.303	0.215	0.202	1.085	0.113
Tp = 14 s	0.807	0.256	0.262	0.221	1.078	0.129
Tp = 16 s	0.726	0.329	0.283	0.202	1.066	0.111
Tp = 18 s	1.284	0.513	0.355	0.272	1.139	0.188

Hmax (m)	surge	sway	yaw	heave	roll	pitch
Tp = 10 s	0.35	0.18	0.13	0.12	0.52	0.08
Tp = 12 s	0.53	0.27	0.18	0.18	1.07	0.11
Tp = 14 s	0.75	0.25	0.22	0.18	1.01	0.11
Tp = 16 s	0.63	0.27	0.26	0.18	1.03	0.10
Tp = 18 s	1.25	0.41	0.30	0.22	1.05	0.16

Hmo (m)	surge	sway	yaw	heave	roll	pitch
Tp = 10 s	0.25	0.14	0.10	0.10	0.28	0.05
Tp = 12 s	0.34	0.18	0.13	0.14	0.74	0.07
Tp = 14 s	0.46	0.18	0.15	0.13	0.63	0.08
Tp = 16 s	0.43	0.22	0.16	0.13	0.63	0.08
Tp = 18 s	0.81	0.33	0.22	0.16	0.64	0.10

Tp (s)	surge	sway	yaw	heave	roll	pitch
Tp = 10 s	182.1	46.3	46.8	2053.3	11.5	10.1
Tp = 12 s	2103.4	12.4	13.5	12.4	12.5	13.7
Tp = 14 s	115.4	30.4	14.8	12.7	13.0	14.0
Tp = 16 s	72.5	46.8	32.2	16.4	16.2	16.1
Tp = 18 s	115.4	49.1	48.2	21.9	15.3	19.6

Hmo/o	surge	sway	yaw	heave	roll	pitch
Tp = 10 s	0.23	0.09	0.06	0.05	0.08	0.02
Tp = 12 s	0.33	0.09	0.06	0.04	0.08	0.02
Tp = 14 s	0.45	0.08	0.07	0.06	0.07	0.03
Tp = 16 s	0.41	0.13	0.09	0.06	0.10	0.02
Tp = 18 s	0.80	0.25	0.16	0.08	0.17	0.04

Tp/o	surge	sway	yaw	heave	roll	pitch
Tp = 10 s	182.1	46.3	46.8	2083.3	1047.0	163.1
Tp = 12 s	2103.4	47.6	52.7	1126.4	47.6	112.2
Tp = 14 s	115.4	46.6	46.6	71.9	50.1	118.8
Tp = 16 s	72.5	46.8	47.9	70.6	46.6	124.1
Tp = 18 s	115.4	49.1	48.2	76.6	49.1	117.0

Hmo/hi	surge	sway	yaw	heave	roll	pitch
Tp = 10 s	0.09	0.10	0.08	0.08	0.26	0.05
Tp = 12 s	0.06	0.16	0.11	0.14	0.73	0.07
Tp = 14 s	0.11	0.16	0.13	0.12	0.63	0.08
Tp = 16 s	0.12	0.17	0.13	0.12	0.62	0.07
Tp = 18 s	0.15	0.21	0.16	0.14	0.61	0.09

Tp/hi	surge	sway	yaw	heave	roll	pitch
Tp = 10 s	19.0	10.5	10.1	10.5	11.5	10.1
Tp = 12 s	12.1	12.4	13.5	12.4	12.5	13.7
Tp = 14 s	14.8	14.2	14.6	12.7	13.0	14.0
Tp = 16 s	20.3	16.4	16.1	16.4	16.2	16.1
Tp = 18 s	25.0	20.9	18.2	21.9	15.3	19.6

SHIP MOTION RESPONSE FOR 4 m WAVES FROM 140 deg

Mean (m)	surge	sway	yaw	heave	roll	pitch
Tp = 10 s	0.008	0.019	0.014	0.009	0.003	0.002
Tp = 12 s	0.014	0.037	0.023	0.004	0.037	0.002
Tp = 14 s	0.014	0.037	0.025	0.004	0.008	0.000
Tp = 16 s	0.058	0.031	0.025	0.024	0.008	0.002
Tp = 18 s	0.032	0.130	0.050	0.014	0.022	0.004

H1 (m)	surge	sway	yaw	heave	roll	pitch
Tp = 10 s	1.343	0.492	0.323	0.331	1.353	0.172
Tp = 12 s	2.160	0.718	0.473	0.403	3.112	0.228
Tp = 14 s	4.135	0.699	0.513	0.481	2.789	0.250
Tp = 16 s	4.086	1.087	0.714	0.649	2.569	0.275
Tp = 18 s	5.657	1.189	0.780	0.613	2.164	0.370

Hmax (m)	surge	sway	yaw	heave	roll	pitch
Tp = 10 s	1.11	0.46	0.26	0.23	1.30	0.16
Tp = 12 s	1.92	0.53	0.41	0.35	2.98	0.19
Tp = 14 s	4.13	0.59	0.46	0.36	2.73	0.21
Tp = 16 s	3.71	1.03	0.52	0.47	2.35	0.21
Tp = 18 s	5.16	1.06	0.70	0.44	2.10	0.31

Hmo (m)	surge	sway	yaw	heave	roll	pitch
Tp = 10 s	0.83	0.27	0.19	0.21	0.78	0.10
Tp = 12 s	1.30	0.45	0.29	0.29	2.08	0.14
Tp = 14 s	2.55	0.46	0.35	0.29	1.76	0.17
Tp = 16 s	2.63	0.60	0.40	0.34	1.60	0.18
Tp = 18 s	3.50	0.85	0.46	0.39	1.32	0.21

Tp (s)	surge	sway	yaw	heave	roll	pitch
Tp = 10 s	115.4	47.6	50.6	210.2	12.4	10.0
Tp = 12 s	120.5	50.3	55.4	12.6	12.6	13.4
Tp = 14 s	115.4	50.6	50.6	70.0	13.0	115.4
Tp = 16 s	71.2	56.9	56.9	70.0	15.8	16.1
Tp = 18 s	112.2	55.7	56.4	20.8	15.1	113.8

Hmo/o	surge	sway	yaw	heave	roll	pitch
Tp = 10 s	0.82	0.17	0.12	0.14	0.13	0.04
Tp = 12 s	1.29	0.32	0.20	0.14	0.22	0.05
Tp = 14 s	2.55	0.36	0.25	0.20	0.27	0.09
Tp = 16 s	2.62	0.47	0.28	0.22	0.29	0.07
Tp = 18 s	3.49	0.75	0.38	0.26	0.40	0.13

Tp/o	surge	sway	yaw	heave	roll	pitch
Tp = 10 s	115.4	47.6	50.6	210.2	48.2	193.1
Tp = 12 s	120.5	50.3	55.4	204.8	50.3	118.8
Tp = 14 s	115.4	50.6	50.6	70.0	50.6	115.4
Tp = 16 s	71.2	56.9	56.9	70.0	56.9	120.5
Tp = 18 s	112.2	55.7	55.4	75.9	56.5	113.8

Hmo/hi	surge	sway	yaw	heave	roll	pitch
Tp = 10 s	0.09	0.21	0.15	0.16	0.77	0.10
Tp = 12 s	0.12	0.32	0.21	0.25	2.04	0.13
Tp = 14 s	0.16	0.28	0.24	0.21	1.74	0.15
Tp = 16 s	0.21	0.36	0.28	0.26	1.67	0.16
Tp = 18 s	0.25	0.41	0.26	0.28	1.26	0.16

Tp/hi	surge	sway	yaw	heave	roll	pitch
Tp = 10 s	17.8	10.5	10.0	10.5	12.4	10.0
Tp = 12 s	13.4	12.6	13.3	12.5	12.6	13.4
Tp = 14 s	19.9	12.9	14.6	12.6	13.0	14.6
Tp = 16 s	25.0	18.5	16.1	16.3	15.8	16.1
Tp = 18 s	21.5	20.8	20.8	20.8	15.1	21.0

SHIP MOTION RESPONSE FOR 6 m WAVES FROM 140 deg

Mean (m)	surge	sway	yaw	heave	roll	pitch
Tp = 10 s	0.088	0.066	0.024	0.022	0.002	0.004
Tp = 12 s	0.053	0.195	0.056	0.009	0.016	0.011
Tp = 14 s	0.067	0.209	0.057	0.012	0.060	0.008
Tp = 16 s	0.112	0.218	0.057	0.010	0.037	0.002
Tp = 18 s	0.053	0.279	0.080	0.033	0.059	0.006

H1 (m)	surge	sway	yaw	heave	roll	pitch
Tp = 10 s	3.076	0.720	0.496	0.621	2.164	0.238
Tp = 12 s	5.325	1.512	0.767	0.783	4.004	0.363
Tp = 14 s	9.310	2.051	1.169	0.808	4.761	0.415
Tp = 16 s	7.814	2.483	1.248	0.958	4.016	0.468
Tp = 18 s	10.139	2.716	1.297	1.066	4.108	0.591

Hmax (m)	surge	sway	yaw	heave	roll	pitch
Tp = 10 s	2.88	0.61	0.45	0.36	2.12	0.21
Tp = 12 s	4.90	1.43	0.66	0.52	3.87	0.25
Tp = 14 s	9.30	1.90	1.03	0.60	4.70	0.32
Tp = 16 s	7.14	2.47	1.04	0.67	3.74	0.33
Tp = 18 s	9.03	2.61	1.17	0.90	3.74	0.57

Hmo (m)	surge	sway	yaw	heave	roll	pitch
Tp = 10 s	2.41	0.43	0.30	0.38	1.35	0.15
Tp = 12 s	3.83	0.88	0.45	0.49	2.66	0.23
Tp = 14 s	6.22	1.44	0.65	0.52	2.62	0.28
Tp = 16 s	4.90	1.56	0.78	0.56	2.17	0.27
Tp = 18 s	6.37	1.91	0.75	0.66	2.24	0.33

Tp (s)	surge	sway	yaw	heave	roll	pitch
Tp = 10 s	70.1	50.0	44.1	1706.7	12.5	112.8
Tp = 12 s	115.6	57.7	40.0	210.2	12.8	115.8
Tp = 14 s	115.4	60.7	43.1	68.9	12.8	113.8
Tp = 16 s	69.4	60.2	42.7	228.3	12.4	17.4
Tp = 18 s	114.9	62.7	44.5	62.7	12.4	114.9

Hmo/o	surge	sway	yaw	heave	roll	pitch
Tp = 10 s	2.41	0.31	0.23	0.31	0.22	0.08
Tp = 12 s	3.61	0.74	0.34	0.35	0.43	0.12
Tp = 14 s	6.22	1.36	0.56	0.41	0.62	0.18
Tp = 16 s	4.90	1.48	0.68	0.42	0.63	0.14
Tp = 18 s	6.36	1.81	0.64	0.50	0.75	0.22

Tp/o	surge	sway	yaw	heave	roll	pitch
Tp = 10 s	70.1	50.0	44.1	1706.7	50.0	205.3
Tp = 12 s	115.6	57.7	40.0	210.2	57.7	115.6
Tp = 14 s	115.4	60.7	43.1	68.9	58.9	113.8
Tp = 16 s	69.4	60.2	42.7	228.3	60.2	120.5
Tp = 18 s	114.9	62.7	44.5	62.7	63.0	114.9

Hmo/hi	surge	sway	yaw	heave	roll	pitch
Tp = 10 s	0.11	0.29	0.19	0.22	1.33	0.13
Tp = 12 s	0.35	0.47	0.30	0.34	2.93	0.19
Tp = 14 s	0.26	0.45	0.33	0.33	2.54	0.21
Tp = 16 s	0.28	0.52	0.38	0.37	2.06	0.23
Tp = 18 s	0.38	0.60	0.41	0.43	2.11	0.25

Tp/hi	surge	sway	yaw	heave	roll	pitch
Tp = 10 s	25.1	10.3	9.9	12.0	12.5	10.0
Tp = 12 s	23.9	12.0	13.0	12.0	12.8	13.1
Tp = 14 s	23.2	12.8	13.8	12.8	12.8	17.6
Tp = 16 s	25.1	20.6	15.9	22.4	12.4	17.4
Tp = 18 s	21.1	20.4	20.4	20.4	12.4	20.6

Appendix 10 Ship motion response

10.d Wave direction 160°

SHIP MOTION RESPONSE FOR 2 m WAVES FROM 160 deg

Mean (m)	surge	sway	yaw	heave	roll	pitch
Tp = 10 s	0.031	0.051	0.003	0.047	0.010	0.003
Tp = 12 s	0.027	0.050	0.004	0.022	0.006	0.004
Tp = 14 s	0.033	0.041	0.001	0.012	0.017	0.001
Tp = 16 s	0.063	0.050	0.017	0.004	0.011	0.003
Tp = 18 s	0.024	0.062	0.020	0.017	0.049	0.001

H1 (m)	surge	sway	yaw	heave	roll	pitch
Tp = 10 s	0.093	0.279	0.189	0.195	0.662	0.135
Tp = 12 s	0.132	0.455	0.282	0.338	2.730	0.201
Tp = 14 s	0.157	0.338	0.283	0.271	2.340	0.195
Tp = 16 s	0.191	0.379	0.321	0.298	2.182	0.197
Tp = 18 s	0.214	0.392	0.296	0.289	1.570	0.179

Hmax (m)	surge	sway	yaw	heave	roll	pitch
Tp = 10 s	0.74	0.53	0.37	0.35	1.78	0.24
Tp = 12 s	0.83	0.83	0.41	0.49	4.46	0.32
Tp = 14 s	2.66	0.95	0.80	0.50	4.61	0.46
Tp = 16 s	1.11	0.78	0.52	0.48	4.12	0.30
Tp = 18 s	2.24	1.35	0.58	0.46	2.85	0.26

Hmo (m)	surge	sway	yaw	heave	roll	pitch
Tp = 10 s	0.59	0.40	0.26	0.22	0.97	0.14
Tp = 12 s	0.66	0.51	0.31	0.35	2.74	0.20
Tp = 14 s	1.42	0.46	0.38	0.31	2.35	0.20
Tp = 16 s	0.86	0.52	0.39	0.34	2.19	0.20
Tp = 18 s	1.68	0.75	0.43	0.34	1.60	0.19

Tp (s)	surge	sway	yaw	heave	roll	pitch
Tp = 10 s	210.2	54.3	54.3	10.3	12.5	10.1
Tp = 12 s	120.9	12.4	11.6	12.1	12.7	11.6
Tp = 14 s	70.0	53.2	41.0	12.4	13.8	14.1
Tp = 16 s	65.6	53.2	34.8	228.3	14.1	14.4
Tp = 18 s	109.2	55.7	55.0	210.2	13.0	17.9

Hmo/o	surge	sway	yaw	heave	roll	pitch
Tp = 10 s	0.58	0.29	0.18	0.11	0.16	0.03
Tp = 12 s	0.65	0.24	0.13	0.09	0.19	0.03
Tp = 14 s	1.41	0.31	0.26	0.16	0.19	0.05
Tp = 16 s	0.84	0.36	0.23	0.16	0.22	0.04
Tp = 18 s	1.67	0.64	0.32	0.17	0.32	0.07

Tp/o	surge	sway	yaw	heave	roll	pitch
Tp = 10 s	210.2	54.3	54.3	210.2	54.6	210.2
Tp = 12 s	120.9	53.6	53.2	204.8	52.9	154.4
Tp = 14 s	70.0	53.2	41.0	210.2	51.5	110.7
Tp = 16 s	65.6	53.2	53.2	228.3	53.9	204.8
Tp = 18 s	109.2	55.7	55.0	210.2	55.4	109.2

Hmo/d	surge	sway	yaw	heave	roll	pitch
Tp = 10 s	0.09	0.28	0.19	0.19	0.96	0.14
Tp = 12 s	0.13	0.45	0.28	0.34	2.73	0.20
Tp = 14 s	0.16	0.34	0.28	0.27	2.34	0.19
Tp = 16 s	0.19	0.38	0.32	0.30	2.18	0.20
Tp = 18 s	0.21	0.39	0.30	0.29	1.57	0.18

Tp/d	surge	sway	yaw	heave	roll	pitch
Tp = 10 s	7.2	10.3	10.1	10.3	12.5	10.1
Tp = 12 s	12.2	12.4	11.6	12.1	12.7	11.6
Tp = 14 s	14.7	12.5	14.6	12.4	13.8	14.1
Tp = 16 s	15.5	16.1	15.8	16.1	14.1	14.4
Tp = 18 s	20.0	20.0	17.9	19.9	13.0	17.9

SHIP MOTION RESPONSE FOR 4 m WAVES FROM 160 deg

Mean (m)	surge	sway	yaw	heave	roll	pitch
Tp = 10 s	0.014	0.061	0.020	0.019	0.005	0.001
Tp = 12 s	0.032	0.091	0.018	0.016	0.041	0.000
Tp = 14 s	0.071	0.220	0.037	0.006	0.000	0.001
Tp = 16 s	0.018	0.161	0.085	0.014	0.017	0.006
Tp = 18 s	0.101	0.197	0.043	0.000	0.014	0.002

H1 (m)	surge	sway	yaw	heave	roll	pitch
Tp = 10 s	2.953	1.235	0.652	0.723	3.118	0.374
Tp = 12 s	3.367	1.702	0.786	0.867	7.108	0.514
Tp = 14 s	8.477	3.025	1.535	1.277	6.648	0.680
Tp = 16 s	5.184	1.823	1.608	1.276	7.593	0.503
Tp = 18 s	10.159	2.627	1.617	1.440	4.828	0.858

Hmax (m)	surge	sway	yaw	heave	roll	pitch
Tp = 10 s	2.84	0.91	0.63	0.58	2.89	0.33
Tp = 12 s	3.36	1.44	0.66	0.75	7.03	0.45
Tp = 14 s	8.40	2.89	1.34	1.12	5.96	0.61
Tp = 16 s	4.15	1.82	1.34	0.77	7.33	0.47
Tp = 18 s	8.33	2.63	1.38	0.88	4.08	0.44

Hmo (m)	surge	sway	yaw	heave	roll	pitch
Tp = 10 s	2.21	0.77	0.44	0.49	2.02	0.23
Tp = 12 s	2.11	0.93	0.53	0.56	4.34	0.31
Tp = 14 s	5.12	1.71	0.79	0.75	3.42	0.33
Tp = 16 s	3.45	1.12	0.76	0.76	3.42	0.34
Tp = 18 s	7.29	1.47	0.91	0.70	2.61	0.36

Tp (s)	surge	sway	yaw	heave	roll	pitch
Tp = 10 s	201.5	54.4	41.8	208.4	12.6	10.0
Tp = 12 s	122.3	56.6	43.1	11.9	13.2	11.6
Tp = 14 s	73.8	66.1	43.3	210.2	12.6	14.2
Tp = 16 s	67.1	57.3	39.8	215.6	14.5	16.8
Tp = 18 s	110.7	61.9	44.5	216.2	13.2	110.7

Hmo/o	surge	sway	yaw	heave	roll	pitch
Tp = 10 s	2.21	0.61	0.33	0.36	0.32	0.09
Tp = 12 s	2.10	0.62	0.30	0.25	0.42	0.08
Tp = 14 s	5.11	1.60	0.65	0.59	0.62	0.16
Tp = 16 s	3.44	0.92	0.57	0.58	0.51	0.12
Tp = 18 s	7.28	1.33	0.80	0.53	0.56	0.21

Tp/o	surge	sway	yaw	heave	roll	pitch
Tp = 10 s	201.6	54.4	41.8	208.4	54.6	208.4
Tp = 12 s	122.3	56.6	43.1	210.2	55.0	124.1
Tp = 14 s	73.8	66.1	43.3	210.2	68.1	204.8
Tp = 16 s	67.1	57.3	39.8	215.6	57.3	215.6
Tp = 18 s	110.7	61.9	44.5	216.2	55.8	110.7

Hmo/d	surge	sway	yaw	heave	roll	pitch
Tp = 10 s	0.12	0.47	0.29	0.33	1.99	0.21
Tp = 12 s	0.19	0.69	0.44	0.49	4.32	0.30
Tp = 14 s	0.30	0.62	0.44	0.48	3.36	0.29
Tp = 16 s	0.30	0.83	0.50	0.50	3.38	0.32
Tp = 18 s	0.36	0.62	0.45	0.46	2.55	0.29

Tp/d	surge	sway	yaw	heave	roll	pitch
Tp = 10 s	20.6	10.4	10.0	10.4	12.6	10.0
Tp = 12 s	14.7	12.1	11.8	11.9	13.2	11.6
Tp = 14 s	23.6	12.6	14.2	12.6	12.6	14.2
Tp = 16 s	20.0	16.5	15.8	16.5	14.5	15.8
Tp = 18 s	24.9	20.2	17.7	20.4	13.2	17.7

SHIP MOTION RESPONSE FOR 6 m WAVES FROM 160 deg

Mean (m)	surge	sway	yaw	heave	roll	pitch
Tp = 10 s	0.124	0.079	0.024	0.058	0.019	0.001
Tp = 12 s	0.018	0.189	0.030	0.572	1.955	0.502
Tp = 14 s	0.110	0.181	0.047	0.065	0.021	0.002
Tp = 16 s	0.108	0.577	0.041	0.073	0.029	0.003
Tp = 18 s	0.138	0.383	0.119	0.064	0.075	0.004

H1 (m)	surge	sway	yaw	heave	roll	pitch
Tp = 10 s	8.426	1.804	0.871	1.263	3.425	0.464
Tp = 12 s	7.389	2.012	1.073	1.255	9.565	0.684
Tp = 14 s	9.087	2.714	1.743	1.362	8.032	0.848
Tp = 16 s	10.673	4.605	1.619	1.865	7.883	0.786
Tp = 18 s	11.502	3.805	1.951	1.871	6.363	0.904

Hmax (m)	surge	sway	yaw	heave	roll	pitch
Tp = 10 s	7.250	1.537	0.738	1.035	3.360	0.345
Tp = 12 s	7.316	1.675	1.059	0.948	9.197	0.595
Tp = 14 s	7.984	2.607	1.350	1.111	8.031	0.653
Tp = 16 s	9.078	4.327	1.348	1.280	6.591	0.604
Tp = 18 s	10.280	3.486	1.759	1.398	6.233	0.591

Hmo (m)	surge	sway	yaw	heave	roll	pitch
Tp = 10 s	6.126	0.964	0.577	0.841	2.309	0.312
Tp = 12 s	4.994	1.227	0.702	0.790	5.691	0.383
Tp = 14 s	6.292	1.438	0.911	0.878	4.452	0.403
Tp = 16 s	7.592	3.283	0.940	1.249	4.121	0.448
Tp = 18 s	9.288	2.598	1.190	1.302	3.740	0.554

Tp (s)	surge	sway	yaw	heave	roll	pitch
Tp = 10 s	205.314	60.845	43.355	210.190	12.644	199.924
Tp = 12 s	120.471	57.312	47.731	204.800	13.107	13.256
Tp = 14 s	71.860	69.424	43.116	1365.333	13.066	14.149
Tp = 16 s	215.579	64.688	45.011	219.571	13.003	211.986
Tp = 18 s	113.837	64.019	39.923	208.393	13.256	113.837

Hmo/o	surge	sway	yaw	heave	roll	pitch
Tp = 10 s	6.123	0.791	0.474	0.750	0.324	0.207
Tp = 12 s	4.987	0.893	0.455	0.540	0.463	0.161
Tp = 14 s	6.285	1.231	0.734	0.690	0.540	0.181
Tp = 16 s	7.581	3.193	0.744	1.111	1.099	0.245
Tp = 18 s	9.276	2.472	1.058	1.154	0.943	0.418

Tp/o	surge	sway	yaw	heave	roll	pitch
Tp = 10 s	205.314	60.845	43.355	210.190	60.845	199.924
Tp = 12 s	120.471	57.312	47.731	204.800	57.702	199.924
Tp = 14 s	71.860	69.424	43.116	1365.333	62.419	113.778
Tp = 16 s	215.579	64.688	45.011	219.571	64.688	211.986
Tp = 18 s	113.837	64.019	39.923	208.393	58.239	113.837

Hmo/d	surge	sway	yaw	heave	roll	pitch
Tp = 10 s	0.20	0.55	0.33	0.38	2.29	0.23
Tp = 12 s	0.28	0.84	0.53	0.58	5.67	0.35
Tp = 14 s	0.29	0.74	0.54	0.54	4.42	0.36
Tp = 16 s	0.41	0.76	0.58	0.57	3.97	0.37
Tp = 18 s	0.48	0.80	0.55	0.60	3.62	0.36

Tp/d	surge	sway	yaw	heave	roll	pitch
Tp = 10 s	24.98	10.41	10.02	10.37	12.64	9.97
Tp = 12 s	14.60	13.11	13.26	11.91	13.11	13.26
Tp = 14 s	19.65	13.00	14.15	12.28	13.07	14.15
Tp = 16 s	21.90	20.11	15.67	19.98	13.00	13.62
Tp = 18 s	24.98	24.58	24.98	24.58	13.26	24.83

Appendix 11 Response amplitude operators of free-floating ship

11.a RAO for surge motion

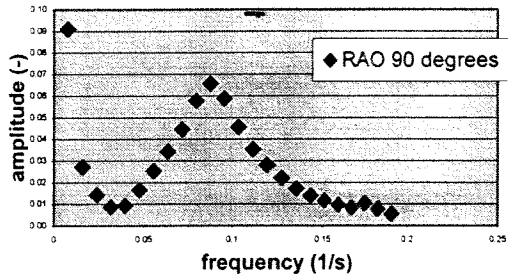

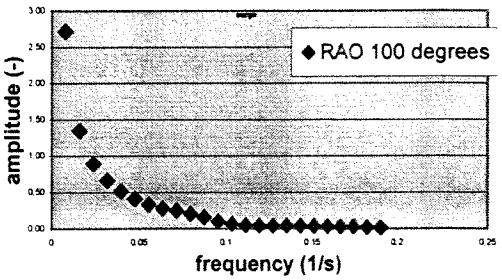

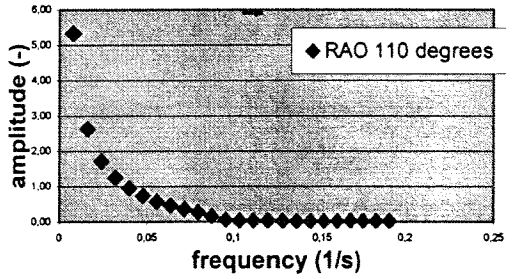

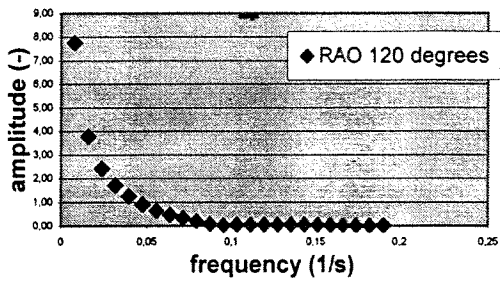

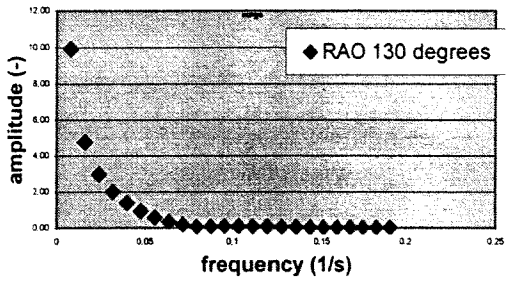

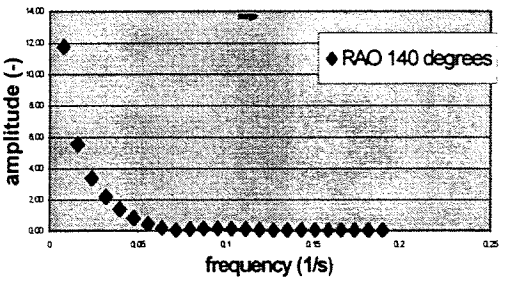

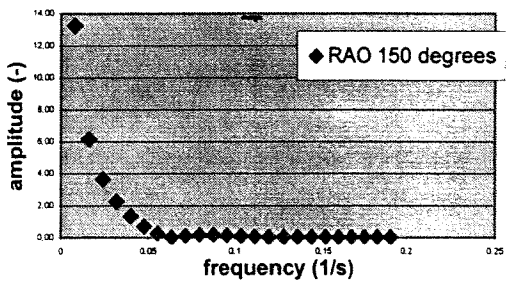

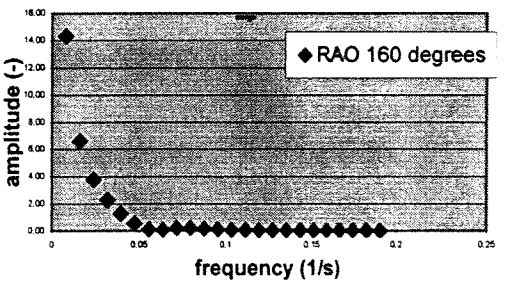

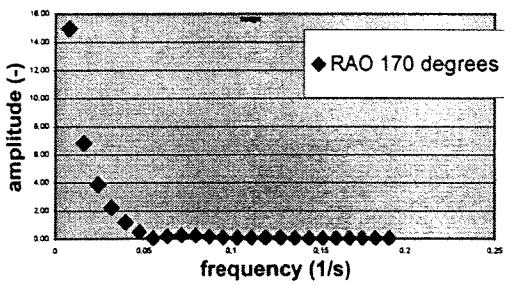

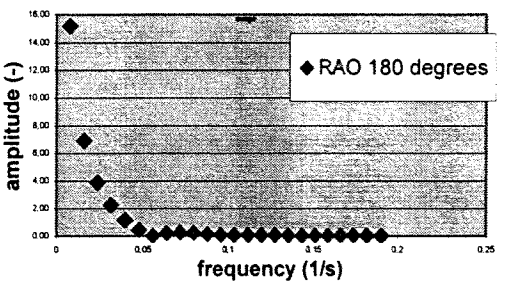

Appendix 11 Response amplitude operators of free-floating ship

11.b RAO for sway motion

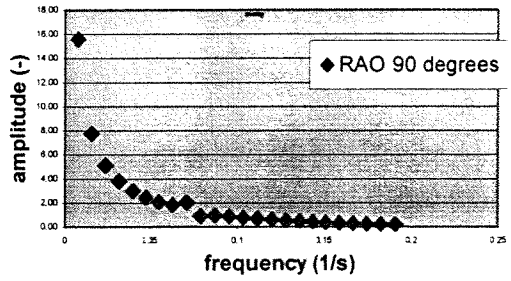

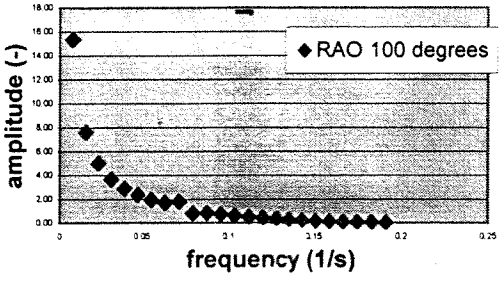

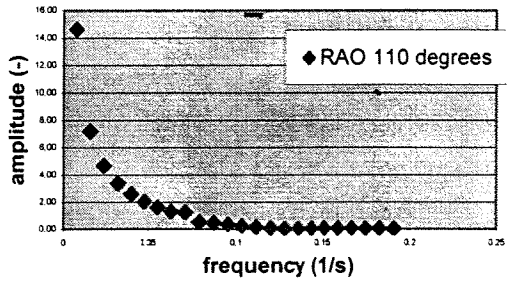

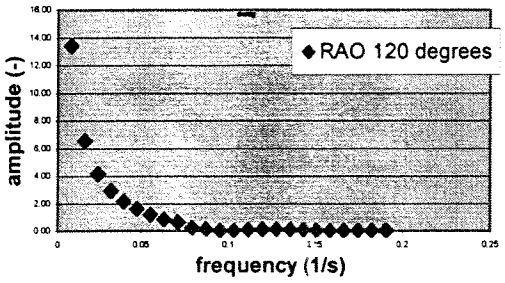

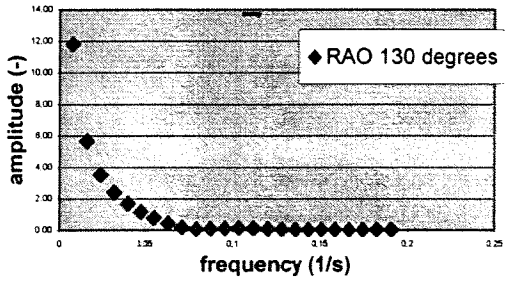

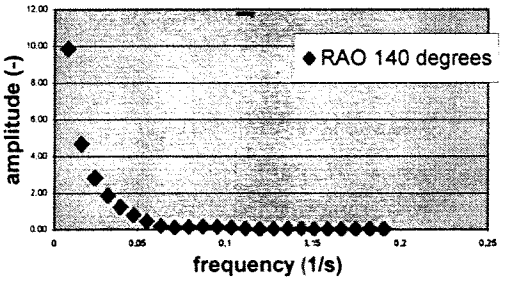

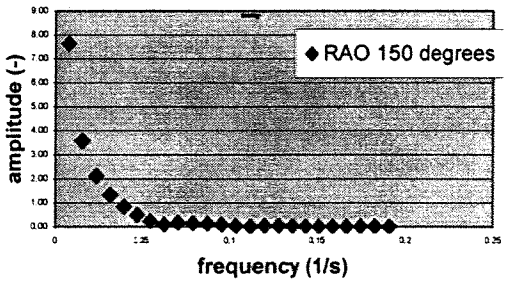

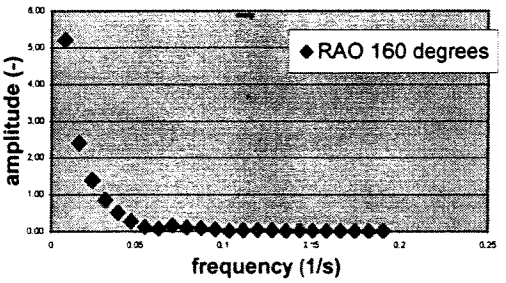

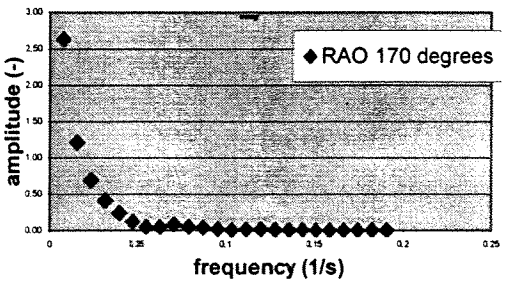

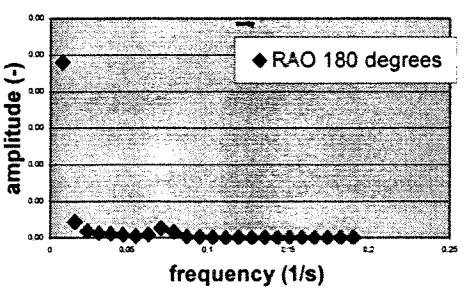

Appendix 11 Response amplitude operators of free-floating ship

11.c RAO for roll motion

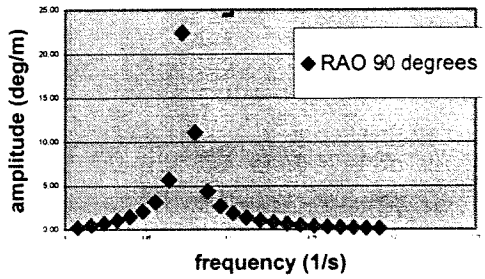

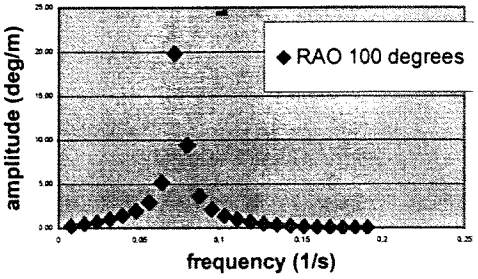

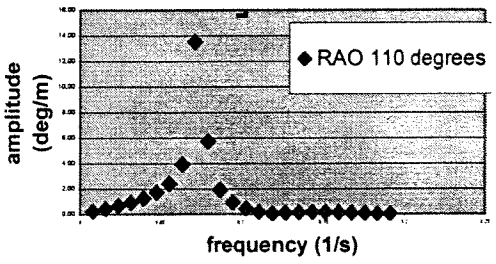

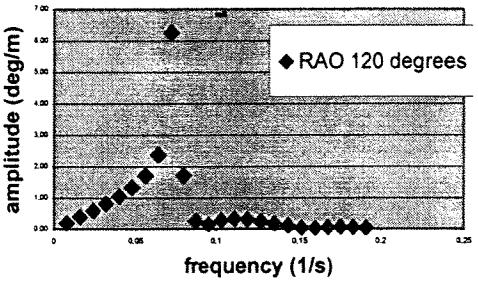

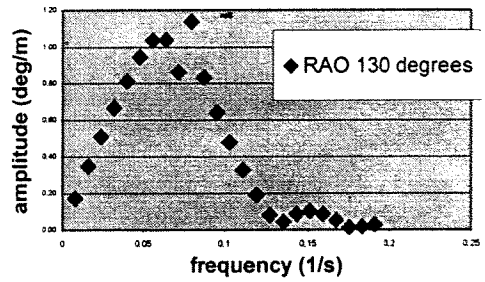

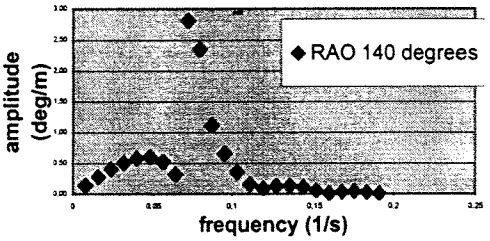

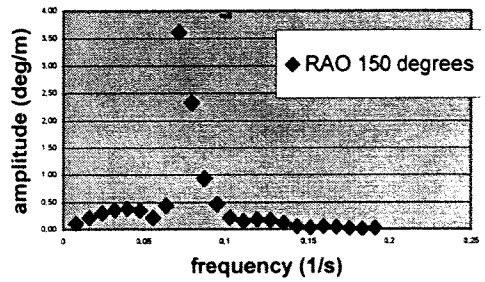

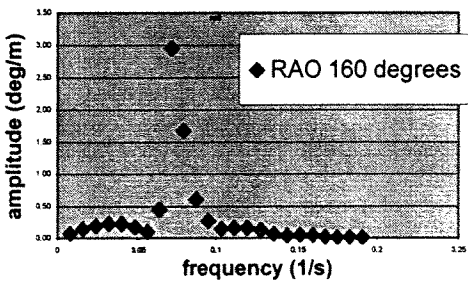

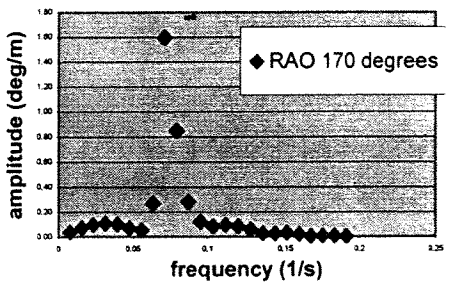

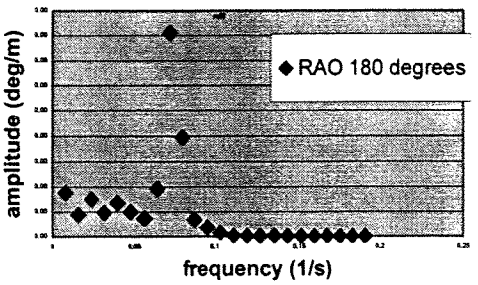

Appendix 12 Linear mass-spring model

This appendix discusses the representation of the moored Coega model ship by a linear mass-spring system.

The equation of (surge) motion for the moored ship is:

$$m_X \cdot \ddot{X} = F_{spring} + F_{damping} + F_{waves} \quad \text{(A-11)}$$

in which

m_X	= mass of the ship (added mass included)
X	= displacement of the ship (surge motion)
F_{spring}	= force due to spring
$F_{damping}$	= force due to damping
F_{waves}	= force due to waves

After substitution of the equations for the spring and the damping forces the equation of (surge) motion becomes:

$$m_X \cdot \ddot{X} + b_X \cdot \dot{X} + c_X \cdot X = \hat{F}_{waves} \cdot \cos(\omega \cdot t) \quad \text{(A-12)}$$

in which

m_X	= mass coefficient
b_X	= damping coefficient
c_X	= spring coefficient
ω	= angular frequency
X	= displacement of the ship (surge motion)
$\hat{F}_{waves}$	= maximum force due to waves

The surge motion resulting from the harmonic wave force is also a harmonic function:

$$X(t) = \hat{X}\cos(\omega t + \theta) \quad \text{(A-13)}$$

Substitution of Equation A-13 in Equation A-12 leads to:

$$\left(c_X - m_X\omega^2\right)\cdot \hat{X}\cos(\omega t + \theta) - b_X\omega \cdot \hat{X}\cos(\omega t + \theta) = \hat{F}\cos(\omega t) \quad \text{(A-14)}$$

The amplitude characteristic $\frac{\hat{X}}{\hat{F}_X}(\omega)$ can be determined from Equation A-15:

$$\frac{\hat{X}}{\hat{F}_X}(\omega) = \sqrt{\left(c_X - m_X\omega^2\right)^2 + \left(b_X\omega\right)^2} \quad \text{(A-15)}$$

Using the programme "DELFRAC", the amplitude characteristic $\frac{\hat{F}_X}{\zeta}(\omega)$ is calculated.

Multiplying the two amplitude characteristics provides the response amplitude operator (RAO) of the moored ship:

$$\frac{\hat{X}}{\hat{\zeta}}(\omega) = \frac{\hat{F}_X}{\hat{\zeta}}(\omega) \cdot \frac{\hat{X}}{\hat{F}_X}(\omega) \qquad \text{(A-16)}$$

Figure A.1 shows this calculated RAO for the moored ship.

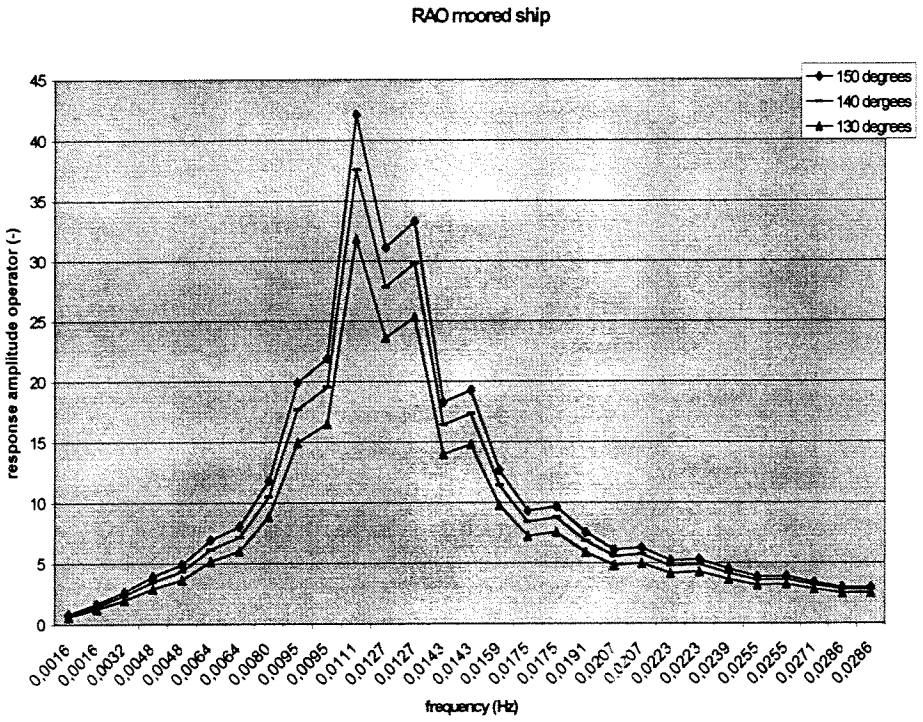

Figure A.1. Response Amplitude Operator of the moored ship

With the RAO of the moored ship and the measured spectral density function of the waves, the spectral density function of the surge motion can be calculated:

$$S_X(\omega) = \left(\frac{\hat{X}}{\hat{\zeta}}(\omega) \right)^2 \cdot S_\zeta(\omega) \qquad \text{(A-17)}$$

By means of the program Excel the surge motion is calculated using Equation A-17. First, the three coefficients of Equation A-12 need to be determined:

$m_x = 1.1 * m = 88\ 770 \cdot 10^3$ kg (this includes the added mass)
$b_x = 0.2 * \sqrt{c_x \cdot m_x}$
$c_x = k_X$

k_X is the stiffness of the mooring system parallel to the quay which is the direction of the surge motion. The stiffness of the mooring system depends on both the load-elongation characteristics of the mooring lines and the angle of the mooring lines to the quay. If there is no pretension in the mooring lines, a change of angle does not influence the stiffness of the mooring system very much. The change of angle is left out of consideration since the lines during the model test are not pretensioned. Then, k_X can be determined by:

$$k_X = \frac{\Delta F}{\Delta X} = k \cdot \cos^2 \phi \qquad \text{(A-18)}$$

in which
ΔF = force in mooring line
$\Delta X = \Delta L / \cos \phi$
ΔL = elongation of the mooring line
k = mooring line stiffness
ϕ = angle of mooring line

Mooring lines 1, 3, 4 and 6 contribute to the total stiffness of the mooring system (see Appendix 6):

- $k_{X1} = 273 \cdot \cos^2 47.3 = 126$ kN/m
- $k_{X3} = 196 \cdot \cos^2 43.3 = 104$ kN/m
- $k_{X4} = 188 \cdot \cos^2 45.4 = 92.7$ kN/m
- $k_{X6} = 291 \cdot \cos^2 44.4 = 149$ kN/m

Total mooring line stiffness parallel to the quay is $k_X = k_{X1} + k_{X3} + k_{X4} + k_{X6} = 472$ kN/m

With this $c_x = k_X = 472$ kN/m
and $b_x = 0.2 * \sqrt{c_x \cdot m_x} = 1.29 \cdot 10^6$ Ns/m

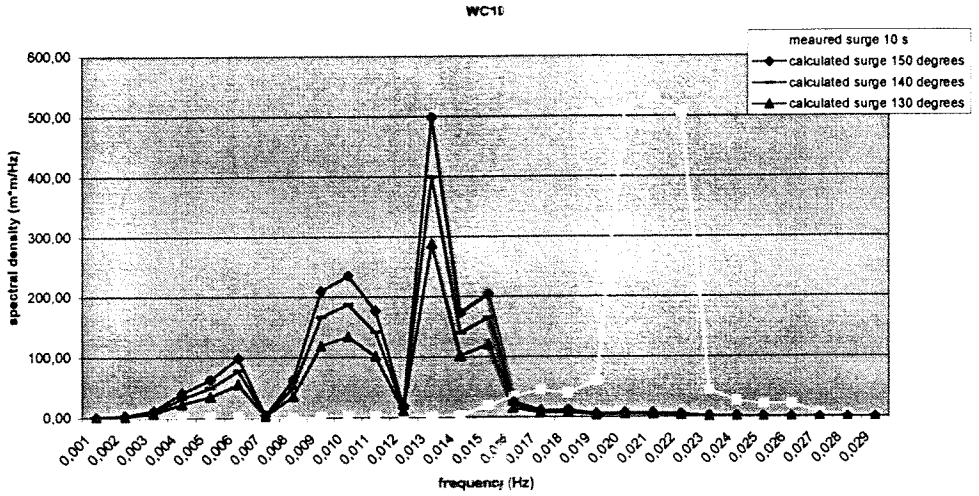
meaured surge 10 s
calculated surge 150 degrees
calculated surge 140 degrees
calculated surge 130 degrees
spectral density (m*m/Hz)
frequency (Hz)

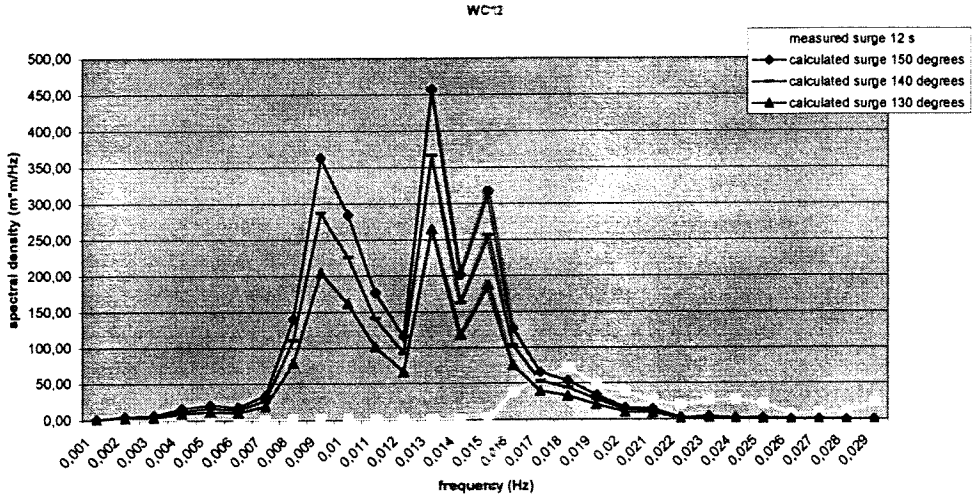
measured surge 12 s
calculated surge 150 degrees
calculated surge 140 degrees
calculated surge 130 degrees
spectral density (m*m/Hz)
frequency (Hz)

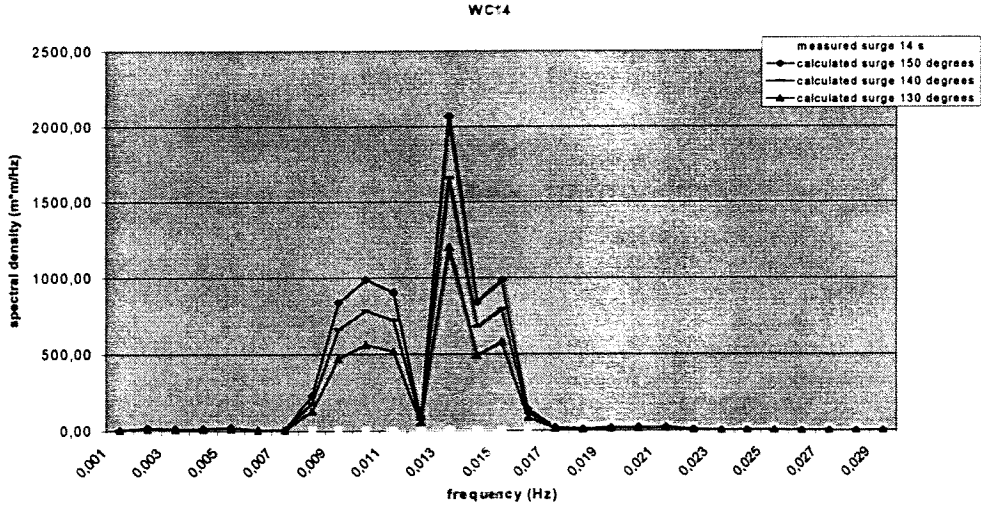
measured surge 14 s
calculated surge 150 degrees
calculated surge 140 degrees
calculated surge 130 degrees
spectral density (m*m/Hz)
frequency (Hz)

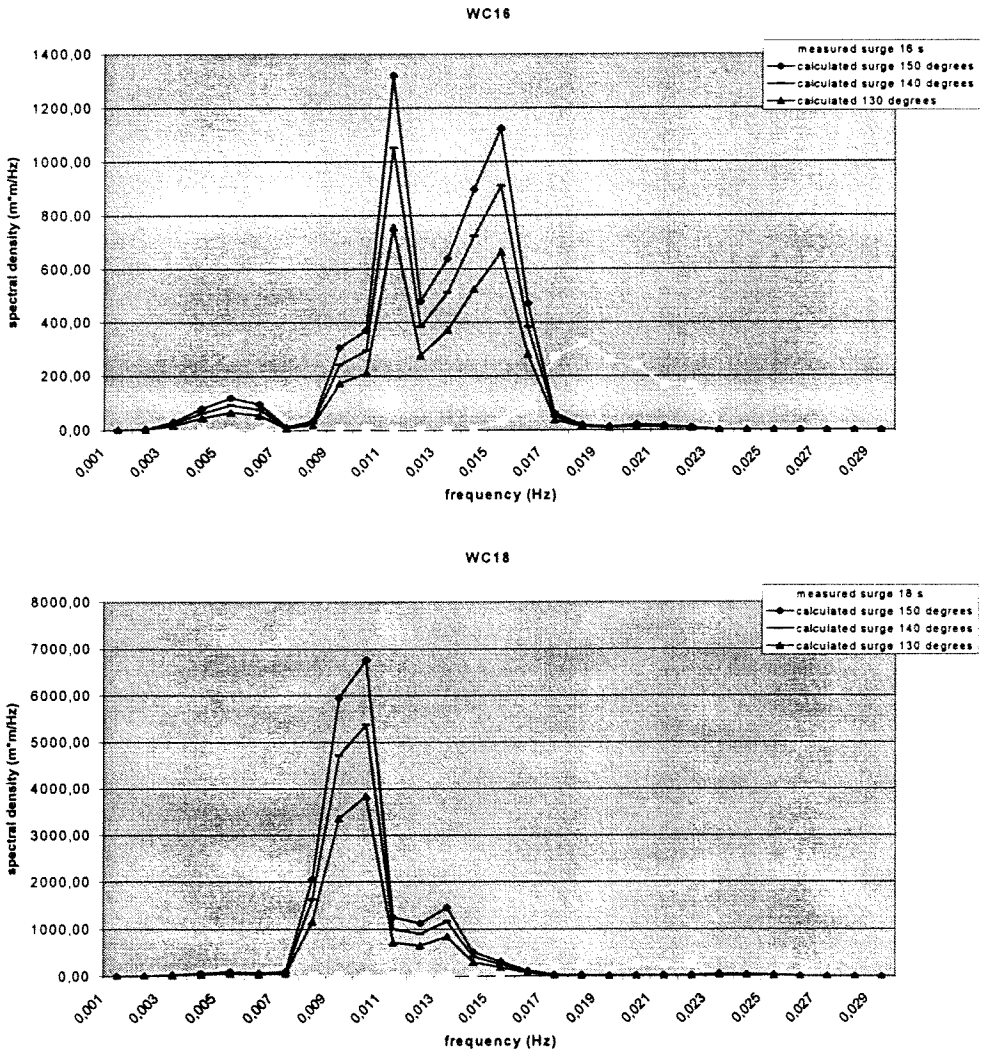

Figure A.2. Calculated and measured surge motion, k_X = 472 kN/m

Figure A.2 shows the energy spectrum of the surge motion calculated according to Equation A-17 and of the surge motion measured in the model tests. The magnitude of the measured and calculated surge motion is equal only for the first wave condition (WC10). The magnitude of the calculated surge motion is several times larger than of the measured surge for WC12 and WC16. The order of magnitude of the measured surge motion for WC14 and WC18 is negligible compared to the magnitude of the calculated surge.

It seems that the damping coefficient is not large enough. This leads to overestimation of the surge motion. Furthermore, the calculated surge shows, for all wave conditions, a peak near frequencies lower than the peak frequency of the measured surge motion. The natural frequency results from the choice of the spring coefficient. Since the spring coefficient determines the damping coefficient, increasing the spring coefficient leads to an increase in damping coefficient.

The natural frequency depends on both the mass of the ship and the spring coefficient:

$$\omega_0 = \sqrt{\frac{c_X}{m_X}} \qquad \text{(A-19)}$$

The measured spectral density curve of WC10 in Figure A.1 shows a peak near a frequency of 0.021 Hz. If this frequency is the natural frequency then, according to Equation A-19, the spring coefficient (c_X) is 1545 kN/m. This coefficient is more than three times larger than the one calculated from the mooring lines. It is noted that the mooring lines 2 and 5 and the fenders are not included in this calculation.

Figure A.3 shows the surge motions calculated with a spring coefficient of $1.55 \cdot 10^6$ N/m together with the surge motion measured in the model tests. Because of a change in spring coefficient, the damping coefficient changes to $b_X = 2.35 \cdot 10^6$ Ns/m.

It can be concluded from Figure A.2 that the measured and calculated surge motions are in the same frequency range. Due to the increase of damping the calculated surge is decreased compared to the calculated surge of Figure A.2.

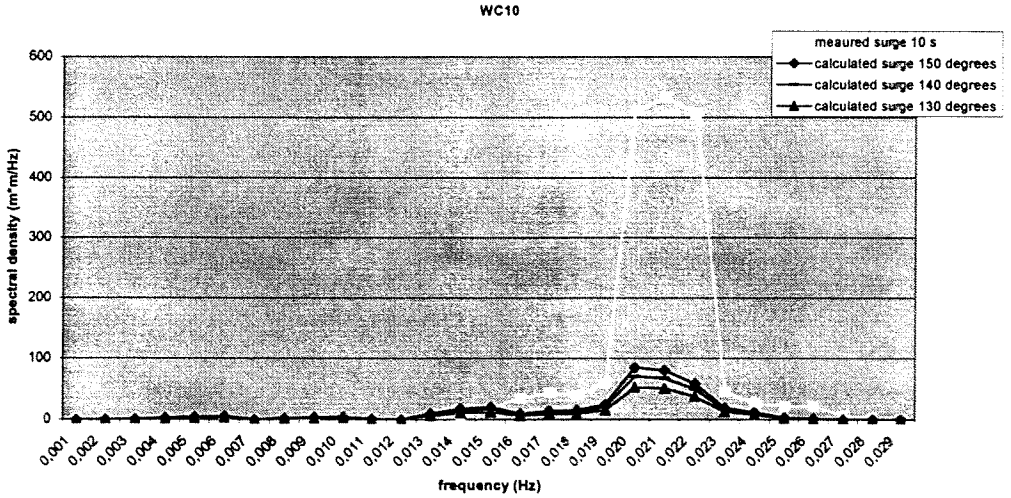

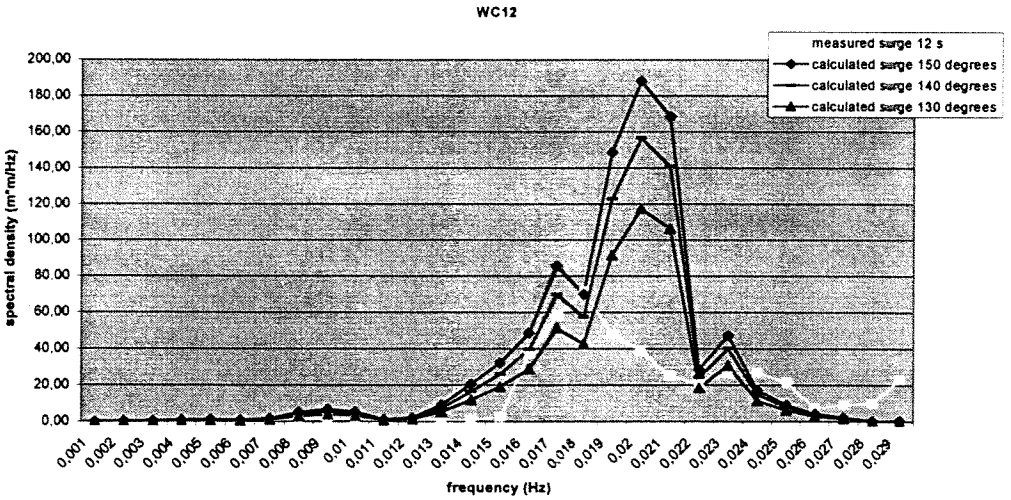

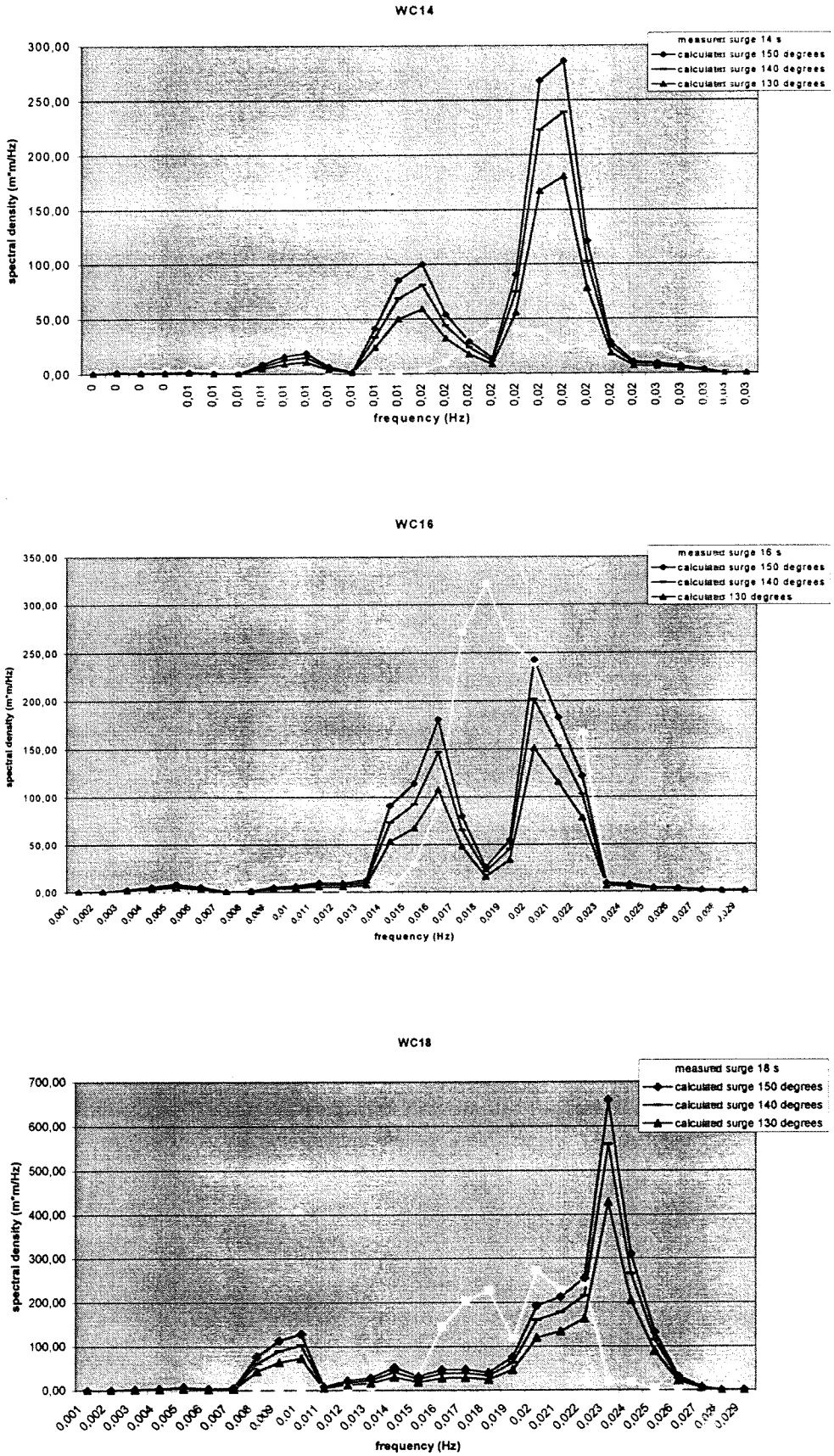

Figure A.3. Calculated and measured surge motion, k_X = 1550 kN/m

Appendix 13 Surge motion due to drift forces

In regular waves the drift force is constant. In irregular waves this drift force is a function of the frequency:

$$\bar{F}_d(\omega) = C(\omega)\cdot\hat{\zeta}^2 \tag{A-20}$$

or

$$C(\omega) = \frac{\bar{F}_d}{\hat{\zeta}^2}(\omega) \tag{A-21}$$

in which
$\bar{F}_d$ = drift force
C = coefficient
ω = angular frequency
$\hat{\zeta}$ = wave amplitude

The mean drift force in irregular waves can be represented by the summation of a large number of wave drift forces in regular waves:

$$\begin{aligned}\bar{F}_d &= \sum_{i=1}^{N}\bar{F}_d(\omega_i) \\ &= \sum_{i=1}^{N} C(\omega_i)\cdot\hat{\zeta}^2 \\ &= \sum_{i=1}^{N} C(\omega_i)\cdot S_\zeta(\omega)\cdot\Delta\omega\end{aligned} \tag{A-22}$$

in which
S_ζ = wave energy spectrum

With $\Delta\omega$ decreasing to zero the mean drift force in irregular waves is:

$$\bar{F}_d = 2\cdot\int_0^\infty \frac{\bar{F}_d}{\hat{\zeta}^2}(\omega)\cdot S_\zeta(\omega)\cdot d\omega \tag{A-23}$$

The spectral density of this drift force at $\omega = 0$ is:

$$S_F(0) = 8\cdot\int_0^\infty\left[\frac{\bar{F}_d}{\hat{\zeta}^2}(\omega)\cdot S_\zeta(\omega)\right]^2\cdot d\omega \tag{A-24}$$

For low frequencies the spectral density of the drift force can be represented by the spectral density at $\omega = 0$. Then the spectral density of the surge motion is calculated as follows:

$$S_X(\omega) = \left[\frac{\hat{X}}{\hat{F}}(\omega)\right]^2 \cdot S_F(\omega) \approx \left[\frac{\hat{X}}{\hat{F}}(\omega)\right]^2 \cdot S_F(0) \qquad \text{(A-25)}$$

in which

S_X = surge energy spectrum
S_F = force energy spectrum
$\frac{\hat{X}}{\hat{F}}(\omega)$ = amplitude characteristic

The significant surge motion follows from the zeroth moment of the surge energy spectrum, which is:

$$M_{0X} = \int_0^\infty S_X(\omega) \cdot d\omega \qquad \text{(A-26)}$$

$$= S_F(0) \cdot \int_0^\infty \left[\frac{\hat{X}}{\hat{F}}(\omega)\right]^2 \cdot d\omega$$

$$= S_F(0) \cdot \frac{\pi}{2 \cdot b \cdot c}$$

in which

M_{0X} = zeroth moment of the surge energy spectrum
b = damping coefficient
c = spring coefficient

Appendix 14 Surge motion due to gradient force

It is suggested that the gradient of the water level can produce surge motion. The gradient creates a harmonic force on the moored ship that can be the cause of surge motion of the moored ship.

$$F_{gradient} = \hat{F}_{gradient} \cdot \cos(\omega t) \tag{A-27}$$

This force can be calculated from the gradient of the water level as follows:

$$F_{gradient} = m \cdot \dot{u} = -m \cdot g \cdot \frac{\partial \zeta}{\partial x} \tag{A-28}$$

The standing wave can be represented by a superposition of two waves:

$$\zeta = \zeta_+ + \zeta_- = \hat{\zeta} \cdot \cos(kx) \cdot \cos(\omega t) \tag{A-29}$$

Then, the gradient of the water level is:

$$\frac{\partial \zeta}{\partial x} = -k \cdot \hat{\zeta} \cdot \sin(kx) \cdot \cos(\omega t) \tag{A-30}$$

At the position of a node cos (kx) = 0, consequently the gradient of the water level becomes:

$$\frac{\partial \zeta}{\partial x} = -k \cdot \hat{\zeta} \cdot \cos(\omega t) \tag{A-31}$$

And the maximum gradient of the waterlevel at the position of the node is:

$$\left(\frac{\partial \zeta}{\partial x}\right)_{\max} = k \cdot \hat{\zeta} = \frac{2\pi}{\lambda} \cdot \frac{H}{2} = \frac{\pi \cdot H}{\lambda} \tag{A-32}$$

Accordingly, the maximum gradient force becomes:

$$\hat{F}_{gradient} = m \cdot g \cdot \left.\frac{\partial \zeta}{\partial x}\right|_{\max} = m \cdot g \cdot \frac{\pi \cdot H}{\lambda} \tag{A-33}$$

As calculated in Section 5.1 the wavelength (λ) is 4 * 560 = 2240 m and the wave period (T_1) is 172 s. The wave height can be determined from the spectral density curve (Appendix 9e).

$$S_\zeta(\omega) \cdot d\omega = \tfrac{1}{2} \cdot \zeta^2 \tag{A-34}$$

in which

$S_\zeta(\omega)$	= spectral density
$d\omega$	= frequency band
ζ	= water elevation

By means of Equation A-34 the wave height is determined to be 0.6 m. Then, the maximum gradient force follows from Equation A-35:

$\hat{F}_{gradient} = 747$ kN

Linear mass-spring system:

$$m_x \cdot \ddot{X} + b_x \cdot \dot{X} + c_x \cdot X = F_{gradient} \quad \text{(A-35)}$$

in which

m_x	= mass coefficient
c_x	= spring coefficient
b_x	= damping coefficient
X	= displacement
$F_{gradient}$	= force due to the gradient of the water level

The solution of the linear mass-spring system is:

$$\hat{X}(\omega) = \frac{\hat{F}_{gradient}}{\sqrt{(k - \omega^2 \cdot m)^2 + (c \cdot \omega)^2}} \quad \text{(A-36)}$$

with

$m_x = 1.1 * m = 88\,770 \cdot 10^3$ kg

$c_x = 472$ kN/m

$b_x = 0.2 * \sqrt{c_x \cdot m_x} = 1.29 \cdot 10^6$ Ns/m

$\omega_x = 2\pi / T_1 = 0.037$ rad/s

The maximum displacement is $\hat{X}(\omega) = 2.1$ m.

The measured surge motion can be determined from the spectral density curve (Appendix 9e).

$$S_\zeta(\omega) \cdot d\omega = \tfrac{1}{2} \cdot X^2 \quad \text{(A-37)}$$

in which

$S_\zeta(\omega)$	= spectral density
$d\omega$	= frequency band
X	= surge motion

By means of Equation A-37 the surge motion is determined to be 4 m. Hence, the calculated surge motion due to the gradient in the water level is two times smaller than the measured significant surge at that frequency band.

Appendix 15 R^2 values per period

15.a R^2 values for relations with regard to roll

Xmo_roll = C *	Hmo	Hmolo	Hmohi
alle Tp	*0,572*	*0,240*	*0,706*
Tp = 10 s	0,801	0,403	0,821
Tp = 12 s	0,233	0,712	0,829
Tp = 14 s	0,820	0,660	[illegible]
Tp = 16 s	0,741	0,410	[illegible]
Tp = 18 s	0,701	0,405	[illegible]

Xmo_roll = C *	Hmo^2	Hmolo^2	Hmohi^2
alle Tp	*0,385*	*0,260*	*0,615*
Tp = 10 s	0,953	0,137	[illegible]
Tp = 12 s	0,079	0,039	[illegible]
Tp = 14 s	0,791	0,504	[illegible]
Tp = 16 s	0,282	0,471	0,607
Tp = 18 s	0,716	0,110	[illegible]

Xmo_roll = C *	Hmo*Tp	Hmolo*Tp	Hmohi*Tp
alle Tp	*0,353*	*0,199*	*0,621*
Tp = 10 s	0,781	0,358	0,818
Tp = 12 s	0,208	0,009	0,807
Tp = 14 s	0,750	0,582	0,824
Tp = 16 s	0,703	0,372	[illegible]
Tp = 18 s	0,455	0,069	[illegible]

Xmo_roll = C *	Hmo*Tp^2	Hmolo*Tp^2	Hmohi*Tp^2
alle Tp	*0,192*	*0,101*	*0,314*
Tp = 10 s	0,758	0,309	0,813
Tp = 12 s	0,180	0,011	0,781
Tp = 14 s	0,659	0,486	0,739
Tp = 16 s	0,656	0,328	[illegible]
Tp = 18 s	0,105	0,093	0,730

Xmo_roll = C *	Hmo^2*Tp	Hmolo^2*Tp	Hmohi^2*Tp
alle Tp	*0,092*	*0,183*	*0,500*
Tp = 10 s	[illegible]	0,089	[illegible]
Tp = 12 s	0,057	0,040	[illegible]
Tp = 14 s	0,777	0,472	[illegible]
Tp = 16 s	0,210	0,459	0,554
Tp = 18 s	0,494	0,201	[illegible]

Xmo_roll = C *	(Hmo*Tp)^2	(Hmolo*Tp)^2	(Hmohi*Tp)^2
alle Tp	*0,260*	*0,107*	*0,234*
Tp = 10 s	[illegible]	0,037	[illegible]
Tp = 12 s	0,033	0,042	[illegible]
Tp = 14 s	0,754	0,433	[illegible]
Tp = 16 s	0,138	0,445	0,494
Tp = 18 s	0,148	0,089	[illegible]

Appendix 15 R^2 values per period

15.b R^2 values for relations with regard to sway

Xmo_sway = C *	Hmo	Hmolo	Hmohi
alle Tp	*0,7*	*0,7*	*0,4*
Tp = 10 s	**0,814**	0,464	**0,755**
Tp = 12 s	0,533	0,654	0,045
Tp = 14 s	**0,824**	**0,813**	**0,771**
Tp = 16 s	**0,804**	**0,802**	0,671
Tp = 18 s	**0,834**	**0,825**	0,621

Xmo_sway = C *	Hmo^2	Hmolo^2	Hmohi^2
alle Tp	*0,686*	*0,617*	*0,336*
Tp = 10 s	0,569	0,216	0,733
Tp = 12 s	0,647	0,657	0,031
Tp = 14 s	0,725	0,654	0,651
Tp = 16 s	0,597	0,498	0,490
Tp = 18 s	0,736	**0,815**	0,509

Xmo_sway = C *	Hmo*Tp	Hmolo*Tp	Hmohi*Tp
alle Tp	*0,785*	*0,749*	*0,631*
Tp = 10 s	**0,808**	0,432	**0,762**
Tp = 12 s	0,547	0,668	0,047
Tp = 14 s	**0,768**	0,744	0,724
Tp = 16 s	**0,795**	**0,777**	0,688
Tp = 18 s	**0,817**	0,712	0,715

Xmo_sway = C *	Hmo*Tp^2	Hmolo*Tp^2	Hmohi*Tp^2
alle Tp	*0,668*	*0,663*	*0,513*
Tp = 10 s	**0,799**	**0,768**	0,395
Tp = 12 s	0,559	0,680	0,680
Tp = 14 s	0,691	0,656	0,656
Tp = 16 s	**0,779**	0,697	0,746
Tp = 18 s	0,702	**0,764**	0,500

Xmo_sway = C *	Hmo^2*Tp	Hmolo^2*Tp	Hmohi^2*Tp
alle Tp	*0,699*	*0,508*	*0,493*
Tp = 10 s	0,951	0,177	0,744
Tp = 12 s	0,668	0,674	0,031
Tp = 14 s	0,728	0,635	0,667
Tp = 16 s	0,554	0,449	0,489
Tp = 18 s	0,935	0,606	0,600

Xmo_sway = C *	(Hmo*Tp)^2	(Hmolo*Tp)^2	(Hmohi*Tp)^2
alle Tp	*0,566*	*0,269*	*0,524*
Tp = 10 s	0,929	0,134	**0,756**
Tp = 12 s	0,687	0,688	0,032
Tp = 14 s	0,721	0,609	0,674
Tp = 16 s	0,509	0,401	0,480
Tp = 18 s	**0,817**	0,316	0,699